Universiteit Leiden
The Netherlands

Osteoprotegerin: a double-edged sword in osteoarthritis development

Rodriguez Ruiz, A.

Citation

Rodriguez Ruiz, A. (2022, October 19). *Osteoprotegerin: a double-edged sword in osteoarthritis development*. Retrieved from https://hdl.handle.net/1887/3484338

Version:	Publisher's Version
License:	Licence agreement concerning inclusion of doctoral thesis in the Institutional Repository of the University of Leiden
Downloaded from:	https://hdl.handle.net/1887/3484338

Note: To cite this publication please use the final published version (if applicable).

OSTEOPROTEGERIN

a double-edged sword in osteoarthritis development

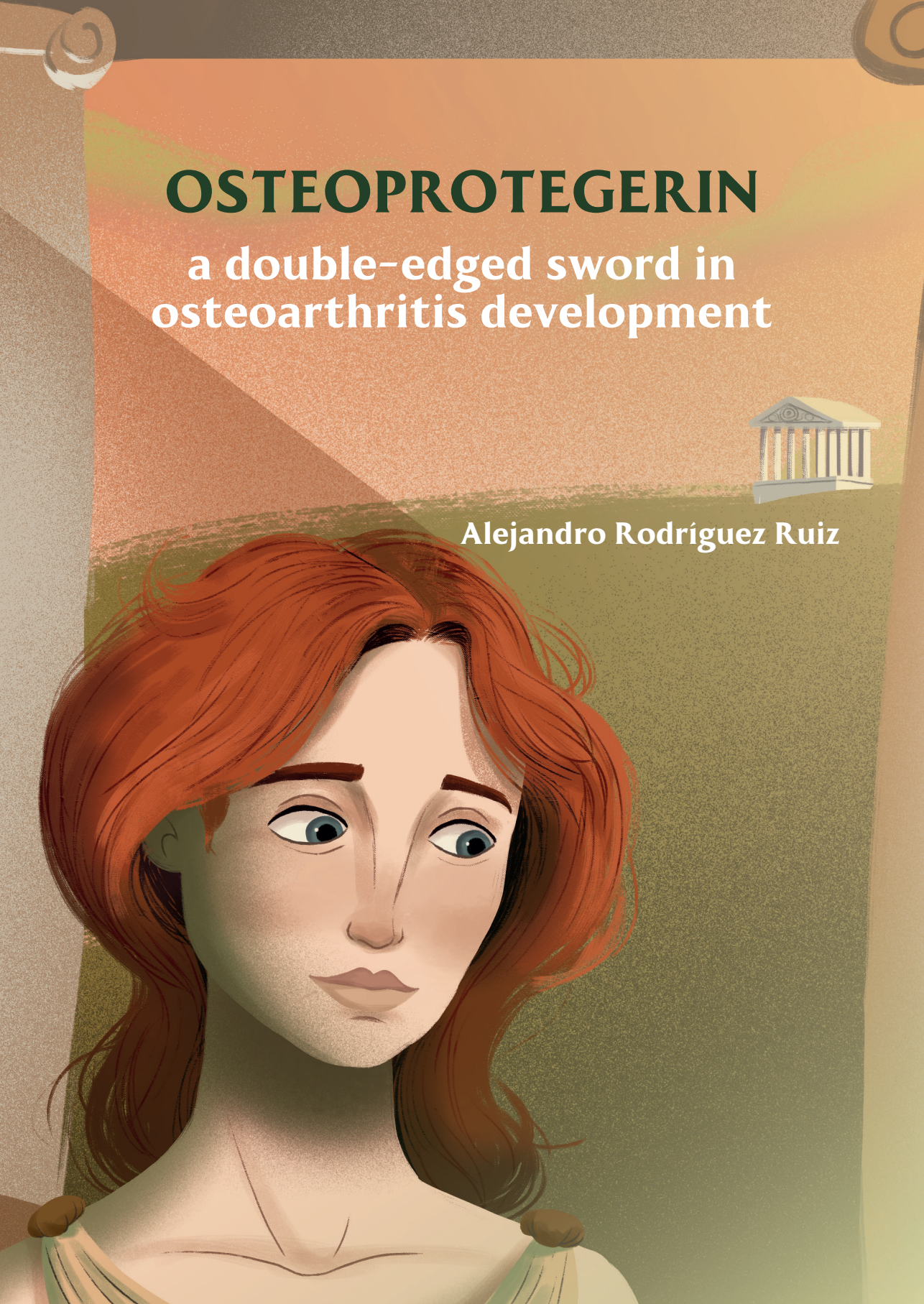

Alejandro Rodríguez Ruiz

Osteoprotegerin, a double-edged sword in osteoarthritis development

Alejandro Rodríguez Ruiz

Osteoprotegerin, a double-edged sword in osteoarthritis development
A. Rodríguez Ruiz

ISBN: 978-94-6458-527-8
Cover design: David Pavón
Lay-out: Publiss | www.publiss.nl
Print: Ridderprint | www.ridderprint.nl

Copyright of each chapter is with the publisher of the journal in which the work has appeared. No part of this thesis may be reproduced, stored in retrieval system or transmitted in any form by any means, without the permission of the author, or when appropriate, of the publisher of the represented published articles.

The research presented in this thesis was performed at the Department of Molecular Epidemiology, Leiden University Medical Center, Leiden, The Netherlands. This research was supported by the Dutch Arthritis Society (DAF-16-1-406 and DAF-16-1-405), and the Dutch Scientific Research council NWO/ZonMW VICI scheme (no. 91816631/528). This work was partly supported by grants from Marie Curie Initial Training Network (Euroclast, FP7-People-2013-ITN: #607447). Data are generated within the scope of the Medical Delta programmes Regenerative Medicine 4D and Improving Mobility with Technology.

Printing of this thesis has been possible thanks to the sponsorship of ChemoMetec, PeproTech, Nederlandse vereniging voor Matrix Biologie (NVMB), Tebu-bio, Sanbio Research & Diagnostics, Proefdiervrij and Medical Delta.

Osteoprotegerin, a double-edged sword in osteoarthritis development

Proefschrift

ter verkrijging van
de graad van doctor aan de Universiteit Leiden,
op het gezag van rector magnificus prof.dr.ir. H. Bijl,
volgens besluit van het college voor promoties
te verdedigen op woensdag 19 oktober 2022
klokke 10.00 uur

door

Alejandro Rodríguez Ruiz

geboren te Valencia, Spanje
in 1992

Promotor:	Prof. dr. I. Meulenbelt
Copromotor:	Dr. Y. F. M. Ramos
Leden promotiecommissie:	Prof. Dr. C. L. Mummery
	Prof. Dr. G. J. V. M. van Osch (Erasmus Medical Centre)
	Dr. T. J. de Vries (Academic Centre for Dentistry Amsterdam)
	Dr. J. Geurts (Lausanne University Hospital)

Table of contents

Chapter 1
General Introduction 7

Chapter 2
The role of *TNFRSF11B* in development of osteoarthritic cartilage 33

Chapter 3
Cartilage from human-induced pluripotent stem cells: comparison with neo-cartilage from chondrocytes and bone marrow mesenchymal stromal cells 57

Chapter 4
Readthrough mutation at CCAL1 locus in *TNFRSF11B* deciphers role of immobilized osteoprotegerin in subchondral bone turnover and cartilage mineralization in humans 87

Chapter 5
General discussion 121

Addendum 137
English Summary 138
Nederlandse samenvatting 141
List of Publications 144
Curriculum vitae 146
Acknowledgements 147

CHAPTER 1

General introduction

OSTEOARTHRITIS

Osteoarthritis (OA) is a chronic age-related degenerative disease of the joints characterized by degradation of the cartilage extracellular matrix (ECM), osteophyte formation, synovitis, and alterations in subchondral bone **(Figure 1A)**. OA affected joints are usually hands, hips and especially knees (1). Multiple risk factors of OA, such as gender, body mass index (BMI), bone mineral density (BMD), injury, and genetics influence the severity, course, and age of onset (2) **(Figure 1B)**. Due to current higher life expectancy, and an increase in metabolic factors such as obesity (3), a steep increase in OA prevalence is anticipated (4, 5). As such, according to the world health organization, in 2050, 15% of the world population over 60 years old will suffer from OA, of whom one third will be severely disabled. Moreover, with increasing OA patients, comorbidities such as stroke, peptic ulcer, and metabolic syndrome will rise in parallel (6).

Clinically, OA is marked by chronic pain, stiffness, and disability of patients (1, 7). Despite debilitating symptoms, no effective therapy is available except for joint replacement (1). Joint replacement, however, does not guarantee complete recovery since almost 25% of patients still experience pain and disability one year after surgery (8). Moreover, costly surgical procedures and lengthy rehabilitation is commonly accompanied with a decline in productivity. Hence, OA has a vast impact on economy, with health care costs accounting for 1-2.5% of gross national products (9, 10). In absence of effective disease modifying treatment strategies, patient care is mainly focused on controlling symptoms and minimizing disability, e.g. by non-steroidal anti-inflammatory drugs (NSAIDs) or life-style interventions, respectively (11, 12). To advance development of effective disease modifying OA treatments a better understanding of its pathophysiological mechanisms is necessary.

Radiographically, OA is assessed by Kellgren and Lawrence grading (0-4), which is based on a combination of characteristics such as joint space narrowing, osteophytosis and scleroses **(13)**. Radiographic OA score, however, does not accommodate emerging information about OA pathophysiological processes, becomes only visible once irreversible damage of joint tissues is a fact, and is insensitive to change (14). A more sensitive technique is magnetic resonance imaging (MRI). This method allows visualization of all joint tissues including cartilage, and is more sensitive to changes in disease over time, hence suitable to test efficacy of novel disease-modifying therapies (15). To score OA severity of hips, hands and knees with MRI the 'hip OA MRI scoring system' (HOAMS), Oslo hand OA MRI (OHOA-MRI), or MRI OA knee score (MOAKS) are applied respectively. These systems evaluate OA progression (0-4) by measuring osteophyte and cyst formation, cartilage loss or bone marrow lesions, among other parameters (16, 17).

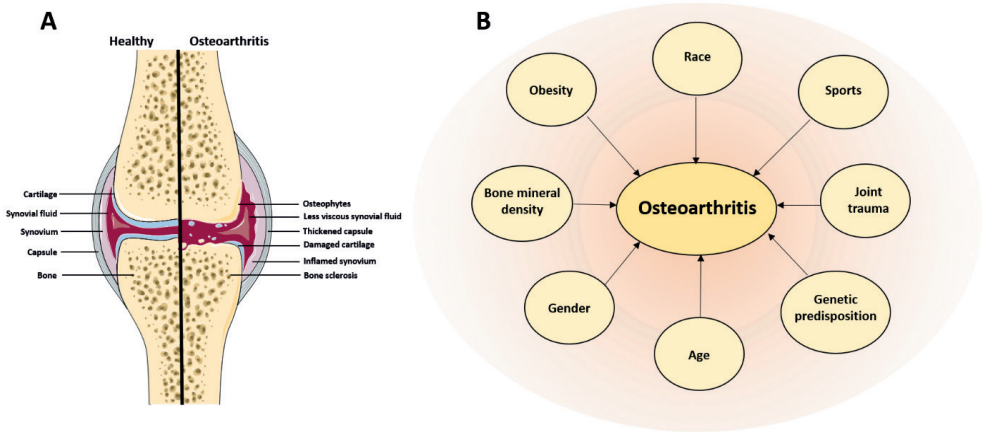

Figure 1. Osteoarthritis development and common risk factors contributing to disease progression. A) Healthy and osteoarthritic knee. **B**) Most common risk factors contributing to OA. Figure adapted from Wieland et al (18).

FORMATION OF OSTEOCHONDRAL COMPARTMENT OF JOINTS

During embryonic development and until young adulthood, bone is generated in a process termed endochondral ossification. Mesenchymal stromal cells (MSCs) condensate and differentiate into chondroprogenitor cells and further differentiate towards chondrocytes that deposit ECM **(Figure 2)**. Subsequently, the ECM network is invaded by osteoprogenitor cells that generate centres of ossification which gradually become hypertrophic and mineralized, while chondrocytes undergo terminal maturation with cartilage breakdown. This is reflected in the higher expression of metalloproteinase 13 (MMP13), that degrades the ECM, and of collagen type I and X that results in its mineralization. Additionally, hypertrophic chondrocytes can also transdifferentiate into osteoblasts, contributing to bone formation upon increased signaling e.g. from the RUNX Family Transcription Factor 2 (RUNX2) (19). In parallel with this process, vascular endothelial growth factor (VEGF) signals induce vessel formation and osteoclast, MSC and osteoprogenitor cells migration to the ECM. Moreover, a secondary ossification centre is formed at the extremes of long bones. This generates a cartilage growth plate, responsible for longitudinal growth of bone. For this, osteoclasts remove the previous cartilage matrix while osteoblasts deposit a novel bone matrix, lengthening bone tissue and ultimately replacing cartilage (20-22). When the primary ossification centre reaches the secondary centre of ossification, the growth plate closes and skeletal maturity is achieved.

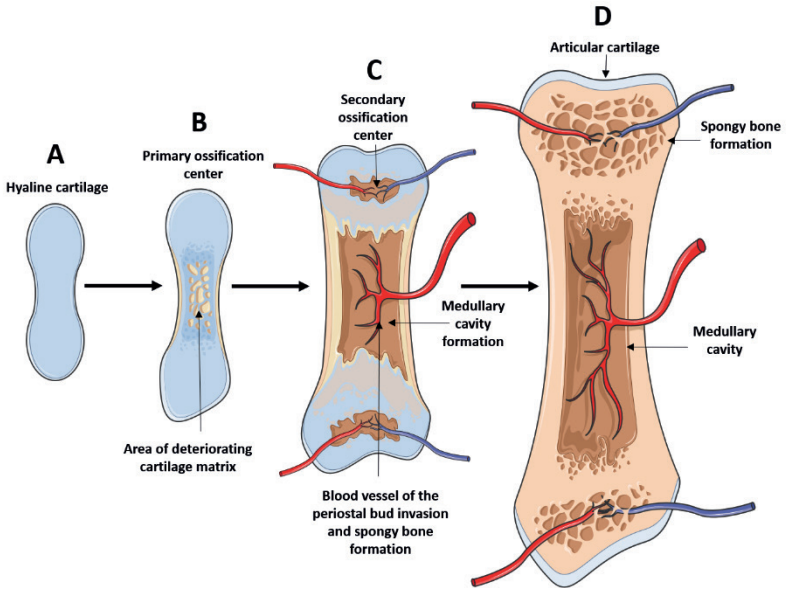

Figure 2. Endochondral ossification from the growth plate. (A) Bone collar forms in the diaphysis of hyaline cartilage. **(B)** Subsequently, cartilage calcifies in the centre of the diaphysis and develops an initial ossification centre where blood vessels of the periosteal bud invades its internal cavities. **(C)** Spongy bone starts forming and diaphysis elongates, generating a medullary cavity. **(D)** In parallel, a secondary ossification centre forms. The extremes of the bones ossify and hyaline cartilage remains on its surface. Adapted from Egawa et al (23).

Healthy (state of) osteochondral compartment

Articular hyaline cartilage is an avascular connective tissue that escapes the endochondral ossification process to cover and protect the end of long bones (24). It contains a structured network of dense ECM produced by a unique cell type, named chondrocyte. From a metabolic perspective, chondrocytes reside in a maturational arrested, near quiescent state in the articular cartilage (25). Nevertheless, during healthy cartilage remodelling, they can become metabolically active to allow ECM breakdown and novel cartilage formation (26, 27). Hence, it is essential that chondrocytes are able to return to their maturational arrested phenotype in order to maintain their healthy steady state. In healthy articular cartilage, different layers can be distinguished depending on its composition and cell morphology (28-30). The superficial zone is formed by flattened chondrocytes, and collagen fibres, and it represents between 10-20% of the total cartilage. The middle zone represents between 40-60% of the total cartilage layer, and has a lower chondrocyte density. The deep zone represents 30% of the total cartilage **(Figure 3A)**. In this layer, chondrocytes are organized in columns, showing the lowest cell density of all cartilage zones. Lastly, the calcified zone contains a reduced number of chondrocytes which are embedded

in a calcified matrix. Remarkably, between the deep and calcified zone there is an interface called tidemark which represents the border between uncalcified and calcified cartilage (24, 31).

Cartilage ECM consists of a mix of collagens, proteoglycans, glycosaminoglycans and glycoproteins responsible for its protective and viscoelastic properties (29, 32, 33). Collagen fibres constitute the primary support of the ECM, provide tensile strength and allow for cell adhesion in cartilage (34). Among all types of collagen, collagen type II (COL2) is the most abundant, reaching 90-95% of total collagen composition (33) and stabilizing the ECM together with proteoglycans. The largest proteoglycan, aggrecan, is distributed within the collagen matrix and forms a complex with the glycosaminoglycan hyaluronic acid. The resulting negative charge causes a strong retention of water in the tissue. The flow of water, upon repetitive loading cycles, distributes nutrients to chondrocytes and withdraws waste products. Additionally, the synovial fluid provides lubrication and osmotic properties necessary to hold mechanical loads and reduce friction on the joints.

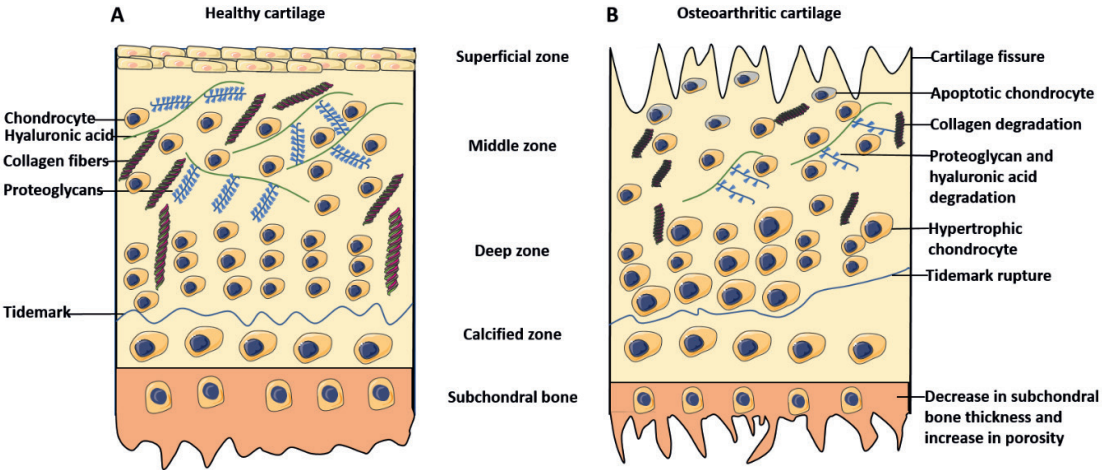

Figure 3. The different zones and cell composition in healthy (A) and osteoarthritic (B) articular cartilage.

Subchondral bone is the rigid tissue underlying calcified cartilage. It is divided in the subchondral cortical plate, with a more compact bone, and the subchondral trabecular bone with a porous composition (35, 36). Subchondral bone distributes mechanical loads across joint surfaces and provides nutrient supply to cartilage (37). It is composed of different cell types that coordinate a highly responsive remodelling process. Osteoblasts initiate mineralization of the ECM, where collagen type I acts as a scaffold for hydroxyapatite crystal deposition (38). The majority of

osteoblasts (90%) becomes embedded in lacunae within the mineralized matrix and forms the osteocytes. Osteocytes are responsible of sensing mechanical loads and controlling bone formation and remodelling processes (39). To accomplish bone resorption, the osteoclasts, a group of haematopoietically-derived cells, ensure that 10% of the total bone mass gets replaced every year (30, 40, 41).

Osteoarthritic osteochondral compartment

OA can severely affect organization of the cartilage ECM. As such, in OA, the superficial cartilage zone starts to present fissures and erosions that slowly progress to the middle zone. Later, loss of proteoglycans and glycosaminogycans follow, all accompanied with a higher chondrocyte proliferation (4, 42). As OA develops, the fissures extend into the deep cartilage zone causing chondrocyte hypertrophy, further proliferation, and ultimately apoptosis. Altogether, OA creates an unbalanced tissue remodeling towards breakdown (42, 43). This is also accompanied by an increase in collagen and proteoglycan breakdown enzymes such as metalloproteinases (44, 45) and aggrecanases. In parallel, there is a reduction of collagen type II, with an increase in collagen type I and collagen type X (46). Subsequently, the calcified zone extends and a rupture of the tidemark can occur, resulting in a new calcified/uncalcified boundary while the physical barrier preventing vessel growth is lost **(Figure 3B)** (47). Remarkably, there is a strong resemblance between OA pathophysiological processes and the terminal differentiation observed in growth plate chondrocytes during endochondral ossification (48-50). As such, both processes result in a regain of growth-plate morphology and end-stage mineralization. To quantify these differences at a histological level, a grading system such as the Mankin score can be applied. For this, joint tissues are scored from zero (normal) to fourteen (most severe) based on cartilage structure, cellularity, proteoglycan content and tidemark disruption (51).

OA in subchondral bone is characterized by an increase in bone remodelling which leads to a thinning of the subchondral plate **(Figure 3B)**. Progression of the OA process results in a reduction of bone turnover, followed by subchondral bone sclerosis and a reduced thickness of the trabeculae (52, 53). Moreover, there is an increase in subchondral bone volume concomitant with reduced subchondral bone mineralization and stiffness due to a lower calcium to collagen ratio (37). To quantify OA progession in subchondral bone, a four-stage evaluation scale (1-4) was developed by Aho et al (54). This method was based on subchondral bone remodelling and increase in subchondral bone volume. Nevertheless, there is no consensus yet about a standardized method to grade subchondral bone OA progession. Besides the cartilage and bone independent processes in OA, a strong interaction between both tissues exists (55, 56). To better understand this interaction and their role in OA pathophysiology further research at a molecular level is necessary (38).

OA PATHOPHYSIOLOGY AT THE MOLECULAR LEVEL

To characterize OA pathophysiology, genome-wide differential gene expression analyses can be performed, while comparing macroscopically intact (preserved) with lesioned OA joint tissues (57). By performing RNA sequencing of macroscopically preserved and lesioned OA cartilage of 35 paired samples of OA patients in the RAAK (Research Arthritis and Articular Cartilage) study, (58) it was revealed that the OA pathophysiological process in cartilage is marked by 2387 differentially expressed genes. Consistent differentially expressed (DE) genes in OA-lesioned cartilage in this study (58) can be found in **Table 1**. These DE genes are enriched in pathways involved in skeletal development, cell adhesion, and extracellular matrix organization. Notable dysregulated genes involved in matrix mineralization that are highly consistent in lesioned versus preserved OA cartilage are *POSTN*, *MGP* and *TNFRSF11B* (58). Moreover, as marked by the consistent differential expression of genes *RUNX2*, *MMP13*, *SOX9*, *DIO2*, *COLX* and *ALPL* with OA, (43, 59) all orchestrating the endochondral ossification process, it was confirmed that chondrocytes entering an OA state recapitulate a growth plate morphology and may be subject to trans-differentiation to osteoblasts. As demonstrated by methylome wide studies of preserved and lesioned OA cartilage, the propensity of articular chondrocytes to undergo terminal maturation is associated with loosening of epigenetically controlled transcription (29, 60, 61) and further supports a shared route between endochondral ossification and OA (59, 62-64).

Additionally, RNA sequencing analyses in preserved versus lesioned subchondral bone of 26 OA patients, resulted in 1569 DE genes that mark the OA pathophysiological process in bone. Some of the most significantly DE genes in OA-subchondral bone can be found in **Table 2**. Of those genes, 305 showed the same direction of effect in cartilage and in subchondral bone, 14 of which were among the 25 highest expressed genes in both tissues (65), indicating crosstalk between articular cartilage and subchondral bone. These genes showed an enrichment in processes related to the extracellular matrix, characterized by up-regulation of *WNT16* and *OGN*, and of the proteinaceous extracellular matrix, characterized by up-regulation of *POSTN* and *ASPN*. Notably, *TNFRSF11B,* a gene involved in bone remodelling, was shown to be consistently and highly upregulated in OA cartilage while it was not differentially expressed in OA bone.

Table 1. Highest upregulated genes in OA cartilage in the RAAK study obtained from RNA sequencing of preserved against lesioned cartilage in 35 OA patients (58).

Gene	Name	Protein function	Effect in OA cartilage
IL11	**Interleukin 11**	**Cytokine stimulator of hematopoietic T cells**	**UP**
P3H2	Prolyl 3-Hydroxylase 2	Enzyme necessary for collagen chain assembly and stability	UP
ISM2	Isthmin 2	Type 1 thrombospondin domain, present in extracellular matrix proteins.	UP
CISH	Cytokine Inducible SH2 Containing Protein	Inhibitor of cytokine signaling	DN
CXCL14	C-X-C Motif Chemokine Ligand 14	Cytokine involved in immunoregulatory and inflammatory processes	UP
CD55	CD55 Molecule (Cromer Blood Group)	Glycoprotein involved in the regulation of the complement cascade	UP
NGF	Nerve Growth Factor	Protein involved in regulation and growth of sympathetic and sensory nervous systems	UP
WNT16	**Wingless-Type MMTV Integration Site Family, Member 16**	**Signaling protein involved in cell fate, developmental processes and patterning in embryogenesis**	**UP**
RIPK4	Receptor Interacting Serine/Threonine Kinase 4	Serine/ threonine protein kinase	UP
LRRC1	Leucine Rich Repeat Containing 1	Gene associated with epilepsy	UP
LAMB3	Laminin Subunit Beta 3	Laminin that belongs to basement membrane proteins	UP
R3HDML	R3H Domain Containing Like	Peptidase inhibitor	UP
PTGES	Prostaglandin E Synthase	Glutathione-dependent prostaglandin E synthase involved in collagen-induced arthritis	UP
TNFRSF11B	TNF Receptor Superfamily Member 11b	Osteoblast-secreted decoy receptor and negative regulator of bone resorption	UP
RELN	Reelin	ECM matrix protein involved in cell-cell interaction in brain development	DN
NPR3	Natriuretic Peptide Receptor 3	Peptide receptors involved in endocytosis of natriuretic peptides	UP
ERFE	Erythroferrone	Protein involved in lipid uptake in adipocytes and hepatocytes	UP
RCAN2	Regulator Of Calcineurin 2	Protein involved in endothelial cell function and angiogenesis	DN
PPP1R14C	**Protein Phosphatase 1 Regulatory Inhibitor Subunit 14C**	**Phosphatase involved in neuronal activity, metabolism, cell division and muscle contraction**	**UP**
SERPINE2	Serpin Family E Member 2	Serine protease inhibitor	UP

Table 2. Highest upregulated genes in OA subchondral bone in the RAAK study obtained from RNA sequencing of preserved against lesioned cartilage in 26 OA patients (65).

Gene	Name	Function	Effect in OA bone
WNT16	**Wingless-Type MMTV Integration Site Family, Member 16**	**Signaling protein involved in cell fate, developmental processes and patterning in embryogenesis**	**UP**
IL11	**Interleukin 11**	**Cytokine stimulator of hematopoietic T cells**	**UP**
GDF6	Growth Differentiation Factor 6	Protein involved in bone formation and activation of SMAD signaling	UP
OGN	Osteoglycin	Regulator of Osteoblast differentiation and ectopic bone formation	UP
ASPN	Asporin	Chondrogenesis regulator and inducer of collagen mineralization	UP
MYO3A	Myosin IIIA	Protein involved in hearing	UP
CRLF1	Cytokine Receptor Like Factor 1	Involved in survival of neuronal cells	UP
GPR158	G Protein-Coupled Receptor 158	Protein highly expressed in the brain	UP
PPP1R14C	**Protein Phosphatase 1 Regulatory Inhibitor Subunit 14C**	**Phosphatase involved in neuronal activity, metabolism, cell division and muscle contraction**	**UP**
MT1G	Metallothionein 1G	Protein related to metal ion transporter pathways	UP
ALX4	ALX Homeobox 4	Transcription factor expressed in the mesenchyme of developing bones limbs, hair, teeth and mammary tissue	UP
P4HA3	Prolyl 4-Hydroxylase Subunit Alpha 3	Component of an enzyme involved in collagen synthesis	UP
FAP	Fibroblast Activation Protein Alpha	Protein involved in fibroblast growth and epithelial mesenchyme interactions	UP
POSTN	Periostin	Protein involved in tissue development being essential for skeletal, dental and cardiac development	UP
HIF3A	Hypoxia Inducible Factor 3 Subunit Alpha	Protein involved in hypoxia	DN
GPC5	Glypican 5	Protein involved in control of cell division and growth regulation	DN
FGF14	Fibroblast Growth Factor 14	Protein involved in embryonic development, cell growth and tissue repair.	DN
KIF1A	Kinesin Family Member 1A	Transporter of organelles along axonal microtubules	DN
SPOCK3	SPARC (Osteonectin), Cwcv And Kazal Like Domains Proteoglycan 3	Calcium-binding protein involved in MMPs inhibition	DN
CHRDL2	Chordin Like 2	Protein expressed in osteoblasts and OA cartilage	DN

GENETIC STUDY DESIGN FOR IDENTIFICATION OF CAUSALITY UNDERLYING DEVELOPMENT OA

The strong genetic component of OA was traditionally identified by studying segregation of OA affected members in families, twin studies, and by exploring early onset families with a Mendelian inheritance pattern of OA (associated) phenotypes (66). Hence, identification of genes that explain the heritable component of OA is a powerful tool to highlight underlying disease pathways.

Genome-wide association studies

Genome-wide association studies (GWAS) are performed to identify single nucleotide polymorphisms (SNPs) that confer risk to common age related OA, as it occurs in the population. **Table 3** shows a selection of genetic variants and their positional genes that have been robustly identified in large comprehensive genome wide association studies in OA up to date (67-71). The functions of these genes confirm that deviations in both cartilage and bone maintenance processes, are major pathways underlying OA pathology in humans. Moreover, follow-up studies have shown that risk SNPs frequently modulate pathology due to altering transcription of the genes in *cis* both in bone and cartilage (72-74). A notable recent example is Matrix Gla Protein (MGP) that regulates extracellular calcium levels via high affinity to its γ-carboxyglutamic acid (Gla) residues. As the OA risk allele (rs1800801; **Table 3**) has been associated with a reduced *MGP* gene expression (75) and with increased vascular calcification (76), this would suggest increased cartilage calcification in carriers of the OA risk allele. Another example was found in the deiodinase iodothyronine type II (D2) gene (*DIO2*). D2 is an enzyme that converts intracellular thyroxine (T4) into triiodothyronine (T3) in specific tissues such growth plate cartilage. Herein, T3 initiates terminal maturation of hypertrophic chondrocytes leading to breakdown and mineralization of cartilage to allow transition to bone (77). In bone, *DIO2* is essential for bone formation and mineralization.

Linkage analysis

Linkage analyses is a powerful tool to identify high impact causal mutations in extended families with an early onset disease phenotype, preferably inherited in a Mendelian inheritance pattern. The value of such familial high impact variants is that identified gene functions and underlying pathways can have shared etiology, hence giving insight into common OA phenotypes (78-81). By applying next generation sequencing of whole genomes or exomes of well selected (definitively affected) family members, genetic variants can be assessed. Subsequently, likely damaging high impact mutations can be prioritized based on for example the amino acid change or location of the mutation (82). Herein,

synonymous variants, tolerated missense variants, intergenic variants and intron variants would likely result in a less strong disease phenotype. On the other hand, variants producing a stop codon or a missense mutation can result in a truncation of the translated protein. To determine the likely effect of a mutation, tools such as Sorts Intolerant From Tolerant (SIFT) and/or polymorphism phenotyping version 2 (PolyPhen) can predict their damaging or neutral effect (83) by using physical and comparative evolutionary considerations.

Table 4 highlights compelling high impact mutations identified in early onset families with OA related phenotypes. Notably, high impact mutations causal to the early onset OA phenotypes are found in relevant extracellular matrix genes such as *COL11A1*, *COL11A2*, *COL2A1* as well as genes functioning in chondrogenic differentiation such as *GDF5* and *SMAD3* (84-87). A compelling example and subject of this thesis, was the identification of a readthrough mutation (c1205A=T; p.Stop402Leu) in *TNFRSF11B* encoding osteoprotegerin (OPG) localized at the chondrocalcinosis locus 1 (CCAL1) (88) in multiple families worldwide (89-91). In these families, the CCAL1 phenotype is defined by early onset OA with characteristic articular cartilage calcification i.e. chondrocalcinosis (92) and low subchondral bone mineralization (91). Being a readthrough mutation resulting in 19 additional amino acids at the C-terminal end of the protein, the mutation was named OPG-XL.

Table 3. Single nucleotide polymorphisms consistently identified in association with OA.

Gene	Single nucleotide polymorphism	Risk allele	Effect	Function	Reference
DIO2	rs225014	C	Catalyzer of thyroid hormone activation	UP	(93)
MGP	rs1800801	T	Regulator of cartilage mineralization	DN	(72)
IL11	rs4252548	T	Cytokine stimulator of hematopoietic T cells	DN	(94)
GDF5	rs143383	T	Regulator of cell growth and differentiation	DN	(95)
SMAD3	rs12901499	G	Signal transducer and transcriptional modulator	UP	(96)
ASPN	Triplet repeat of the codon for aspartic acid	-	Cartilage extracellular protein involved in chondrogenesis and mineralization	UP	(97)

Table 4. High impact mutations in early onset OA families.

Gene	Name	Protein function	Mutation	Reference
COL2A1	Collagen type II α1	Major structural component in cartilage	p.Arg275Cys	(98)
			p.Gly204Ala	(86)
			p.Arg719Cys	(99)
COL11A1	Collagen type XI α1	Minor fibrillar collagen in cartilage, alpha chain 1	p.Pro446Gln	
COL11A2	Collagen type XI α2	Minor fibrillar collagen in cartilage, alpha chain 2	p.Arg53Trp	(100)
COMP	Cartilage oligomeric matrix protein	Extracellular matrix protein present in cartilage	p.Arg718Trp	(85)
TNFRSF11B	Tumor necrosis factor receptor superfamily member 11b	Extracellular regulator of osteoclastogenesis	p.Ter402Leu	(88)
GDF5	Growth differentiation factor 5	TGF-beta family member protein involved in skeletal development	p.Leu441Pro	
			p.Arg438Leu	(101)
SMAD3	Mothers against decapentaplegic homolog 3	Protein involved in TGF-beta signaling and skeletal development	p.Arg287Trp	
			p.Thr261I1e	
			p.Thr247fsX61	(102)

OSTEOPROTEGERIN; ROLE IN CARTILAGE AND BONE PHYSIOLOGY

OPG is a decoy receptor which competes for binding of nuclear factor KB ligand (RANKL) to the receptor activator of the nuclear KB factor (RANK). Together, this triad is well known for regulating osteoclastogenesis (103), hence playing a critical role in bone homeostasis, endochondral ossification, and bone remodelling (5, 6) **(Figure 4)**. More recently, by using a heparan sulphate (HS)-binding deficient mutant OPG mouse model, it was found that OPG not only binds to free RANKL but also to RANKL as a membrane-bound form on osteoblasts through interaction of its C-terminus with heparan sulphate. This binding appears indispensable for RANKL mediated inhibition of osteoclastogenesis due to immobilization of secreted OPG on the osteoblast membrane and formation of a stable HS-OPG-RANKL complex (104-106). Mice with aberrations in this triad, generated several skeletal diseases ranging from spontaneous fractures and osteoporosis to osteopetrosis (103, 107). For instance, infant mice treated with OPG for 12 weeks, developed a denser bone phenotype, while OPG knock-out mice showed a decrease in BMD and high incidence of bone fractures (108). Moreover, it was shown that RANKL stimulates osteoclast fission to produce transcriptionally distinct osteomorphs, which in turn, recycle towards large multinucleated osteoclasts or polykaryons by fusion, under tight control of OPG (109, 110).

Despite the large body of literature on the OPG-RANK-RANKL triad in bone homeostasis, the role of OPG in cartilage remains elusive. Nonetheless, a specific role of *TNFRSF11B* and its ligand *TNFSF11* encoding RANKL in cartilage (patho)physiology has been highlighted by transcriptome wide studies. Herein, *TNFRSF11B* and *TNFSF11* but not *TNFRSF11A* encoding RANK show high expression and are robustly responsive to OA cartilage pathophysiology, as marked by consistent high upregulation in human OA affected relative to preserved (57, 58) or healthy (111) cartilage. In contrast, differential expression of *TNFRSF11B* or *TNSF11* in subchondral bone underlying preserved and lesioned areas of OA cartilage was not observed (65). Other than that, with *TNFSF11* being a robust OA risk gene identified in the largest genome wide association study to date (112) aberrant function of OPG/RANKL clearly indicates its relevance in common OA pathology.

Next to the indicated separate roles of OPG in bone and cartilage, accumulating evidence suggests that OPG may also play a role in the dynamic interaction between articular cartilage and (subchondral) bone metabolism. The direction of changes of subchondral bone density and mineralization in osteoarthritis patients, however, remains unclear and possibly dependent on the subtype. This controversy is exemplified by a study of osteoarthritis patients that were shown to benefit from treatment with strontium ranelate, which is a drug licensed for osteoporosis and acts by increasing bone formation while decreasing bone resorption via stimulation of OPG (113). In absence of an effective OA therapy, these studies have gained a lot of attention but also elicited debate, since they contradict to epidemiological studies indicating that individuals with high systemic bone mass are at increased risk for the incidence of osteoarthritis. Additional studies, subsequently confirmed that indeed strontium ranelate administration resulted in an increase in cartilage deposition and a decrease in MMP release, with upregulation of osteoblast formation and reduced subchondral bone remodelling (114, 115) . On the other hand, in an OA guinea pig model, Chu et al (116) showed that upon strontium ranelate administration there was an increase in osteophyte size, which is a known characteristic of OA development. Taken together, these findings would suggest the involvement of OPG in other biological processes related to cartilage formation, independent from its known function in bone homeostasis (117, 118).

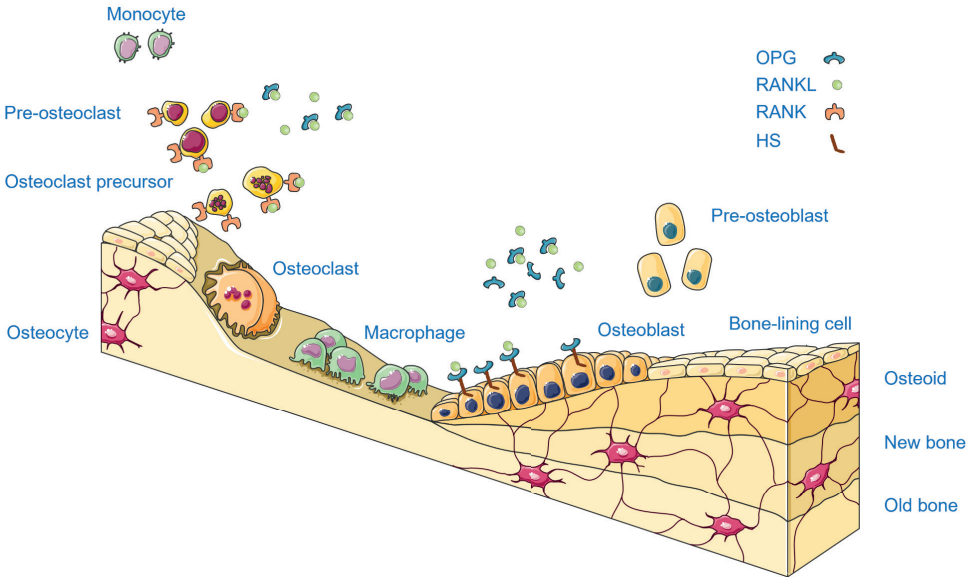

Figure 4. Role of Osteoprotegerin in bone resorption. OPG is a soluble decoy receptor that inhibits differentiation of osteoclast precursors by competing for its binding of RANKL to RANK. This results in less osteoclasts available and inhibition of bone resorption.

HUMAN DISEASE MODELS IN OA

To allow translation of identified strong OA risk genes towards underlying biological mechanisms, studies on target discovery, and drug testing; a human model system that incorporates disease relevant tissue units is necessary. Moreover, such models require the possibility to perturb the system with essential genetic and/or environmental cues to trigger OA-like changes. For instance, to study underlying biological mechanisms of OA risk genes, it is important to be able to change the expression levels of these genes and/or apply genetic engineering tools to introduce high impact OA mutations (119). Some of the current OA models that allow these perturbations will be described in the following paragraphs.

In vitro models

A two dimensional (2D) *in vitro* model allows culture of either primary cartilage or bone cells or immortalized cell lines on flat surfaces, hence representing a simplified osteochondral system. It allows high throughput screening, for instance, upon lentiviral induction or inhibition of a specific gene, or upon exposure to therapeutic compounds. Nevertheless, the lack of nutrient and oxygen gradients, fast chondrocyte dedifferentiation, or the lack of extracellular matrix production,

arise as important challenges for accurately reproducing OA. Three-dimensional (3D) *in vitro* models optionally employed with a variety of different cells such as human primary articular chondrocytes (hPACs), osteoblasts and mesenchymal stromal cells (MSCs) can better address these issues (120, 121). Yet, hPACs, osteoblasts and MSCs can only be obtained after invasive procedures, while there is a large heterogeneity in chondrogenic capacity between donors (122-124). Moreover, primary cells have a tendency to rapidly become senescent during *in vitro* expansion (124-126). Nonetheless, 3D in vitro models have highlighted relevant functions of some proteins. For instance, cartilage oligomeric matrix protein (COMP) overexpression in bovine chondrocytes resulted in a collagen formation with a smaller diameter (127). Another example can be found upon overexpressing DIO2 in human chondrocytes (128), resulting in a lower ECM deposition and a higher catabolic and mineralization response.

Ex vivo models

Ex vivo models culturing human osteochondral explants can also be used to study OA. This human model offers a reliable method to study the interaction between different cell types and the interplay between aged cartilage and bone (129). Moreover, osteochondral explants can be used to investigate joint mechanobiology. For instance Houtman et al showed a catabolic response in chondrocyte signaling upon loading human explants (130). Unfortunately in these models, specific medium requirements for each cell type are necessary to maintain the cell inherent phenotype over a longer time period, while genetic engineering strategies cannot be applied (120).

In vivo models

In vivo models of small animals, especially mice and rats, are frequently used to study OA. For this aim, surgically and chemically induced models can trigger OA development by disturbing joint biomechanics and/or by administering compounds such as collagenase, which is detrimental to joint health. Additionally, genetic manipulation such as a knock-in or knock-out experiments can be applied to prove gene causality in an *in vivo* complex system. For instance, Bomer et al showed the relevance of *DIO2* in a knock-out mouse model. Data of the study showed that DIO2 knock out mice relative to wild type littermates were protected against cartilage damage upon force running (131). In another study by Wu et al, OPG transgenic mice were generated and showed an increase BMD and trabecular tibia number and thickness when compared to wild type mice (132). Nevertheless, differences in joint structure and loading regimes, with an absence of spontaneous OA in some animal models, fail to represent to gradual development of OA in humans with aging. Moreover, animal research must progressively integrate the principle of 3Rs: replacement, reduction and

refinement, only performing research in animal models when strictly necessary.

Induced pluripotent stem cells

In 2006, Yamanaka generated embryonic stem cell-like cells by introducing four reprogramming factors (Oct-4, Sox-2, Klf4 and c-Myc) into fibroblast mouse cells and termed these cells as induced pluripotent stem cells (iPSCs). These cells were able to differentiate into the three germ layers while maintaining the genetic background of the donor. As a result, iPSC technology was later applied to human cells and became a method not only for disease modeling, follow up of genetic studies or regenerative medicine, but also for high-throughput drug screening and personalized medicine (133, 134). Additionally, iPS-cell production can be scaled, while the use of such immortal-like cells avoids the need for biopsies and repeated surgeries on patients. Moreover, iPSC technology easily allows to study the causative effect of point mutations (135) by performing genome editing tools such as Clustered Regularly Interspaced Short Palindromic Repeats (CRISPR) (136). In this system, a RNA guided endonuclease induces double stranded breaks in the genome after recognition of a protospacer adjacent motive (PAM). When this technology is combined with a repaired or mutation template, an iPSC isogenic control or point-mutation line can be generated, making this system ideal for studying specific mutations (137). Nevertheless, issues can arise due to the strong variation in differentiation efficiencies between iPSC lines and clones (138, 139) and a tendency to generate fibrous cartilage matrix (124, 140). Hence, even though several protocols are available, the optimal method for generation of chondrocytes and osteoblasts from iPSCs remains to be established. Some studies comparing human bone marrow-derived mesenchymal stromal cells (BMSCs) and iPSC-derived mesenchymal stromal cells (iMSCs) suggest major functional and genetic differences, not only between cells but also between neo-cartilage and neo-bone derived from both cell types (141, 142). However, in these studies, iMSCs were generated via the formation of cell aggregates called embryoid bodies (EBs), often variable and with low efficiency (141, 142), while direct monolayer generation was shown to be more robust (143).

Alternatively, a stepwise approach can be taken to generate neo-cartilage from hiPSCs via chondroprogenitor cells (iCPCs) (144-146). Notably, differentiation of iPSCs with this protocol mimics each developmental step through anterior primitive streak formation and successive emergence of iCPCs, diminishing variability between independent differentiations. Unfortunately, a major disadvantage of this method is the inability to generate bone and its inefficiency to expand hiCPCs, due to the rapid loss of their chondrogenic potential (145). Therefore, heterogeneity in the resulting cell population, urges for efficient and cell expandable step-wise differentiation approaches where a better study of fundamental biological processes is required (147, 148). Only when these signals

and complex interactions are better understood they can be used as accurate follow up models.

AIMS AND CONTENTS OF THIS THESIS

The role of OPG, encoded by *TNFRSF11B*, in bone development is commonly known, however its function in cartilage remains elusive. Its high expression in OA lesioned cartilage and identification of a readthrough mutation in a family with early onset OA suggest a crucial role for OPG in the homeostasis of this tissue.

To address the role of OPG in cartilage, in **Chapter 2** we will overexpress *TNFRSF11B* in preserved chondrocytes with a lentiviral construct to determine its likely function as a trigger of OA. Additionally, gene expression levels of a unique RNA sequencing dataset of preserved against lesioned cartilage will be correlated to *TNFRSF11B* and used as a readout to determine downstream effects of this process.

Once the function of *TNFRSF11B* is determined in cartilage, we will investigate the effects of its readthrough mutation in the early onset OA family. Nevertheless obtaining cartilage and bone tissue from them is dependent on joint replacement surgeries of the few family members that carry the mutation. Remarkably, iPSC technology can be used to generate neo-cartilage and neo-osseous tissue that later can be researched in an *in vitro* model. With this aim in mind, in **Chapter 3** we will establish the optimal method for iPSC derived neo-cartilage generation while comparing two differentiation protocols with cartilage deposited by primary cells. Once the optimal method for neo-cartilage and neo-bone is achieved, an iPSC line from an early onset family member carrier of a mutation in *TNFRSF11B* at the CCAL1 locus will be generated in **Chapter 4**. The mutation will be rescued by applying CRISPR/Cas9. Subsequently, taking the established optimal approach for *in vitro* iPSC-derived OA modelling determined in **Chapter 3**, neo-cartilage and neo-bone will be generated from both lines. By doing so, we will get substantial understanding of the molecular background underlying their phenotypes. Finally, monocyte-derived osteoclasts of OPG-XL carriers will be generated and their osteoclast activity researched. In parallel with the *in vitro* experiments, family members with and without the mutation will take part on different tests to evaluate their joints status, BMD and OA stage. With this thesis we expect to determine the role of OPG in cartilage and discover the functional effects of the readthrough mutation, which will ultimately help to address the role of OPG in OA development.

REFERENCES

1. Hunter DJ, Bierma-Zeinstra S. Osteoarthritis. Lancet. 2019;393(10182):1745-59.
2. Fernandez-Moreno M, Rego I, Carreira-Garcia V, Blanco FJ. Genetics in osteoarthritis. Curr Genomics. 2008;9(8):542-7.
3. Hootman JM, Helmick CG. Projections of US prevalence of arthritis and associated activity limitations. Arthritis Rheum. 2006;54(1):226-9.
4. Chen D, Shen J, Zhao W, Wang T, Han L, Hamilton JL, et al. Osteoarthritis: toward a comprehensive understanding of pathological mechanism. Bone Res. 2017;5:16044.
5. Cucchiarini M, de Girolamo L, Filardo G, Oliveira JM, Orth P, Pape D, et al. Basic science of osteoarthritis. J Exp Orthop. 2016;3(1):22.
6. Swain S, Sarmanova A, Coupland C, Doherty M, Zhang W. Comorbidities in Osteoarthritis: A Systematic Review and Meta-Analysis of Observational Studies. Arthritis Care Res (Hoboken). 2020;72(7):991-1000.
7. Hunter DJ, Schofield D, Callander E. The individual and socioeconomic impact of osteoarthritis. Nat Rev Rheumatol. 2014;10(7):437-41.
8. Wylde V, Hewlett S, Learmonth ID, Dieppe P. Persistent pain after joint replacement: prevalence, sensory qualities, and postoperative determinants. Pain. 2011;152(3):566-72.
9. Litwic A, Edwards MH, Dennison EM, Cooper C. Epidemiology and burden of osteoarthritis. Br Med Bull. 2013;105:185-99.
10. Chen A, Gupte C, Akhtar K, Smith P, Cobb J. The Global Economic Cost of Osteoarthritis: How the UK Compares. Arthritis. 2012;2012:698709.
11. Pope JE, McCrea K, Stevens A, Ouimet JM. The relationship between NSAID use and osteoarthritis (OA) severity in patients with hip and knee OA: results of a case control study of NSAID use comparing those requiring hip and knee replacements to those in whom surgery was not recommended. Med Sci Monit. 2008;14(12):CR604-10.
12. Mobasheri A, Batt M. An update on the pathophysiology of osteoarthritis. Ann Phys Rehabil Med. 2016;59(5-6):333-9.
13. KELLGREN JH, LAWRENCE JS. Radiological assessment of osteo-arthrosis. Ann Rheum Dis. 1957;16(4):494-502.
14. Guermazi A, Roemer FW, Burstein D, Hayashi D. Why radiography should no longer be considered a surrogate outcome measure for longitudinal assessment of cartilage in knee osteoarthritis. Arthritis Res Ther. 2011;13(6):247.
15. Roemer FW, Demehri S, Omoumi P, Link TM, Kijowski R, Saarakkala S, et al. State of the Art: Imaging of Osteoarthritis-Revisited 2020. Radiology. 2020;296(1):5-21.
16. Hunter DJ, Guermazi A, Lo GH, Grainger AJ, Conaghan PG, Boudreau RM, et al. Evolution of semi-quantitative whole joint assessment of knee OA: MOAKS (MRI Osteoarthritis Knee Score). Osteoarthritis Cartilage. 2011;19(8):990-1002.
17. Roemer FW, Hunter DJ, Winterstein A, Li L, Kim YJ, Cibere J, et al. Hip Osteoarthritis MRI Scoring System (HOAMS): reliability and associations with radiographic and clinical findings. Osteoarthritis Cartilage. 2011;19(8):946-62.
18. Wieland HA, Michaelis M, Kirschbaum BJ, Rudolphi KA. Osteoarthritis - an untreatable disease? Nat Rev Drug Discov. 2005;4(4):331-44.
19. Qin X, Jiang Q, Nagano K, Moriishi T, Miyazaki T, Komori H, et al. Runx2 is essential for the transdifferentiation of chondrocytes into osteoblasts. PLoS Genet. 2020;16(11):e1009169.
20. Aghajanian P, Mohan S. The art of building bone: emerging role of chondrocyte-to-osteoblast transdifferentiation in endochondral ossification. Bone Res. 2018;6:19.
21. Yang L, Tsang KY, Tang HC, Chan D, Cheah KS. Hypertrophic chondrocytes can become osteoblasts and osteocytes in endochondral bone formation. Proc Natl Acad Sci U S A. 2014;111(33):12097-102.

22. Ripmeester EGJ, Timur UT, Caron MMJ, Welting TJM. Recent Insights into the Contribution of the Changing Hypertrophic Chondrocyte Phenotype in the Development and Progression of Osteoarthritis. Front Bioeng Biotechnol. 2018;6:18.
23. Egawa S, Miura S, Yokoyama H, Endo T, Tamura K. Growth and differentiation of a long bone in limb development, repair and regeneration. Dev Growth Differ. 2014;56(5):410-24.
24. Bhosale AM, Richardson JB. Articular cartilage: structure, injuries and review of management. Br Med Bull. 2008;87:77-95.
25. Lapadula G, Iannone F. Metabolic activity of chondrocytes in human osteoarthritis as a result of cell-extracellular matrix interactions. Semin Arthritis Rheum. 2005;34(6 Suppl 2):9-12.
26. Dreier R. Hypertrophic differentiation of chondrocytes in osteoarthritis: the developmental aspect of degenerative joint disorders. Arthritis Res Ther. 2010;12(5):216.
27. Lian C, Wang X, Qiu X, Wu Z, Gao B, Liu L, et al. Collagen type II suppresses articular chondrocyte hypertrophy and osteoarthritis progression by promoting integrin beta1-SMAD1 interaction. Bone Res. 2019;7:8.
28. Purcell P, Trainor PA. The Mighty Chondrocyte: No Bones about It. J Dent Res. 2015;94(12):1625-7.
29. Akkiraju H, Nohe A. Role of Chondrocytes in Cartilage Formation, Progression of Osteoarthritis and Cartilage Regeneration. J Dev Biol. 2015;3(4):177-92.
30. Goldring MB, Goldring SR. Articular cartilage and subchondral bone in the pathogenesis of osteoarthritis. Ann N Y Acad Sci. 2010;1192:230-7.
31. Lewis PB, McCarty LP, 3rd, Kang RW, Cole BJ. Basic science and treatment options for articular cartilage injuries. J Orthop Sports Phys Ther. 2006;36(10):717-27.
32. Singh P, Marcu KB, Goldring MB, Otero M. Phenotypic instability of chondrocytes in osteoarthritis: on a path to hypertrophy. Ann N Y Acad Sci. 2019;1442(1):17-34.
33. Carballo CB, Nakagawa Y, Sekiya I, Rodeo SA. Basic Science of Articular Cartilage. Clin Sports Med. 2017;36(3):413-25.
34. Grogan SP, Chen X, Sovani S, Taniguchi N, Colwell CW, Jr., Lotz MK, et al. Influence of cartilage extracellular matrix molecules on cell phenotype and neocartilage formation. Tissue Eng Part A. 2014;20(1-2):264-74.
35. Reznikov N, Chase H, Brumfeld V, Shahar R, Weiner S. The 3D structure of the collagen fibril network in human trabecular bone: relation to trabecular organization. Bone. 2015;71:189-95.
36. Sepriano A, Roman-Blas JA, Little RD, Pimentel-Santos F, Arribas JM, Largo R, et al. DXA in the assessment of subchondral bone mineral density in knee osteoarthritis--A semi-standardized protocol after systematic review. Semin Arthritis Rheum. 2015;45(3):275-83.
37. Li G, Yin J, Gao J, Cheng TS, Pavlos NJ, Zhang C, et al. Subchondral bone in osteoarthritis: insight into risk factors and microstructural changes. Arthritis Res Ther. 2013;15(6):223.
38. Findlay DM, Kuliwaba JS. Bone-cartilage crosstalk: a conversation for understanding osteoarthritis. Bone Res. 2016;4:16028.
39. Oftadeh R, Perez-Viloria M, Villa-Camacho JC, Vaziri A, Nazarian A. Biomechanics and mechanobiology of trabecular bone: a review. J Biomech Eng. 2015;137(1).
40. Neogi T. Clinical significance of bone changes in osteoarthritis. Ther Adv Musculoskelet Dis. 2012;4(4):259-67.
41. Langdahl B, Ferrari S, Dempster DW. Bone modeling and remodeling: potential as therapeutic targets for the treatment of osteoporosis. Ther Adv Musculoskelet Dis. 2016;8(6):225-35.
42. Roseti L, Desando G, Cavallo C, Petretta M, Grigolo B. Articular Cartilage Regeneration in Osteoarthritis. Cells. 2019;8(11).
43. Mackie EJ, Ahmed YA, Tatarczuch L, Chen KS, Mirams M. Endochondral ossification: how cartilage is converted into bone in the developing skeleton. Int J Biochem Cell Biol. 2008;40(1):46-62.
44. Mehana EE, Khafaga AF, El-Blehi SS. The role of matrix metalloproteinases in osteoarthritis pathogenesis: An updated review. Life Sci. 2019;234:116786.

45. Rose BJ, Kooyman DL. A Tale of Two Joints: The Role of Matrix Metalloproteases in Cartilage Biology. Dis Markers. 2016;2016:4895050.
46. He Y, Manon-Jensen T, Arendt-Nielsen L, Petersen KK, Christiansen T, Samuels J, et al. Potential diagnostic value of a type X collagen neo-epitope biomarker for knee osteoarthritis. Osteoarthritis Cartilage. 2019;27(4):611-20.
47. Pritzker KP, Gay S, Jimenez SA, Ostergaard K, Pelletier JP, Revell PA, et al. Osteoarthritis cartilage histopathology: grading and staging. Osteoarthritis Cartilage. 2006;14(1):13-29.
48. van der Kraan PM, van den Berg WB. Chondrocyte hypertrophy and osteoarthritis: role in initiation and progression of cartilage degeneration? Osteoarthritis Cartilage. 2012;20(3):223-32.
49. Xiao ZF, Su GY, Hou Y, Chen SD, Lin DK. Cartilage degradation in osteoarthritis: A process of osteochondral remodeling resembles the endochondral ossification in growth plate? Med Hypotheses. 2018;121:183-7.
50. Hosaka Y, Saito T, Sugita S, Hikata T, Kobayashi H, Fukai A, et al. Notch signaling in chondrocytes modulates endochondral ossification and osteoarthritis development. Proc Natl Acad Sci U S A. 2013;110(5):1875-80.
51. Pauli C, Whiteside R, Heras FL, Nesic D, Koziol J, Grogan SP, et al. Comparison of cartilage histopathology assessment systems on human knee joints at all stages of osteoarthritis development. Osteoarthritis Cartilage. 2012;20(6):476-85.
52. Hurwitz DE, Sumner DR, Block JA. Bone density, dynamic joint loading and joint degeneration. A review. Cells Tissues Organs. 2001;169(3):201-9.
53. Guilak F. Biomechanical factors in osteoarthritis. Best Pract Res Clin Rheumatol. 2011;25(6):815-23.
54. Aho OM, Finnila M, Thevenot J, Saarakkala S, Lehenkari P. Subchondral bone histology and grading in osteoarthritis. PLoS One. 2017;12(3):e0173726.
55. Castaneda S, Roman-Blas JA, Largo R, Herrero-Beaumont G. Subchondral bone as a key target for osteoarthritis treatment. Biochem Pharmacol. 2012;83(3):315-23.
56. Cox LG, van Rietbergen B, van Donkelaar CC, Ito K. Bone structural changes in osteoarthritis as a result of mechanoregulated bone adaptation: a modeling approach. Osteoarthritis Cartilage. 2011;19(6):676-82.
57. Ramos YF, den Hollander W, Bovee JV, Bomer N, van der Breggen R, Lakenberg N, et al. Genes involved in the osteoarthritis process identified through genome wide expression analysis in articular cartilage; the RAAK study. PLoS One. 2014;9(7):e103056.
58. Coutinho de Almeida R, Ramos YFM, Mahfouz A, den Hollander W, Lakenberg N, Houtman E, et al. RNA sequencing data integration reveals an miRNA interactome of osteoarthritis cartilage. Ann Rheum Dis. 2019;78(2):270-7.
59. Chen H, Ghori-Javed FY, Rashid H, Adhami MD, Serra R, Gutierrez SE, et al. Runx2 regulates endochondral ossification through control of chondrocyte proliferation and differentiation. J Bone Miner Res. 2014;29(12):2653-65.
60. Catheline SE, Hoak D, Chang M, Ketz JP, Hilton MJ, Zuscik MJ, et al. Chondrocyte-Specific RUNX2 Overexpression Accelerates Post-traumatic Osteoarthritis Progression in Adult Mice. J Bone Miner Res. 2019;34(9):1676-89.
61. Wang M, Sampson ER, Jin H, Li J, Ke QH, Im HJ, et al. MMP13 is a critical target gene during the progression of osteoarthritis. Arthritis Res Ther. 2013;15(1):R5.
62. Fan X, Wu X, Crawford R, Xiao Y, Prasadam I. Macro, Micro, and Molecular. Changes of the Osteochondral Interface in Osteoarthritis Development. Front Cell Dev Biol. 2021;9:659654.
63. Saito T, Fukai A, Mabuchi A, Ikeda T, Yano F, Ohba S, et al. Transcriptional regulation of endochondral ossification by HIF-2alpha during skeletal growth and osteoarthritis development. Nat Med. 2010;16(6):678-86.
64. den Hollander W, Meulenbelt I. DNA Methylation in Osteoarthritis. Curr Genomics. 2015;16(6):419-26.

65. Tuerlings M, van Hoolwerff M, Houtman E, Suchiman E, Lakenberg N, Mei H, et al. RNA sequencing reveals interacting key determinants of osteoarthritis acting in subchondral bone and articular cartilage. Arthritis Rheumatol. 2020.
66. Spector TD, MacGregor AJ. Risk factors for osteoarthritis: genetics. Osteoarthritis Cartilage. 2004;12 Suppl A:S39-44.
67. Peffers MJ, Balaskas P, Smagul A. Osteoarthritis year in review 2017: genetics and epigenetics. Osteoarthritis Cartilage. 2018;26(3):304-11.
68. Styrkarsdottir U, Helgason H, Sigurdsson A, Norddahl GL, Agustsdottir AB, Reynard LN, et al. Whole-genome sequencing identifies rare genotypes in COMP and CHADL associated with high risk of hip osteoarthritis. Nat Genet. 2017;49(5):801-5.
69. Tachmazidou I, Hatzikotoulas K, Southam L, Esparza-Gordillo J, Haberland V, Zheng J, et al. Identification of new therapeutic targets for osteoarthritis through genome-wide analyses of UK Biobank data. Nat Genet. 2019;51(2):230-6.
70. Jia X, Zhang F, Bai J, Gao L, Zhang X, Sun H, et al. Combinational analysis of linkage and exome sequencing identifies the causative mutation in a Chinese family with congenital cataract. BMC Med Genet. 2013;14:107.
71. Boer CG, Hatzikotoulas K, Southam L, Stefansdottir L, Zhang Y, Coutinho de Almeida R, et al. Deciphering osteoarthritis genetics across 826,690 individuals from 9 populations. Cell. 2021;184(18):4784-818 e17.
72. Houtman E, Coutinho de Almeida R, Tuerlings M, Suchiman HED, Broekhuis D, Nelissen R, et al. Characterization of dynamic changes in Matrix Gla Protein (MGP) gene expression as function of genetic risk alleles, osteoarthritis relevant stimuli, and the vitamin K inhibitor warfarin. Osteoarthritis Cartilage. 2021.
73. Bos SD, Bovee JV, Duijnisveld BJ, Raine EV, van Dalen WJ, Ramos YF, et al. Increased type II deiodinase protein in OA-affected cartilage and allelic imbalance of OA risk polymorphism rs225014 at DIO2 in human OA joint tissues. Ann Rheum Dis. 2012;71(7):1254-8.
74. Loughlin J. Genetic contribution to osteoarthritis development: current state of evidence. Curr Opin Rheumatol. 2015;27(3):284-8.
75. Tunon-Le Poultel D, Cannata-Andia JB, Roman-Garcia P, Diaz-Lopez JB, Coto E, Gomez C, et al. Association of matrix Gla protein gene functional polymorphisms with loss of bone mineral density and progression of aortic calcification. Osteoporos Int. 2014;25(4):1237-46.
76. Sheng K, Zhang P, Lin W, Cheng J, Li J, Chen J. Association of Matrix Gla protein gene (rs1800801, rs1800802, rs4236) polymorphism with vascular calcification and atherosclerotic disease: a meta-analysis. Sci Rep. 2017;7(1):8713.
77. Gereben B, Zavacki AM, Ribich S, Kim BW, Huang SA, Simonides WS, et al. Cellular and molecular basis of deiodinase-regulated thyroid hormone signaling. Endocr Rev. 2008;29(7):898-938.
78. Wu L, Schaid DJ, Sicotte H, Wieben ED, Li H, Petersen GM. Case-only exome sequencing and complex disease susceptibility gene discovery: study design considerations. J Med Genet. 2015;52(1):10-6.
79. Do R, Kathiresan S, Abecasis GR. Exome sequencing and complex disease: practical aspects of rare variant association studies. Hum Mol Genet. 2012;21(R1):R1-9.
80. Skarp S, Kamarainen OP, Wei GH, Jakkula E, Kiviranta I, Kroger H, et al. Whole exome sequencing in Finnish families identifies new candidate genes for osteoarthritis. PLoS One. 2018;13(8):e0203313.
81. Auer PL, Lettre G. Rare variant association studies: considerations, challenges and opportunities. Genome Med. 2015;7(1):16.
82. Suravajhala P, Benso A. Prioritizing single-nucleotide polymorphisms and variants associated with clinical mastitis. Adv Appl Bioinform Chem. 2017;10:57-64.
83. Eilbeck K, Quinlan A, Yandell M. Settling the score: variant prioritization and Mendelian disease. Nat Rev Genet. 2017;18(10):599-612.

84. Jackson GC, Marcus-Soekarman D, Stolte-Dijkstra I, Verrips A, Taylor JA, Briggs MD. Type IX collagen gene mutations can result in multiple epiphyseal dysplasia that is associated with osteochondritis dissecans and a mild myopathy. Am J Med Genet A. 2010;152A(4):863-9.
85. Mu SC, Lin YJ, Liu HC, Wu JY, Li SC, Michael Lee MT, et al. A mutation in cartilage oligomeric matrix protein (COMP) causes early-onset osteoarthritis in a large kindred study. Ann Hum Genet. 2011;75(5):575-83.
86. Kannu P, Bateman JF, Randle S, Cowie S, du Sart D, McGrath S, et al. Premature arthritis is a distinct type II collagen phenotype. Arthritis Rheum. 2010;62(5):1421-30.
87. Aury-Landas J, Marcelli C, Leclercq S, Boumediene K, Bauge C. Genetic Determinism of Primary Early-Onset Osteoarthritis. Trends Mol Med. 2016;22(1):38-52.
88. Ramos YF, Bos SD, van der Breggen R, Kloppenburg M, Ye K, Lameijer EW, et al. A gain of function mutation in *TNFRSF11B* encoding osteoprotegerin causes osteoarthritis with chondrocalcinosis. Ann Rheum Dis. 2015;74(9):1756-62.
89. Baldwin CT, Farrer LA, Adair R, Dharmavaram R, Jimenez S, Anderson L. Linkage of early-onset osteoarthritis and chondrocalcinosis to human chromosome 8q. Am J Hum Genet. 1995;56(3):692-7.
90. Mitton-Fitzgerald E, Gohr CM, Williams CJ, Ortiz A, Mbalaviele G, Rosenthal AK. Effects of the *TNFRSF11B* Mutation Associated With Calcium Pyrophosphate Deposition Disease in Osteoclastogenesis in a Murine Model. Arthritis & Rheumatology. 2021;73(8):1543-9.
91. Williams CJ, Qazi U, Bernstein M, Charniak A, Gohr C, Mitton-Fitzgerald E, et al. Mutations in osteoprotegerin account for the CCAL1 locus in calcium pyrophosphate deposition disease. Osteoarthritis Cartilage. 2018;26(6):797-806.
92. Meulenbelt I, Bijkerk C, Breedveld FC, Slagboom PE. Genetic linkage analysis of 14 candidate gene loci in a family with autosomal dominant osteoarthritis without dysplasia. J Med Genet. 1997;34(12):1024-7.
93. Meulenbelt I, Min JL, Bos S, Riyazi N, Houwing-Duistermaat JJ, van der Wijk HJ, et al. Identification of DIO2 as a new susceptibility locus for symptomatic osteoarthritis. Hum Mol Genet. 2008;17(12):1867-75.
94. Styrkarsdottir U, Lund SH, Thorleifsson G, Zink F, Stefansson OA, Sigurdsson JK, et al. Meta-analysis of Icelandic and UK data sets identifies missense variants in SMO, IL11, COL11A1 and 13 more new loci associated with osteoarthritis. Nat Genet. 2018;50(12):1681-7.
95. Chapman K, Takahashi A, Meulenbelt I, Watson C, Rodriguez-Lopez J, Egli R, et al. A meta-analysis of European and Asian cohorts reveals a global role of a functional SNP in the 5' UTR of GDF5 with osteoarthritis susceptibility. Hum Mol Genet. 2008;17(10):1497-504.
96. Valdes AM, Spector TD, Tamm A, Kisand K, Doherty SA, Dennison EM, et al. Genetic variation in the SMAD3 gene is associated with hip and knee osteoarthritis. Arthritis Rheum. 2010;62(8):2347-52.
97. Nakamura T, Shi D, Tzetis M, Rodriguez-Lopez J, Miyamoto Y, Tsezou A, et al. Meta-analysis of association between the ASPN D-repeat and osteoarthritis. Hum Mol Genet. 2007;16(14):1676-81.
98. Lankisch P, Honscheid A, Schaper J, Borkhardt A, Laws HJ. COL2A1 mutation as a cause of premature osteoarthritis in a 13-year-old child. Joint Bone Spine. 2014;81(1):83-5.
99. Ala-Kokko L, Baldwin CT, Moskowitz RW, Prockop DJ. Single base mutation in the type II procollagen gene (COL2A1) as a cause of primary osteoarthritis associated with a mild chondrodysplasia. Proc Natl Acad Sci U S A. 1990;87(17):6565-8.
100. Jakkula E, Melkoniemi M, Kiviranta I, Lohiniva J, Raina SS, Perala M, et al. The role of sequence variations within the genes encoding collagen II, IX and XI in non-syndromic, early-onset osteoarthritis. Osteoarthritis Cartilage. 2005;13(6):497-507.
101. Seemann P, Schwappacher R, Kjaer KW, Krakow D, Lehmann K, Dawson K, et al. Activating and deactivating mutations in the receptor interaction site of GDF5 cause symphalangism or brachydactyly type A2. J Clin Invest. 2005;115(9):2373-81.
102. van de Laar IM, Oldenburg RA, Pals G, Roos-Hesselink JW, de Graaf BM, Verhagen JM, et al.

Mutations in SMAD3 cause a syndromic form of aortic aneurysms and dissections with early-onset osteoarthritis. Nat Genet. 2011;43(2):121-6.

103. Feige U. Osteoprotegerin. Ann Rheum Dis. 2001;60 Suppl 3:iii81-4.
104. Li M, Yang S, Xu D. Heparan Sulfate Regulates the Structure and Function of Osteoprotegerin in Osteoclastogenesis. The Journal of biological chemistry. 2016;291(46):24160-71.
105. Li M, Xu D. Antiresorptive activity of osteoprotegerin requires an intact heparan sulfate-binding site. Proceedings of the National Academy of Sciences. 2020;117(29):17187-94.
106. Li M, Yang S, Xu D. Heparan Sulfate Regulates the Structure and Function of Osteoprotegerin in Osteoclastogenesis. J Biol Chem. 2016;291(46):24160-71.
107. Min H, Morony S, Sarosi I, Dunstan CR, Capparelli C, Scully S, et al. Osteoprotegerin reverses osteoporosis by inhibiting endosteal osteoclasts and prevents vascular calcification by blocking a process resembling osteoclastogenesis. J Exp Med. 2000;192(4):463-74.
108. Bargman R, Posham R, Boskey A, Carter E, DiCarlo E, Verdelis K, et al. High- and low-dose OPG-Fc cause osteopetrosis-like changes in infant mice. Pediatr Res. 2012;72(5):495-501.
109. McDonald MM, Khoo WH, Ng PY, Xiao Y, Zamerli J, Thatcher P, et al. Osteoclasts recycle via osteomorphs during RANKL-stimulated bone resorption. Cell. 2021;184(7):1940.
110. Bucay N, Sarosi I, Dunstan CR, Morony S, Tarpley J, Capparelli C, et al. osteoprotegerin-deficient mice develop early onset osteoporosis and arterial calcification. Genes Dev. 1998;12(9):1260-8.
111. Ijiri K, Zerbini LF, Peng H, Otu HH, Tsuchimochi K, Otero M, et al. Differential expression of GADD45beta in normal and osteoarthritic cartilage: potential role in homeostasis of articular chondrocytes. Arthritis Rheum. 2008;58(7):2075-87.
112. Boer CG, Hatzikotoulas K, Southam L, Stefánsdóttir L, Zhang Y, Coutinho de Almeida R, et al. Deciphering osteoarthritis genetics across 826,690 individuals from 9 populations. Cell. 2021;184(18):4784-818.e17.
113. Saidak Z, Marie PJ. Strontium signaling: molecular mechanisms and therapeutic implications in osteoporosis. Pharmacol Ther. 2012;136(2):216-26.
114. Rodrigues TA, Freire AO, Bonfim BF, Cartagenes MSS, Garcia JBS. Strontium ranelate as a possible disease-modifying osteoarthritis drug: a systematic review. Braz J Med Biol Res. 2018;51(8):e7440.
115. Reginster JY, Beaudart C, Neuprez A, Bruyere O. Strontium ranelate in the treatment of knee osteoarthritis: new insights and emerging clinical evidence. Ther Adv Musculoskelet Dis. 2013;5(5):268-76.
116. Chu JG, Dai MW, Wang Y, Tian FM, Song HP, Xiao YP, et al. Strontium ranelate causes osteophytes overgrowth in a model of early phase osteoarthritis. BMC Musculoskelet Disord. 2017;18(1):78.
117. Zhu H, Yan H, Ma J, Zhang H, Zhang J, Hu Z, et al. CCAL1 enhances osteoarthritis through the NF-kappaB/AMPK signaling pathway. FEBS Open Bio. 2020;10(12):2553-63.
118. Snelling S, Rout R, Davidson R, Clark I, Carr A, Hulley PA, et al. A gene expression study of normal and damaged cartilage in anteromedial gonarthrosis, a phenotype of osteoarthritis. Osteoarthritis Cartilage. 2014;22(2):334-43.
119. Freedman ML, Monteiro AN, Gayther SA, Coetzee GA, Risch A, Plass C, et al. Principles for the post-GWAS functional characterization of cancer risk loci. Nat Genet. 2011;43(6):513-8.
120. Samvelyan HJ, Hughes D, Stevens C, Staines KA. Models of Osteoarthritis: Relevance and New Insights. Calcif Tissue Int. 2021;109(3):243-56.
121. Bomer N, den Hollander W, Suchiman H, Houtman E, Slieker RC, Heijmans BT, et al. Neo-cartilage engineered from primary chondrocytes is epigenetically similar to autologous cartilage, in contrast to using mesenchymal stem cells. Osteoarthritis Cartilage. 2016;24(8):1423-30.
122. Stenberg J, de Windt TS, Synnergren J, Hynsjo L, van der Lee J, Saris DB, et al. Clinical Outcome 3 Years After Autologous Chondrocyte Implantation Does Not Correlate With the Expression of a Predefined Gene Marker Set in Chondrocytes Prior to Implantation but Is Associated With Critical Signaling Pathways. Orthop J Sports Med. 2014;2(9):2325967114550781.

123. Ebert JR, Fallon M, Ackland TR, Janes GC, Wood DJ. Minimum 10-Year Clinical and Radiological Outcomes of a Randomized Controlled Trial Evaluating 2 Different Approaches to Full Weightbearing After Matrix-Induced Autologous Chondrocyte Implantation. Am J Sports Med. 2020;48(1):133-42.

124. de Windt TS, Vonk LA, Slaper-Cortenbach ICM, Nizak R, van Rijen MHP, Saris DBF. Allogeneic MSCs and Recycled Autologous Chondrons Mixed in a One-Stage Cartilage Cell Transplantion: A First-in-Man Trial in 35 Patients. Stem Cells. 2017;35(8):1984-93.

125. Fellows CR, Matta C, Zakany R, Khan IM, Mobasheri A. Adipose, Bone Marrow and Synovial Joint-Derived Mesenchymal Stem Cells for Cartilage Repair. Front Genet. 2016;7:213.

126. Barry F. MSC Therapy for Osteoarthritis: An Unfinished Story. J Orthop Res. 2019;37(6):1229-35.

127. Bastiaansen-Jenniskens YM, de Bart AC, Koevoet W, Jansen KM, Verhaar JA, van Osch GJ, et al. Elevated Levels of Cartilage Oligomeric Matrix Protein during In Vitro Cartilage Matrix Generation Decrease Collagen Fibril Diameter. Cartilage. 2010;1(3):200-10.

128. Bomer N, den Hollander W, Ramos YF, Bos SD, van der Breggen R, Lakenberg N, et al. Underlying molecular mechanisms of DIO2 susceptibility in symptomatic osteoarthritis. Ann Rheum Dis. 2015;74(8):1571-9.

129. Houtman E, Tuerlings M, Riechelman J, Suchiman E, van der Wal RJP, Nelissen R, et al. Elucidating mechano-pathology of osteoarthritis: transcriptome-wide differences in mechanically stressed aged human cartilage explants. Arthritis Res Ther. 2021;23(1):215.

130. Houtman E, van Hoolwerff M, Lakenberg N, Suchiman EHD, van der Linden-van der Zwaag E, Nelissen R, et al. Human Osteochondral Explants: Reliable Biomimetic Models to Investigate Disease Mechanisms and Develop Personalized Treatments for Osteoarthritis. Rheumatol Ther. 2021;8(1):499-515.

131. Bomer N, Cornelis FM, Ramos YF, den Hollander W, Storms L, van der Breggen R, et al. The effect of forced exercise on knee joints in Dio2(-/-) mice: type II iodothyronine deiodinase-deficient mice are less prone to develop OA-like cartilage damage upon excessive mechanical stress. Ann Rheum Dis. 2016;75(3):571-7.

132. Wu Y, Liu J, Guo H, Luo Q, Yu Z, Liao E, et al. Establishment of OPG Transgenic Mice and the Effect of OPG on Bone Microarchitecture. Int J Endocrinol. 2013;2013:125932.

133. Liu H, Yang L, Yu FF, Wang S, Wu C, Qu C, et al. The potential of induced pluripotent stem cells as a tool to study skeletal dysplasias and cartilage-related pathologic conditions. Osteoarthritis Cartilage. 2017;25(5):616-24.

134. Takahashi K, Yamanaka S. Induction of pluripotent stem cells from mouse embryonic and adult fibroblast cultures by defined factors. Cell. 2006;126(4):663-76.

135. Shi Y, Inoue H, Wu JC, Yamanaka S. Induced pluripotent stem cell technology: a decade of progress. Nat Rev Drug Discov. 2017;16(2):115-30.

136. Geng BC, Choi KH, Wang SZ, Chen P, Pan XD, Dong NG, et al. A simple, quick, and efficient CRISPR/Cas9 genome editing method for human induced pluripotent stem cells. Acta Pharmacol Sin. 2020;41(11):1427-32.

137. Ben Jehuda R, Shemer Y, Binah O. Genome Editing in Induced Pluripotent Stem Cells using CRISPR/Cas9. Stem Cell Rev Rep. 2018;14(3):323-36.

138. Castro-Vinuelas R, Sanjurjo-Rodriguez C, Pineiro-Ramil M, Hermida-Gomez T, Rodriguez-Fernandez S, Oreiro N, et al. Generation and characterization of human induced pluripotent stem cells (iPSCs) from hand osteoarthritis patient-derived fibroblasts. Sci Rep. 2020;10(1):4272.

139. Lin Z, Li Z, Li EN, Li X, Del Duke CJ, Shen H, et al. Osteochondral Tissue Chip Derived From iPSCs: Modeling OA Pathologies and Testing Drugs. Front Bioeng Biotechnol. 2019;7:411.

140. Nakayama N, Pothiawala A, Lee JY, Matthias N, Umeda K, Ang BK, et al. Human pluripotent stem cell-derived chondroprogenitors for cartilage tissue engineering. Cell Mol Life Sci. 2020;77(13):2543-63.

141. Xu M, Shaw G, Murphy M, Barry F. Induced Pluripotent Stem Cell-Derived Mesenchymal Stromal Cells Are Functionally and Genetically Different From Bone Marrow-Derived Mesenchymal Stromal Cells. Stem Cells. 2019;37(6):754-65.

142. Diederichs S, Tuan RS. Functional comparison of human-induced pluripotent stem cell-derived mesenchymal cells and bone marrow-derived mesenchymal stromal cells from the same donor. Stem Cells Dev. 2014;23(14):1594-610.

143. Diederichs S, Klampfleuthner FAM, Moradi B, Richter W. Chondral Differentiation of Induced Pluripotent Stem Cells Without Progression Into the Endochondral Pathway. Front Cell Dev Biol. 2019;7:270.

144. Nejadnik H, Diecke S, Lenkov OD, Chapelin F, Donig J, Tong X, et al. Improved approach for chondrogenic differentiation of human induced pluripotent stem cells. Stem Cell Rev Rep. 2015;11(2):242-53.

145. Adkar SS, Wu CL, Willard VP, Dicks A, Ettyreddy A, Steward N, et al. Step-Wise Chondrogenesis of Human Induced Pluripotent Stem Cells and Purification Via a Reporter Allele Generated by CRISPR-Cas9 Genome Editing. Stem Cells. 2019;37(1):65-76.

146. Dicks A, Wu CL, Steward N, Adkar SS, Gersbach CA, Guilak F. Prospective isolation of chondroprogenitors from human iPSCs based on cell surface markers identified using a CRISPR-Cas9-generated reporter. Stem Cell Res Ther. 2020;11(1):66.

147. Guzzo RM, Gibson J, Xu RH, Lee FY, Drissi H. Efficient differentiation of human iPSC-derived mesenchymal stem cells to chondroprogenitor cells. J Cell Biochem. 2013;114(2):480-90.

148. Wu CL, Dicks A, Steward N, Tang R, Katz DB, Choi YR, et al. Single cell transcriptomic analysis of human pluripotent stem cell chondrogenesis. Nat Commun. 2021;12(1):362.

CHAPTER 2

The role of *TNFRSF11B* in development of osteoarthritic cartilage

Alejandro Rodríguez Ruiz[1], Margo Tuerlings[1], Ankita Das[1], Rodrigo Coutinho de Almeida[1], H. Eka Suchiman[1], Rob GHH Nelissen[2], Yolande FM Ramos[1§*], and Ingrid Meulenbelt[1§]

[1]Department of Biomedical Data Sciences, Section Molecular Epidemiology and [2]Department of Orthopaedics, Leiden University Medical Center, Leiden, The Netherlands

Rheumatology (Oxford). 2022 Feb; 61(2): 856–864.

ABSTRACT

Objectives: Osteoarthritis (OA) is a complex genetic disease with different risk factors contributing to its development. One of the genes, *TNFRSF11B*, previously identified with gain-of-function mutation in a family with early-onset OA with chondrocalcinosis, is among the highest upregulated genes in lesioned OA cartilage (RAAK-study). Here, we determined the role of *TNFRSF11B* overexpression in development of OA.

Methods: Human primary articular chondrocytes (9 donors RAAK study) were transduced using lentiviral particles with or without *TNFRSF11B*. Cells were cultured for 1 week in a 3D *in-vitro* chondrogenic model . *TNFRSF11B* overexpression was confirmed by RT-qPCR, immunohistochemistry and ELISA. Effects of *TNFRSF11B* overexpression on cartilage matrix deposition, matrix mineralization, and genes highly correlated to *TNFRSF11B* in RNA-sequencing dataset (r>|0.75|) were determined by RT-qPCR. Additionally, glycosaminoglycans and collagen deposition were visualized with Alcian blue staining and immunohistochemistry (COL1 and COL2).

Results: Overexpression of *TNFRSF11B* resulted in strong upregulation of *MMP13*, *COL2A1* and *COL1A1*. Likewise, mineralization and osteoblast characteristic markers *RUNX2*, *ASPN* and *OGN* showed a consistent increase. Among 30 genes highly correlated to *TNFRSF11B*, expression of only eight changed significantly, with *BMP6* showing highest increase (9-fold) while expression of RANK and RANKL remained unchanged indicating previously unknown downstream pathways of *TNFRSF11B* in cartilage.

Conclusion: Results of our 3D *in vitro* chondrogenesis model indicate that upregulation of *TNFRSF11B* in lesioned OA cartilage may act as a direct driving factor for chondrocyte to osteoblast transition observed in OA pathophysiology. This transition does not appear to act via the OPG/RANK/RANKL triad common in bone remodeling.

Key messages:

- *TNFRSF11B* in cartilage is a direct driving factor for chondrocyte-to-osteoblast transition observed in OA pathophysiology.
- Chondrocyte-to-osteoblast transition in cartilage does not act via the OPG/RANK/RANKL triad, common in bone remodeling.
- Likely, the *TNFRSF11B*-induced cartilage mineralization is accomplished via BMP6 signaling.

INTRODUCTION

Osteoarthritis (OA) is a common degenerative disorder characterized by cartilage extracellular matrix degradation (ECM) and changes in subchondral bone. Being marked by pain and disability, no effective therapy is available, and current treatments are focused on pain relief or joint surgery at end-stage disease, creating a great social and economic burden (1, 2). To characterize the OA pathophysiological process, multiple studies (3-5) have performed transcriptome-wide analyses of preserved and lesioned cartilage. Among the most consistent and highly upregulated genes in lesioned OA cartilage is the tumor necrosis factor receptor superfamily member 11b (*TNFRSF11B*) at the CCAL1 (chondrocalcinosis) locus (4, 6), encoding osteoprotegerin (OPG). OPG is a decoy receptor for the binding of nuclear factor KB ligand (RANKL) to the receptor activator of the nuclear KB factor (RANK). Together, this triad is well known for tightly regulating osteoclastogenesis, hence playing a critical role in bone formation, endochondral ossification, and bone remodelling (5, 6). A gain of function mutation in OPG (c1205A=>T; p.Stop402Leu) was identified in multiple families with early onset osteoarthritis (FOA) characterized by chondrocalcinosis (6, 7). With this mutation, the underlying importance of OPG was further confirmed, not only in bone turnover but also in cartilage homeostasis and OA onset. Given the eminent cross-talk between bone and cartilage, it was suggested that aberrant OPG function can affect the delicate balance between subchondral bone formation and resorption (8), making OPG essential in joint homeostasis. A drug called strontium ranelate has been administered in the clinic in order to fight osteoporosis by increasing OPG expression and impairing bone resorption processes (9). This drug is also used to treat OA, but controversial results have been shown in preclinical and clinical studies (10, 11). To study whether the observed upregulation of *TNFRSF11B* in OA can trigger unbeneficial mineralization of cartilage, a tailored human 3D *in vitro* OA tissue model was applied in which aberrant gene function was mimicked by lentiviral overexpression of *TNFRSF11B* in spherical cartilage pellets. Potential effects on anabolic, catabolic and mineralization markers involved in cartilage homeostasis were investigated. Moreover, to better comprehend the pathways in which *TNFRSF11B* acts in articular cartilage and during OA, a selected panel of genes that showed high co-expression with *TNFRSF11B* during OA pathophysiology was studied.

MATERIALS AND METHODS

Sample description

RNA sequencing data previously obtained of N=57 preserved and N=44 lesioned OA cartilage samples (RAAK study) and previously assessed (4), were taken for *in silico TNFRSF11B* correlation analyses. RNA sequencing was used to identify genes

co-expressed with *TNFRSF11B,* where a Spearman correlation was performed. Genes were considered to be correlated if the P-value was lower than 0.05 and the absolute r-value was higher than 0.75. Quality control of the data was performed as previously described (4). Human primary articular chondrocytes (hPACs) obtained from knee replacement surgeries of N=9 participants (4 females and 5 males with average age of 69.4±11.1) of the RAAK study were isolated and cultured to perform lentiviral transduction.

Cloning of TNFRSF11B in lentivirus plasmid

The Porf9-H*TNFRSF11B* V04 plasmid and the pLV.CMV.bc.eGFP lentivirus vector (kindly provided by Prof. Dr. R. Hoeben) were digested with AgeI and NheI (New England Biolabs). The full gene *TNFRSF11B* was ligated into the AgeI and NheI sites of the K4_pLV.CMV.bc.eGFP plasmid by using the Takara Mighty Mix ligation kit (Takara Bio Europe AB). DNA was obtained by Maxiprep Kit (ThermoFisher), and Sanger sequencing was performed to confirm successful cloning of the lentivirus plasmid.

Lentiviral production and cell culture

Lentiviral production was performed in HEK293T cells using the Lenti-vpak Lentiviral Packaging Kit (Origene Technologies). In short, HEK 293T cells were expanded in DMEM high glucose (Gibco), supplemented with 10% fetal calf serum (FCS, Gibco) 100U/mL penicillin, 100ug/ml streptomycin (Gibco), and lentivirus particles were collected and titrated.

Following their isolation, hPACs were transduced at passage 1 with either control (pLV.CMV.bc.eGFP) or *TNFRSF11B* Lentivirus (MOI of 1). After 16 hours, the medium was refreshed (DMEM high glucose (Gibco) supplemented with 10% FCS (Gibco), 100 U/ml penicillin and 100 ug/ml streptomycin (Gibco), and 0.5 ng/ml bFGF-2 (PeproTech)) and hPACs were further cultured for another passage. Subsequently, neo-cartilage was generated from 250,000 transduced hPACs in 3D pellets for seven days, as described before (12), and keeping the conditions between both groups equal. All data were analyzed 7 days following the 3D chondrogenesis. Cells were counted with the Nucleocounter NC-200 (Chemometec).

RNA isolation and RT-qPCR

RNA was isolated from four biological replicates for each patient and condition (control and *TNFRSF11B*-overexpressing chondrocytes) while pooling two pellets together to generate two independent samples for downstream analyses. Isolations were performed as described previously (12). Total mRNA (150 ng) was processed with the first strand cDNA kit according to the manufacturer's protocol (Roche Applied Science). CDNA was further diluted five times, and preamplification with

TaqMan preamp master mix (Thermo Fisher Scientific Inc.) was performed. Gene expression was measured (**Supplementary Table S1**) with RT-qPCR (Quantstudio), and average of the two biological replicates was determined as relative levels (–ΔCt values) using expression levels of glyceraldehyde 3-phosphate dehydrogenase (*GAPDH*) and Acidic ribosomal phosphoprotein P0 (*ARP*) as housekeeping genes. Quality control of the results was performed as described before (12).

Selection criteria for gene expression analyses

TNFRSF11B expression was analyzed to quantify overexpression. To determine matrix homeostasis, metabolic activity and mineralization status, a list of 16 relevant genes was selected from the literature (**Supplementary Table S1**). Additionally, to identify potential new downstream pathways, a two-step approach was taken for selection of genes. Firstly, a *TNFRSF11B* co-expression network was created based on correlations of genes significantly differentially expressed between preserved (N = 57) and lesioned (N = 44) OA cartilage from our previously published RNA sequencing dataset (N=2387 genes) (4). Genes with $r \geq |0.80|$ were selected for expression analysis (N=21 genes). Secondly, genes with $r > |0.75|$ were designated on basis of their functionality in cartilage homeostasis and mineralization (6 genes), or based on previously identified protein-protein interactions with *TNFRSF11B* within the online available webtool STRING (13) (three genes). This resulted in a total of 30 genes. Finally, *GAPDH* and *ARP* were used as housekeeping genes.

Histology and immunohistochemistry

Following chondrogenesis, pellets were fixed in 4% formaldehyde and embedded in paraffin. After sectioning, deparaffinization and rehydration sections were analyzed by histology (1% Alcian Blue 8-GX (Sigma-Aldrich)) and immunohistochemistry (COL2 (MAB1330; Milipore; 1:100), COL1 (ab34710; Abcam), and OPG (EPR3592; Epitomics; 1:100)), as described before (12). Pixel intensity quantification was performed for Alcian Blue staining by ImageJ, and surface area of the pellets were measured with the CellSens Dimension software (Olympus).

ELISA and DMMB assay

The osteoprotegerin human instant ELISA™ Kit (Thermofisher) and the Dimethylmethylene Blue assay (DMMB; Sigma-Aldrich), respectively, were used following the manufacturer's instructions for OPG and GAG quantification in the conditioned media of three independent pellets with or without *TNFRSF11B* overexpression for each patient.

Statistical analysis

To determine statistical differences between the controls and samples with *TNFRSF11B* overexpression, a paired sample t-test was performed. P-value <0.05 was considered significant.

RESULTS

No change in matrix deposition upon TNFRSF11B overexpression

Lentiviral transduction of primary chondrocytes resulted in consistent and significant upregulation of *TNFRSF11B* mRNA as well as OPG protein (**Supplementary Figure S1**). Following *TNFRSF11B* overexpression, hPACs were subjected to a 3D *in vitro* chondrogenesis model, and neo-cartilage formation was characterized at day seven.

Alcian Blue staining was performed to visualize pellets and the presence of glycosaminoglycans (GAGs). The relative pixel intensity of the GAG staining showed no significant differences in the presence of higher OPG levels (n=18, P-value=3.4×10^{-1}; **Figure 1**). Likewise, GAG release in the medium was similar (n=27, P-value=5.3×10^{-1}). Furthermore, no significant difference in pellet size was observed between controls and *TNFRSF11B* (n=72, P-value=5.5×10^{-1}). Together, these data indicate that *TNFRSF11B* upregulation does not change capacity of chondrocytes to deposit matrix at day 7.

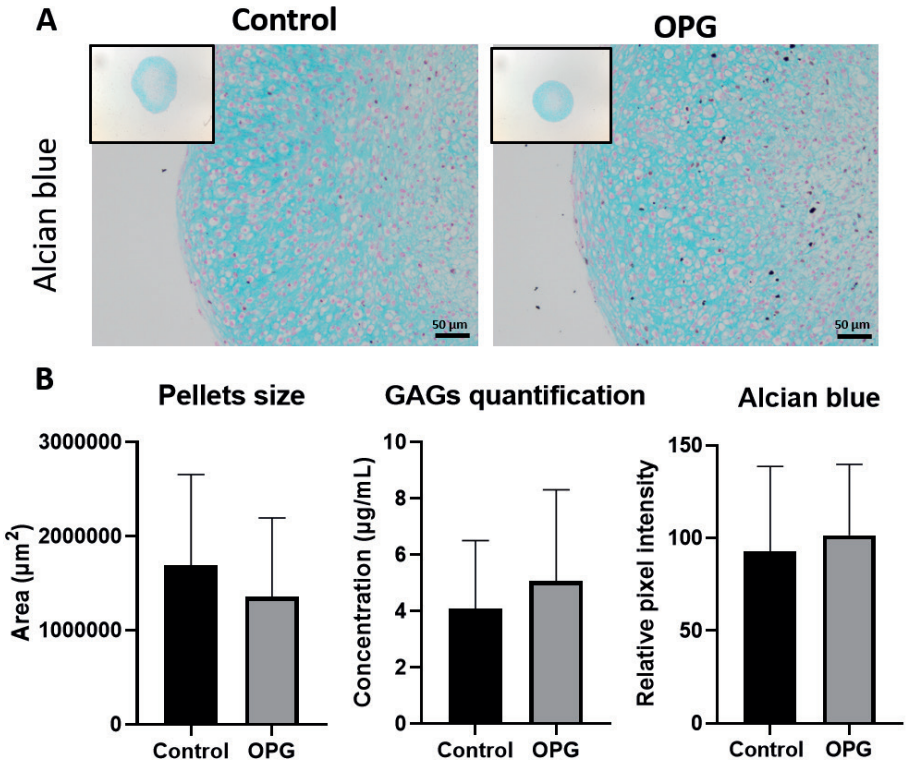

Figure 1. Neo-cartilage deposition upon *TNFRSF11B* overexpression. A) Representative images of 1-week neo-cartilage pellets as indicated (left: control chondrocytes; right: chondrocytes with *TNFRSF11B* overexpression). Scale bars: 50 µm. **B)** Area of the pellets (n=72), GAG-release in the medium (n=27), and Alcian blue pixel intensity quantification (n=18) for control and *TNFRSF11B* overexpressing chondrocytes.

Collagen type I and collagen type II become upregulated upon TNFRSF11B overexpression

To study the effect of *TNFRSF11B* overexpression on matrix characteristics, RT-qPCR was performed for anabolic and catabolic genes involved in cartilage homeostasis (**Supplementary Table S2, Figure 2**). Of note was the high and significant upregulation of *MMP13* (FD=14.76, P-value=2.0x10^{-3}) following overexpression of *TNFRSF11B* (**Figure 2**). Furthermore, overexpression of *TNFRSF11B* resulted in significantly higher upregulation of *COL2A1* (FD=4.77, P-value=4.8x10^{-4}) and *COL1A1* (FD=1.88, P-value=1.3x10^{-2}) and a modest downregulation of *COMP* (FD=0.69, P-value=2.0x10^{-2}) during chondrogenesis. Hypertrophic marker *COL10A1* showed no significant difference (FD=4.24, P-value=6.3x10^{-1}). Immunohistochemistry of collagen type 2 (COL2) and collagen type 1 (COL1) showed a visual higher expression for both collagens in the OPG overexpressing group concurrent with respective gene expression levels (**Figure 3**). As such, COL1 staining showed a

darker and wider layer of staining towards the edges of the pellet when compared to the control group. COL2 differences were less strong between both conditions, nevertheless a more consistent staining was observed in the ECM and retained within the cells cytoplasm in the OPG overexpressing group.

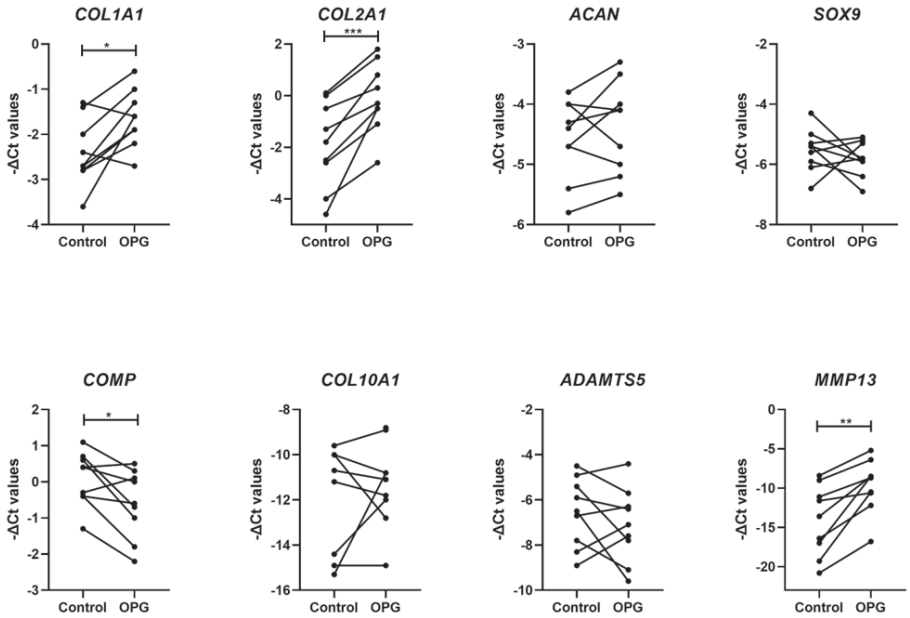

Figure 2. Expression of matrix-related genes in neo-cartilage. Results show line plots for -ΔCt values of genes in 1-week neo-cartilage pellets (control chondrocytes versus chondrocytes with *TNFRSF11B* overexpression (n=18; * P-value< 0.05; ** P-value< 10^{-3}; *** P-value< 10^{-6}).

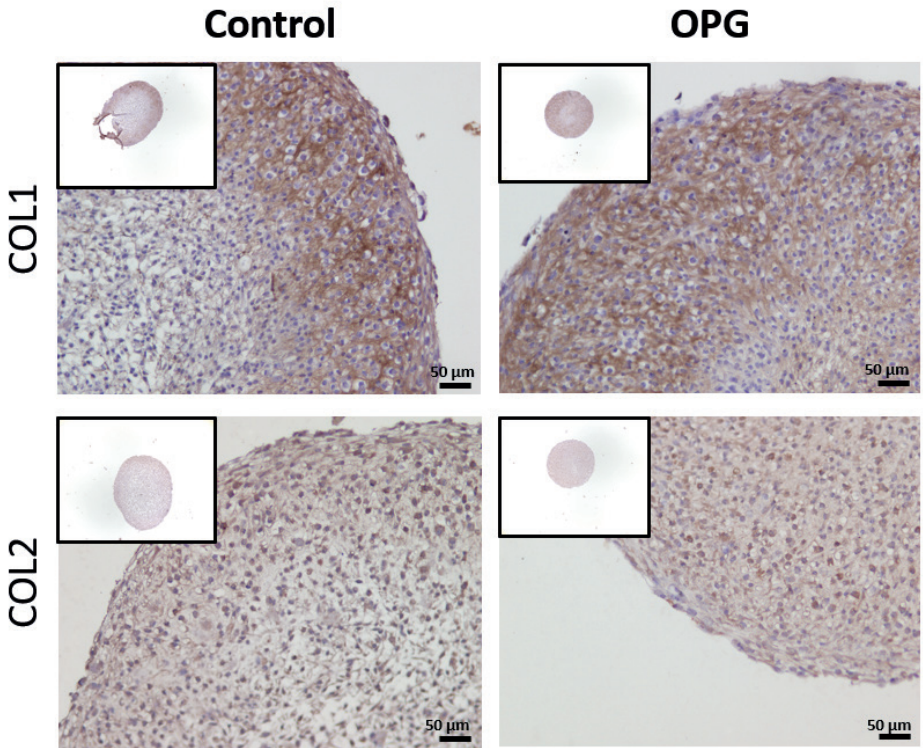

Figure 3. COL1 and COL2 immunohistochemistry of neo-cartilage. Representative images of 1-week neo-cartilage pellets as indicated (left: control chondrocytes; right: chondrocytes with *TNFRSF11B* overexpression). Scale bars: 50µm.

High gene expression of osteogenic markers, yet no alteration in the TNFRSF11B triad upon TNFRSF11B overexpression

To investigate our hypothesis that upregulation of *TNFRSF11B* with OA pathophysiology directly induces cartilage mineralization, we next explored the expression of genes involved in matrix mineralization (**Supplementary table S2**). First, we explored expression of *TNFRSF11A* encoding RANK and *TNFSF11* encoding RANKL, which together with OPG are known to tightly regulate bone turnover. Remarkably (**Figure 4**), neither *TNFSF11* (FD=1.06, P-value=3.9×10^{-1}) nor *TNFRSF11A* (FD=2.45, P-value=7.8×10^{-1}), did significantly respond to the lentiviral-induced upregulation of *TNFRSF11B*. Nonetheless, the osteogenic markers *RUNX2* (FD=4.51, P-value=4.0×10^{-3}), *POSTN* (FD=1.75, P-value=4.0×10^{-2}), *OGN* (FD=1.68, P-value=2.3×10^{-2}) and *ASPN* (FD=2.61, P-value=1.0×10^{-2}), were significantly higher upregulated in chondrocytes upon *TNFRSF11B* overexpression.

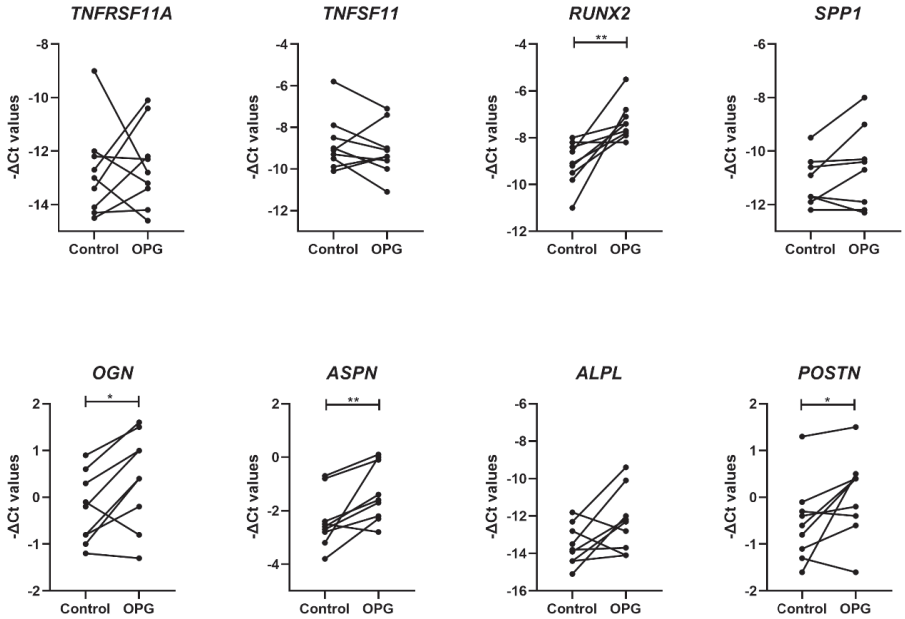

Figure 4. Expression of osteogenic-related genes in neo-cartilage. Results show line plots for -ΔCt values of mineralization and bone formation genes in 1-week neo-cartilage pellets (control chondrocytes versus chondrocytes with *TNFRSF11B* overexpression (n=18; * P-value< 0.05; ** P-value< 10^{-3} ;*** P-value< 10^{-6}).

A novel set of signaling pathways is discovered in highly correlated genes with TNFRSF11B upon TNFRSF11B overexpression

After assessing the effect of *TNFRSF11B*-induced overexpression on known related genes, we next performed an exploratory analysis to identify potential novel *TNFRSF11B* signaling pathways in cartilage. To do so, we generated a *TNFRSF11B* co-expression network with differentially expressed genes between preserved and lesioned OA cartilage as previously assessed (N=2387 genes) (4). We found 51 genes highly correlated with *TNFRSF11B* with absolute r-values ≥ 0.75 (**Supplementary Table S3**). Among the highest positively correlated genes, we found *CDH19* (r=0.88), *ATP1A1* (r=0.87), and *DIXDC1* (r=0.85), whereas the highest inverse correlation was observed for *SLC15A3* (r=-0.81), *MAPK11* (r=-0.81), and *HLA-E* (r=-0.8). Of these 51 genes, 30 were selected for expression analysis based on their correlation with *TNFRSF11B* and additional functional connection in STRING (**Supplementary Figure S2**). As shown in **Supplementary Table S4** and **Figure 5**, we found eight genes to be significantly differentially expressed upon lentiviral-induced *TNFRSF11B* overexpression. The strongest increased expression was found for *BMP6* (FD=9.34, P-value=2.6x10^{-2}) while the *SLC15A3* gene was 2.5-fold downregulated (FD=0.4, P-value=4.0x10^{-3}). Around

2-fold increase was observed for *FITM2* (FD=2.28, P-value=1.4x10^{-2}), *CDON* (FD=2.03, P-value=5.0x10^{-3}), and *SLC16A7* (FD=1.97, P-value=1.8x10^{-2}). Moderate effects were found for *CDH19* (FD=1.53, P-value=4.5x10^{-2}), *P3H2* (FD=1.48, P-value=4.7x10^{-2}), and *WNT16* (FD=0.81, P-value=4.3x10^{-2}).

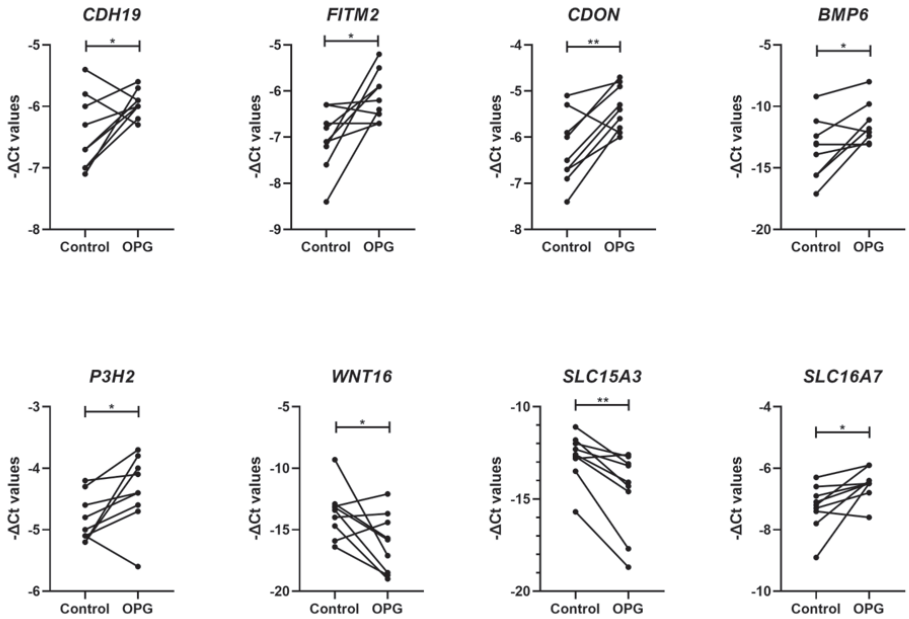

Figure 5. Expression of *TNFRSF11B*-correlated genes in neo-cartilage. Results show line plots for -ΔCt values of *TNFRSF11B*-correlated genes in 1-week neo-cartilage pellets (control chondrocytes versus chondrocytes with *TNFRSF11B* overexpression (n=18; * P-value< 0.05; ** P-value< 10^{-3}; *** P-value< 10^{-6}).

DISCUSSION

In the current study, we investigated the role of increased *TNFRSF11B* in OA pathophysiology. To this end, lentiviral upregulation of *TNFRSF11B* was established in a 3D *in vitro* chondrogenic model (**Supplementary Figure S1**). As reflected by the particularly high upregulation of *MMP13* (FD=14.76, P-value=2.0x10^{-3}) in combination with the upregulation of characteristic osteogenic genes *RUNX2, POSTN, BMP6, ASPN,* and *OGN* and in absence of differential expression of the mineralization markers *COL10A1* and *ALPL,* we advocate that *TNFRSF11B* affects OA pathophysiology by advancing chondrocyte to osteoblast transition (14). This finding is in line with the observed chondrocalcinosis phenotype observed in previously described members of the family with early-onset OA and carriers of readthrough mutation in *TNFRSF11B* also known as the CCAL1 locus (7).

With *TNFRSF11B* encoding the decoy receptor OPG, which competes for binding of RANKL to the RANK receptor, we next examined expression of *TNFRSF11A* (encoding RANK) and *TNFSF11* (encoding RANKL) upon *TNFRSF11B* upregulation. Even though this triad, and particularly the RANKL/OPG ratio, is known to be an important determinant of bone mass and skeletal integrity (5, 6), no significant changes in *TNFRSF11A* or *TNFSF11* levels were observed (**Figure 4, Supplementary Table S2**). This, together with the fact that we did not find high correlation of expression between *TNFRSF11B* with *TNFRSF11A* or *TNFSF11* in preserved and lesioned OA cartilage, would suggest that in cartilage the interaction among the triad may not play such an important role as in bone. This is in line with the finding of Komuro *et al*. and Tat *et al*. (14, 15), showing no alterations in RANK and OPG expression upon adding exogenous RANKL to chondrocytes.

OPG at high concentration is well known to decrease tumor necrosis factor-related apoptosis-inducing ligand (TRAIL) in chondrocytes, as such inhibiting apoptosis (15, 16).Given that we observed high upregulation of *MMP13* in combination with the upregulation of characteristic osteogenic genes *RUNX2, POSTN, BMP6, ASPN,* and *OGN* (**Figure 4**), which is an opposite response to that of OPG binding to TRAIL (17), we advocate that OPG rather affects OA pathophysiology in cartilage by advancing chondrocyte to osteoblast transition (14). On the other hand, in our spherical neo-cartilage pellets model, we have studied the effect of OPG overexpression at an early timepoint in postmitotic chondrocytes that are stimulated to deposit matrix without further proliferation. As such this model may not be optimal to provide insight into TRAIL-related signaling role of OPG.

In order to determine the co-expression network of OPG signaling in articular cartilage and with OA pathophysiology, we explored a previously assessed RNA sequencing dataset of preserved and lesioned OA cartilage for correlation with *TNFRSF11B* (4). We found 51 genes that highly correlated with *TNFRSF11B* ($r \geq 0.75$), such as *CDH19* (r=0.88) encoding for cadherins involved in calcium-dependent cell-cell adhesion, or *SLC15A3* (r=-0.81) encoding histidine and osteoclast transporters (18). From this network, expression of 30 genes were compared between control and *TNFRSF11B* overexpressing chondrocytes. Despite the high correlations with *TNFRSF11B*, notably only eight genes were found to be responsive to *TNFRSF11B* upregulation (26.6%; *CDON*, *BMP6*, *CDH19*, *P3H2, WNT16, SLC16A7, SLC15A3* and *FITM2)*. This may be explained partly by the fact that genes are upstream of OPG. Alternatively, genes may be correlated to *TNFRSF11B* as a general result of ongoing OA disease processes. Notable among the *TNFRSF11B* correlated and responsive genes were *BMP6* and *SLC15A3* (**Figure 5**). *BMP6* (r=0.77), encoding bone morphogenic protein 6, is well known to be involved in bone formation (19), and *SLC15A3* (r=-0.81) an osteoclast transporter of which lower expression would likely result in a reduction of the number of available osteoclasts. Additionally,

we identified increased expression of *FITM2* (r=0.76) and *SLC16A7* (r=0.77), genes involved in lipid droplet formation and metabolite transport, respectively. Lipid droplets have been reported in OA cartilage (20) and during the osteogenesis process, where osteoprogenitors and osteoblasts synthesize them to use them as energy supplies for the differentiation process (21). More importantly, it has recently been confirmed in mice that fat metabolism is a critical antagonist of cartilage health and integrity (22). Notable as being co-expressed and highly responsive to *TNFRSF11B* was *CDON* (Cell Adhesion Associated, Oncogene Regulated; r=0.83). Although little is known about its direct role in cartilage or bone homeostasis, cadherin signaling is known to be essential for successful cell differentiation, as it has been previously shown for osteogenesis (23, 24). Lastly, expression of *ANKH* (r=0.84), a gene previously associated with chondrocalcinosis and early OA (25, 26), was not affected by *TNFRSF11B* upregulation. This would confirm the work performed in porcine chondrocytes by Williams et al. (6) and translate it to primary human chondrocytes where *ANKH* would affect chondrocalcinosis by a *TNFRSF11B*-independent mechanism.

Remarkably, the study by Zhu et al. (27), showed a different signaling outcome upon overexpression of OPG (CCAL1) in primary human chondrocytes from OA patients. In contrast to results shown here, they observed a fibrotic effect, dominated by reduced expression of *COL2A1* and *SOX9* and a higher expression of *COL1A1*. Several factors may have contributed to this disparity in results. Likely, the most important difference is the use of a 2D model that was previously demonstrated to rather result in a hypertrophic phenotype (28).

Additionally, a previously published trial claimed minimal but debatable effects in OA joints upon treatment with strontium ranelate, a drug licensed for osteoporosis (29, 30). Strontium ranelate increased bone formation while decreasing bone resorption via stimulation of OPG and was thought to target unbeneficial changes in subchondral bone with OA. Considering our current results showing the effect of OPG on cartilage, we advocate that the risk of such an oral treatment to OA patients is seriously underestimated and bound to considerably increase the burden of OA.

A potential limitation of our study is that we have mainly focused on gene expression responses of hPACs by RT-qPCR at day 7 of matrix deposition. Henceforth, due to the early timepoint taken for these analyses and the inherently lower sensitivity and more challenging quantification methods that regular protein analyses such as immunoblotting offer, we have not extensively quantified our changes at a protein level. To further confirm, for example, whether the high upregulation of *MMP13* results in significant changes in protein expression or, for that matter matrix degeneration, later harvesting timepoints (day 14 or day 21) and increasing sample sizes may be required.

In conclusion, we here highlighted the role of *TNFRSF11B* upregulation in OA pathophysiology. Results of our 3D *in vitro* chondrogenesis model indicate that the observed consistent upregulation of *TNFRSF11B* in lesioned OA cartilage may act as a direct driving factor for chondrocyte to osteoblast transition occurring in OA pathophysiology. Moreover, we showed that this transition does not act via the OPG/RANK/RANKL triad, known for that matter in bone remodeling. Together, our results merit further exploration of *TNFRSF11B* as a promising disease OA modifying factor.

Acknowledgements

We thank all the participants of the RAAK study. The LUMC has and is supporting the RAAK study. We thank all the members of our group for valuable discussion and feedback, especially Evelyn Houtman and Ritchie Timmermans. We also thank Enrike van der Linden, Demiën Broekhuis, Peter van Schie, Shaho Hasan, Maartje Meijer, Daisy Latijnhouwers and Geert Spierenburg for collecting the RAAK material. We thank the Sequence Analysis Support Core (SASC) of the Leiden University Medical Center for their support.

Funding

Research leading to these results has received funding from the Dutch Arthritis Society (DAF-16-1-406), and the Dutch Scientific Research council NWO/ZonMW VICI scheme (nr 91816631/528). Data is generated within the scope of the Medical Delta programs Regenerative Medicine 4D ('Generating complex tissues with stem cells and printing technology and Improving Mobility with Technology').

Disclosure of potential conflicts of interest

None declared.

Data availability statement

The data that support the funding of this study are available from the corresponding author upon request.

Ethics approval and consent to participate

The Medical Ethics Committee of the LUMC gave approval for the RAAK study (P08.239). Written informed consent was obtained from all donors.

REFERENCES

1. Chen D, Shen J, Zhao W, Wang T, Han L, Hamilton JL, et al. Osteoarthritis: toward a comprehensive understanding of pathological mechanism. Bone Res. 2017;5:16044.
2. Cucchiarini M, de Girolamo L, Filardo G, Oliveira JM, Orth P, Pape D, et al. Basic science of osteoarthritis. J Exp Orthop. 2016;3(1):22.
3. Dunn SL, Soul J, Anand S, Schwartz JM, Boot-Handford RP, Hardingham TE. Gene expression changes in damaged osteoarthritic cartilage identify a signature of non-chondrogenic and mechanical responses. Osteoarthritis Cartilage. 2016;24(8):1431-40.
4. Coutinho de Almeida R, Ramos YFM, Mahfouz A, den Hollander W, Lakenberg N, Houtman E, et al. RNA sequencing data integration reveals an miRNA interactome of osteoarthritis cartilage. Ann Rheum Dis. 2019;78(2):270-7.
5. Styrkarsdottir U, Lund SH, Thorleifsson G, Zink F, Stefansson OA, Sigurdsson JK, et al. Meta-analysis of Icelandic and UK data sets identifies missense variants in SMO, IL11, COL11A1 and 13 more new loci associated with osteoarthritis. Nat Genet. 2018;50(12):1681-7.
6. Williams CJ, Qazi U, Bernstein M, Charniak A, Gohr C, Mitton-Fitzgerald E, et al. Mutations in osteoprotegerin account for the CCAL1 locus in calcium pyrophosphate deposition disease. Osteoarthritis Cartilage. 2018;26(6):797-806.
7. Ramos YF, Bos SD, van der Breggen R, Kloppenburg M, Ye K, Lameijer EW, et al. A gain of function mutation in *TNFRSF11B* encoding osteoprotegerin causes osteoarthritis with chondrocalcinosis. Ann Rheum Dis. 2015;74(9):1756-62.
8. Pelletier JP, Boileau C, Brunet J, Boily M, Lajeunesse D, Reboul P, et al. The inhibition of subchondral bone resorption in the early phase of experimental dog osteoarthritis by licofelone is associated with a reduction in the synthesis of MMP-13 and cathepsin K. Bone. 2004;34(3):527-38.
9. Cianferotti L, D'Asta F, Brandi ML. A review on strontium ranelate long-term antifracture efficacy in the treatment of postmenopausal osteoporosis. Ther Adv Musculoskelet Dis. 2013;5(3):127-39.
10. Rodrigues TA, Freire AO, Bonfim BF, Cartagenes MSS, Garcia JBS. Strontium ranelate as a possible disease-modifying osteoarthritis drug: a systematic review. Braz J Med Biol Res. 2018;51(8):e7440.
11. Chu JG, Dai MW, Wang Y, Tian FM, Song HP, Xiao YP, et al. Strontium ranelate causes osteophytes overgrowth in a model of early phase osteoarthritis. BMC Musculoskelet Disord. 2017;18(1):78.
12. Bomer N, den Hollander W, Ramos YF, Bos SD, van der Breggen R, Lakenberg N, et al. Underlying molecular mechanisms of DIO2 susceptibility in symptomatic osteoarthritis. Ann Rheum Dis. 2015;74(8):1571-9.
13. Szklarczyk D, Gable AL, Lyon D, Junge A, Wyder S, Huerta-Cepas J, et al. STRING v11: protein-protein association networks with increased coverage, supporting functional discovery in genome-wide experimental datasets. Nucleic Acids Res. 2019;47(D1):D607-D13.
14. Aghajanian P, Mohan S. The art of building bone: emerging role of chondrocyte-to-osteoblast transdifferentiation in endochondral ossification. Bone Res. 2018;6:19.
15. Park DR, Kim J, Kim GM, Lee H, Kim M, Hwang D, et al. Osteoclast-associated receptor blockade prevents articular cartilage destruction via chondrocyte apoptosis regulation. Nat Commun. 2020;11(1):4343.
16. Shimizu S, Asou Y, Itoh S, Chung UI, Kawaguchi H, Shinomiya K, et al. Prevention of cartilage destruction with intraarticular osteoclastogenesis inhibitory factor/osteoprotegerin in a murine model of osteoarthritis. Arthritis Rheum. 2007;56(10):3358-65.
17. Qin X, Jiang Q, Nagano K, Moriishi T, Miyazaki T, Komori H, et al. Runx2 is essential for the transdifferentiation of chondrocytes into osteoblasts. PLoS Genet. 2020;16(11):e1009169.

18. Song F, Yi Y, Li C, Hu Y, Wang J, Smith DE, et al. Regulation and biological role of the peptide/histidine transporter SLC15A3 in Toll-like receptor-mediated inflammatory responses in macrophage. Cell Death Dis. 2018;9(7):770.
19. Wu M, Chen G, Li YP. TGF-beta and BMP signaling in osteoblast, skeletal development, and bone formation, homeostasis and disease. Bone Res. 2016;4:16009.
20. Mansfield JC, Winlove CP. Lipid distribution, composition and uptake in bovine articular cartilage studied using Raman micro-spectrometry and confocal microscopy. J Anat. 2017;231(1):156-66.
21. Rendina-Ruedy E, Guntur AR, Rosen CJ. Intracellular lipid droplets support osteoblast function. Adipocyte. 2017;6(3):250-8.
22. Collins KH, Lenz KL, Pollitt EN, Ferguson D, Hutson I, Springer LE, et al. Adipose tissue is a critical regulator of osteoarthritis. Proc Natl Acad Sci U S A. 2021;118(1).
23. Lee JK, Hu JC, Yamada S, Athanasiou KA. Initiation of Chondrocyte Self-Assembly Requires an Intact Cytoskeletal Network. Tissue Eng Part A. 2016;22(3-4):318-25.
24. Kawaguchi J, Kii I, Sugiyama Y, Takeshita S, Kudo A. The transition of cadherin expression in osteoblast differentiation from mesenchymal cells: consistent expression of cadherin-11 in osteoblast lineage. J Bone Miner Res. 2001;16(2):260-9.
25. Gruber BL, Couto AR, Armas JB, Brown MA, Finzel K, Terkeltaub RA. Novel ANKH amino terminus mutation (Pro5Ser) associated with early-onset calcium pyrophosphate disease with associated phosphaturia. J Clin Rheumatol. 2012;18(4):192-5.
26. Abhishek A, Doherty M. Pathophysiology of articular chondrocalcinosis--role of ANKH. Nat Rev Rheumatol. 2011;7(2):96-104.
27. Zhu H, Yan H, Ma J, Zhang H, Zhang J, Hu Z, et al. CCAL1 enhances osteoarthritis through the NF-kappaB/AMPK signaling pathway. FEBS Open Bio. 2020;10(12):2553-63.
28. Caron MM, Emans PJ, Coolsen MM, Voss L, Surtel DA, Cremers A, et al. Redifferentiation of dedifferentiated human articular chondrocytes: comparison of 2D and 3D cultures. Osteoarthritis Cartilage. 2012;20(10):1170-8.
29. Reginster JY. Efficacy and safety of strontium ranelate in the treatment of knee osteoarthritis: results of a double-blind randomised, placebo-controlled trial. Ann Rheum Dis. 2014;73(2):e8.
30. Lafeber FP, van Laar JM. Strontium ranelate: ready for clinical use as disease-modifying osteoarthritis drug? Ann Rheum Dis. 2013;72(2):157-61.

Supplementary Figures:

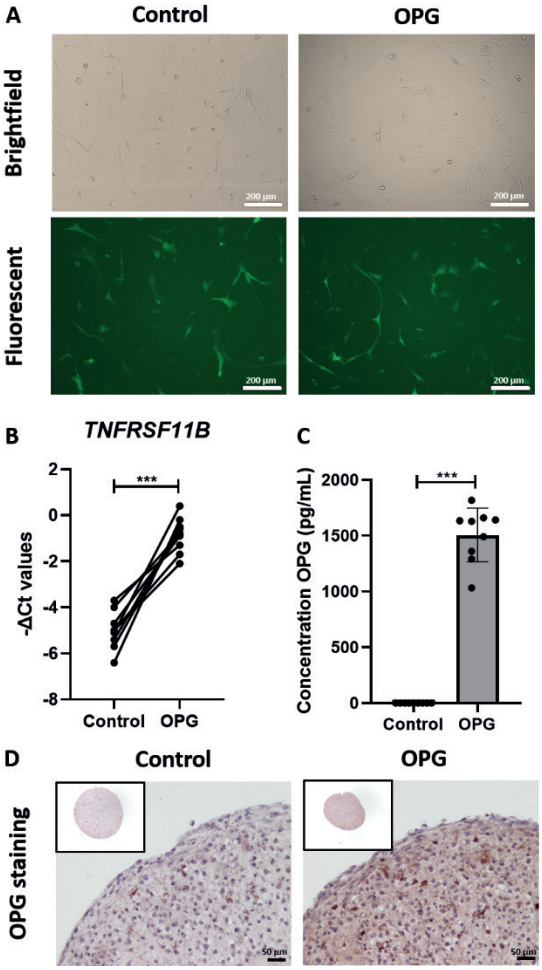

Supplementary Figure S1. Overexpression of *TNFRSF11B* in chondrocytes and quantification of the overexpression by RT-qPCR and ELISA at day 7. A) Representative brightfield and fluorescent images (GFP) of the transduction performed in chondrocytes of the control vector and of the *TNFRSF11B* gene. **B)** RT-qPCR of *TNFRSF11B* in the control samples against *TNFRSF11B* overexpression. **C)** Quantification of OPG (pg/mL) in collected medium measured by ELISA. **D)** OPG staining of the neo-cartilage matrix. Scale bars: 50 µm.

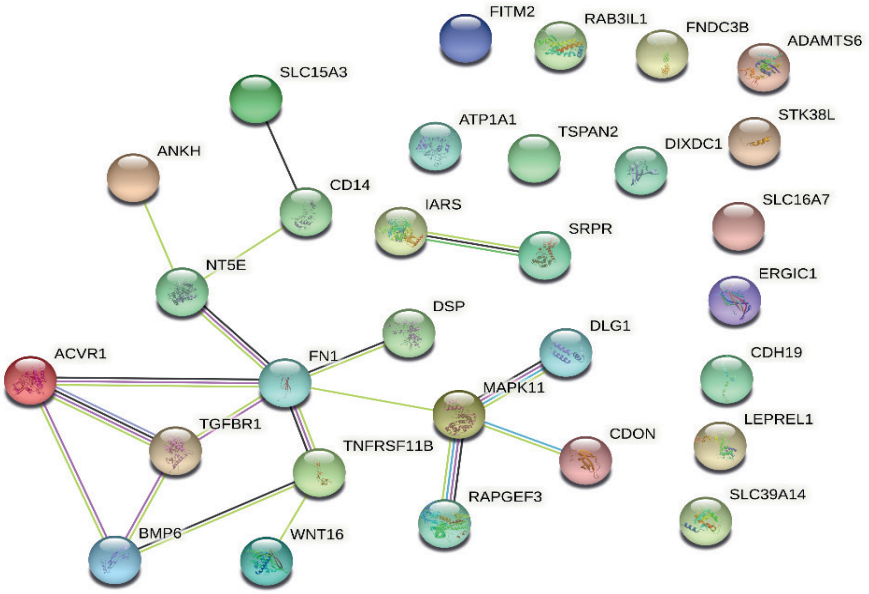

Supplementary Figure S2. Protein-protein interaction network of the 30 selected highly correlated genes to *TNFRSF11B* in STRING. 21 genes with a r≥|0.80|, and 9 genes with a r>|0.75| were added to the online available webtool STRING with a medium confidence interval of 0.4 and a PPI enrichment P-value of 2.11×10^{-6}.

Supplementary Tables:

Supplementary Table S1. Primer sequences of genes related to cartilage matrix, mineralization and highly correlated to *TNFRSF11B*.

	Primer Sequences	
Matrix Genes	**Fwd**	**Rvs**
ADAMTS5	5′-TGGCTCACGAAATCGGACAT-3′	5′-GCGCTTATCTTCTGTGGAACC-3′
ACAN	5′AGAGACTCACACAGTCGAAACAGC-3′	5′-CTATGTTACAGTGCTCGCCAGTG-3′
ARP	5′-CACCATTGAAATCCTGAGTGATGT-3′	5′-TGACCAGCCGAAAGGAGAAG-3′
COL10A1	5′-GGCAACAGCATTATGACCCA-3′	5′-TGAGATCGATGATGGCACTCC-3′
COL1A1	5′-GTGCTAAAGGTGCCAATGGT-3′	5′-ACCAGGTTCACCGCTGTTAC -3′
COL2A1	5′-CTACCCCAATCCAGCAAACGT-3′	5′-AGGTGATGTTCTGGGAGCCTT-3′
COMP	5′-ACAATGACGGAGTCCCTGAC-3′	5′-TCTGCATCAAAGTCGTCCTG-3′
GAPDH	5′-TGCCATGTAGACCCCTTGAAG-3′	5′-ATGGTACATGACAAGGTGCGG-3′
MMP13	5′-TTGAGCTGGACTCATTGTCG-3′	5′-GGAGCCTCTCAGTCATGGAG-3′
SOX9	5′-CCCCAACAGATCGCCTACAG-3′	5′-CTGGAGTTCTGGTGGTCGGT-3′
Mineralization genes	**Fwd**	**Rvs**
ALPL	5′-CAAAGGCTTCTTCTTGCTGGTG-3′	5′-CCTGCTTGGCTTTTCCTTCA-3′
ASPN	5′-ACACGTTTTGGAAATGAGTGC-3′	5′-GAACACCGTCACCCCTTCAA-3′
OGN	5′-TGATGAAATGCCCACGTGTC-3′	5′-TTTGGTAAGGGTGGTACAGCA-3′
POSTN	5′-TACACTTTGCTGGCACCTGT-3′	5′-TTTAAGGAGGCGCTGATCCA-3′
RUNX2	5′-CAATTTCCTCCTTGCCCCTCA-3′	5′-TCGGATCTACGGGAATACGCA-3′
SPP1	5′-GCCAGTTGCAGCCTTCTCA-3′	5′-AAAAGCAAATCACTGCAATTCTCA-3′
TNFRSF11A	5′-GAAGCTCAGCCTTTTGCTCA-3′	5′-GGGAACCAGATGGGATGTCG-3′
TNFRSF11B	5′-TTGATGGAAAGCTTACCGGGA-3′	5′-TCTGGTCACTGGGTTTGCATG-3′
TNFSF11	5′-CAACAAGGACACAGTGTGCAA-3′	5′-AGGTACAGTTGGTCCAGGGT-3′
***TNFRSF11B*-correlated genes**	**Fwd**	**Rvs**
ACVR1	AGGGCTCATCACCACCAATG	GTAATCTGGCGAGCCACTGT
ADAMTS6	5′-GGTGCAGATACCAAGAGGCT-3′	5′-GCCAGTCAATAGTCCAGGCA-3′
ANKH	5′-GTCTGCATGGCTCTGTCACT-3′	5′-AGGCAAAGTCCACTCCGATG-3′
ATP1A1	5′-TGTACCTGGGTGTGGTGCTA-3′	5′-ATCACAAGGGCTTGCTGAGG-3′
BMP6	5′-GCGGACATGGTCATGAGCTT-3′	5′-ACCTCACCCTCAGGAATCTG-3′
CD14	5′-AGCCACAGGACTTGCACTTT-3′	5′-TGCTTGGGCAATGCTCAGTA-3′
CDH19	5′-TGAGCACCAGAACCACTACG-3′	5′-AAGTGGTGGAAGCCTCAGTG-3′
CDON	5′-ACACCACTCTCTCAGGAGCA-3′	5′-AAGGTGGGAATAGCCACTGC-3′
DIXDC1	5′-CCCAGTCAGAAGAGAAGGCA-3′	5′-GCCGCCAGTCTCGAGATAAT-3′
DLG1	5′-TCTTCCCTCTCCTCCCACTG-3′	5′-GTACTGGGGGAGGATTTGCC-3′

***TNFRSF11B*-correlated genes**	**Fwd**	**Rvs**
DSP	5'-ATGTACTATTCTCGGCGCGG-3'	5'-GTGTTCTGGTTCTGGTGCCT-3'
ERGIC1	5'-TCTGCTGCTGCCTCTTCATC-3'	5'-CCTTGTCTGGGTCATCGACA-3'
FITM2	5'-ACTGATCACTCTGCTGTGGC-3'	5'-GCCATCAGAGGGAGGCATTT-3'
FN1	5'-CCGACCAGAAGTTTGGGTTC-3'	5'-CACGACCATTCCCAACACAC-3'
FNDC3B	5'-CCTGGAACCGTGTATCGCTT-3'	5'-GGTGCTTTGCATTGTCCAGG-3'
HLA-E	5'-GGCCTGGTTCTCCTTGGATC-3'	5'-GCTCCCTCCTTTTCCACCTG-3'
IARS	5'-GGTTGTCCACCAAGCTCCTT-3'	5'-GTTGTGAAGCAGCCTGAAGC-3'
MAPK11	5'-GCCGACCTGAACAACATCGT-3'	5'-TTCAGGTCCCGGTGGATGAT-3'
NT5E	5'-ATTGCACTGGGACATTCGGG-3'	5'-TGGAAGGTGGATTGCCTGTG-3'
P3H2	5'-AGAGAAGCCAAGCCACACAT-3'	5'-GCTTGTTCGAAGTGCCTGAT-3'
RAB3IL1	5'-CAGGAGCGTTGTCTGGAACA-3'	5'-CCAGTGGGTGCAGATTCAGA-3'
RAPGEF3	5'-TCCAGTGCTCATGACCCAAC-3'	5'-ATGGAAGTGGTGCAGAAGGG-3'
SLC15A3	5'-AGGACATCGCCAACTTCCAG-3'	5'-AGACCCTGCAGGACATAGGT-3'
SLC16A7	5'-GGACTCTTGGTGCCAACAGA-3	5'-ACCACAATCCAACCCCATCC-3'
SLC39A14	5'-GAAGGCCCTACTCAACCACC-3'	5'-GTGGGCAGTGAAGAGGTCTC-3'
SRPRA	5'-GGCGTTAATGGAGTGGGGAA-3'	5'-TCACAGGCAGCAATGAGGAC-3'
STK38L	5'-TGAAGAGAGAGAAACCAGGCAG-3'	5'-TTCTTTGCGAGCGTGTTGTG-3'
TGFBR1	5'-TGCAGACTTAGGACTGGCAG-3'	5'-GAGAACTTCAGGGGCCATGT-3'
TSPAN2	5'-CAGGGGAAAAGGCAATGGGA-3'	5'-GCTCCTTTGGGCATGTAGGT-3'
WNT16	5'-AACACCACGGGCAAAGAAAAC-3'	5'-ATCAACTTGGCGACAGCCT-3'

Supplementary table S2. Cartilage health and mineralization gene changes measured by RT-qPCR upon lentiviral induced overexpression of *TNFRSF11B* in a 3D *in vitro* chondrogenesis model. Significant data are highlighted in bold.

Cartilage health			**Mineralization**		
Genes	**FD**	**P value**	**Genes**	**FD**	**P value**
ACAN	1.21	$2.7x10^{-1}$	*ALPL*	4.22	$7.2x10^{-2}$
ADAMTS5	1.03	$3.0x10^{-1}$	***ASPN***	**2.61**	$\mathbf{1.0x10^{-2}}$
COL10A1	4.24	$6.3x10^{-1}$	***OGN***	**1.68**	$\mathbf{2.3x10^{-2}}$
COL1A1	**1.88**	$\mathbf{1.3x10^{-2}}$	***POSTN***	**1.75**	$\mathbf{4.0x10^{-2}}$
COL2A1	**4.77**	$\mathbf{4.8x10^{-4}}$	***RUNX2***	**4.51**	$\mathbf{4.0x10^{-3}}$
COMP	**0.69**	$\mathbf{2.0x10^{-2}}$	*SPP1*	1.94	$1.6x10^{-1}$
MMP13	**14.76**	$\mathbf{2.0x10^{-3}}$	*TNFRSF11A*	2.45	$7.8x10^{-1}$
SOX9	1.02	$4.3x10^{-1}$	*TNFSF11*	1.06	$3.9x10^{-1}$

Supplementary table S3. 51 *TNFRSF11B*-correlated genes from RNA-seq data with an r-value higher than 0.75.

Genes highly correlated to *TNFRSF11B*			
R-value	**Gene**	**R-value**	**Gene**
0.88	*CDH19*	-0.78	*PARP10*
0.87	*ATP1A1*	0.78	*ADGRG2*
0.85	*DIXDC1*	-0.78	*CD14*
0.85	*FN1*	-0.77	*SNCG*
0.84	*STK38L*	0.77	*GLP2R*
0.84	*ANKH*	0.77	*R3HDML*
0.84	*TGFBR1*	0.77	*SLC16A7*
0.83	*CDON*	0.77	*BMP6*
0.82	*NT5E*	0.76	*CDK2AP1*
-0.81	*SLC15A3*	0.76	*PAPSS2*
0.81	*ERGIC1*	-0.76	*RAPGEF3*
0.81	*ADAMTS6*	0.76	*CDH10*
0.81	*DSP*	0.76	*IARS*
-0.81	*MAPK11*	0.76	*SLC7A1*
0.80	*SLC39A14*	0.76	*CD109*
0.80	*TSPAN2*	0.76	*PGM2L1*
0.80	*DLG1*	0.76	*TES*
-0.80	*HLA.E*	0.76	*FITM2*
0.80	*SRPRA*	0.76	*CLVS2*
0.79	*P3H2*	-0.76	*FLOT2*
-0.79	*RAB3IL1*	0.75	*ACVR1*
0.79	*DSG2*	0.75	*PPP4R4*
0.79	*TMCO3*	0.75	*GALNT7*
0.79	*SLC1A1*	0.75	*RCAN3*
0.78	*RFTN2*	0.75	*WNT16*
0.78	*FNDC3B*		

Supplementary table S4. Genes highly correlated to *TNFRSF11B* analyzed by RT-qPCR upon lentiviral induced overexpression of *TNFRSF11B* in a 3D *in vitro* chondrogenesis model. Significant data are highlighted in bold.

Expression of genes highly correlated to *TNFRSF11B*					
Genes	**FD**	**P value**	**Genes**	**FD**	**P value**
CDH19	**1.53**	**$4.5x10^{-2}$**	*TSPAN2*	1.23	$1.5x10^{-1}$
ATP1A1	1.01	$6.3x10^{-1}$	*DLG1*	1.06	$6.8x10^{-1}$
DIXDC1	1.13	$7.7x10^{-1}$	*HLA.E*	1.04	$9.0x10^{-1}$
FN1	1.34	$3.0x10^{-1}$	*SRPRA*	1.27	$2.3x10^{-1}$
STK38L	1.23	$3.6x10^{-1}$	***P3H2***	**1.48**	**$4.7x10^{-2}$**
ANKH	1.34	$1.8x10^{-1}$	*RAB3IL1*	1.30	$9.5x10^{-1}$
TGFBR1	1.10	$8.6x10^{-1}$	***BMP6***	**9.34**	**$2.6x10^{-2}$**
CDON	**2.03**	**$5.0x10^{-3}$**	***WNT16***	**0.81**	**$4.3x10^{-2}$**
NT5E	1.29	$2.5x10^{-1}$	*ACVR1*	1.31	$5.5x10^{-1}$
SLC15A3	**0.40**	**$4.0x10^{-3}$**	*FNDC3B*	1.19	$3.0x10^{-1}$
ERGIC1	1.12	$4.7x10^{-1}$	*CD14*	1.38	$4.8x10^{-1}$
ADAMTS6	1.20	$5.4x10^{-1}$	***SLC16A7***	**1.97**	**$1.8x10^{-2}$**
DSP	0.92	$1.8x10^{-1}$	*RAPGEF3*	1.36	$6.6x10^{-1}$
MAPK11	1.94	$4.5x10^{-1}$	*IARS*	1.26	$1.1x10^{-1}$
SLC39A14	1.03	$9.6x10^{-1}$	***FITM2***	**2.28**	**$1.4x10^{-2}$**

CHAPTER 3

Cartilage from human induced pluripotent stem cells: comparison with neo-cartilage from chondrocytes and bone marrow mesenchymal stromal cells

Alejandro Rodríguez Ruiz[1], Amanda Dicks[2], Margo Tuerlings[1], Koen Schepers[3], Melissa van Pel[3,4], Rob GHH Nelissen[5], Christian Freund[6,7], Christine Mummery[6,7], Valeria Orlova[6], Farshid Guilak[2], Ingrid Meulenbelt[1], and Yolande FM Ramos[1]

[1]Dept. of Biomedical Data Sciences, Section Molecular Epidemiology, Leiden University Medical Center, LUMC, Leiden, The Netherlands; [2]Dept. Orthopedic Surgery, Washington University and Shriners Hospitals for Children, St. Louis, USA; [3]Dept. Immunohematology and Blood transfusion, LUMC; [4]NECSTGEN, Leiden, The Netherlands; [5]Dept. Orthopaedics, LUMC; [6]Dept. Anatomy, LUMC; [7]LUMC hiPSC Hotel.

Cell and Tissue Research. 2021 Nov;386(2):309-320.

ABSTRACT:

Objectives: Cartilage has little intrinsic capacity for repair, so transplantation of exogenous cartilage cells is considered a realistic option for cartilage regeneration. We explored whether human-induced pluripotent stem cells (hiPSCs) could represent such unlimited cell sources for neo-cartilage comparable to human primary articular chondrocytes (hPACs) or human bone marrow derived mesenchymal stromal cells (hBMSCs).

Methods: Chondroprogenitor cells (hiCPCs) and hiPSC-derived mesenchymal stromal cells (hiMSCs) were generated from two independent hiPSC lines and characterized by morphology, fow cytometry, and differentiation potential. Chondrogenesis was compared to hBMSCs and hPACs by histology, immunohistochemistry, and RT-qPCR, while similarities were estimated based on Pearson correlations using a panel of 20 relevant genes.

Results: Our data show successful differentiations of hiPSC into hiMSCs and hiCPCs. Characteristic hBMSC markers were shared between hBMSCs and hiMSCs, with the exception of CD146 and CD45. However, neo-cartilage generated from hiMSCs showed low resemblances when compared to hBMSCs (53%) and hPACs (39%) characterized by lower collagen type 2 and higher collagen type 1 expression. Contrarily, hiCPC neo-cartilage generated neo-cartilage more similar to hPACs (65%), with stronger expression of matrix deposition markers.

Conclusion: Our study shows that taking a stepwise approach to generate neo-cartilage from hiPSCs via chondroprogenitor cells results in strong similarities to neo-cartilage of hPACs within 3 weeks following chondrogenesis, making them a potential candidate for regenerative therapies. Contrarily, neo-cartilage deposited by hiMSCs seems more prone to hypertrophic characteristics compared to hPACs. We therefore compared chondrocytes derived from hiMSCs and hiCPCs with hPACs and hBMSCs to outline similarities and differences between their neo-cartilage and establish their potential suitability for regenerative medicine and disease modelling.

Key messages:

- Neo-cartilage deposited from hiCPCs is 65% similar to hPAC neo-cartilage with stronger expression of matrix deposition markers.
- Neo-cartilage deposited from hiMSCs shows a 53% similarity to hBMSCs with higher expression of hypertrophic markers.

INTRODUCTION

Articular cartilage, the smooth and lubricated tissue lining the end of long bones, plays an important role in mobility by ensuring frictionless articulation while withstanding compressive forces during joint loading. It is composed entirely of chondrocytes, responsible for maintaining tissue homeostasis upon stress, by synthesizing a dense cartilage extracellular matrix (ECM), rich in collagens, proteoglycans, and sulphated glycosaminoglycans (s-GAGs) (1, 2). However, due to a lack of blood supply or lymphatic vessels, cartilage is essentially unable to regenerate, contributing to development of diseases such as osteoarthritis (OA) (3, 4) and making cartilage regeneration therapies essential to fighting this debilitating condition. Some therapies, based on administering human primary articular chondrocytes (hPACs) and/or mesenchymal stromal cells (MSCs), have been shown to produce stable and healthy neo-cartilage that can be used in implants and for *in vitro* disease models (5-7).

Previously, we showed the potential of hPAC-derived neo-cartilage for cartilage regeneration based on their 99% similarity of genome-wide methylation to autologous cartilage (8). While autologous neo-cartilage would avoid the immunogenic response that allogenic cells may cause, this technique is relatively invasive for patients since, prior to implantation, a biopsy of the articular cartilage is needed. Alternatively, MSCs can be obtained from several tissues and have the potential to differentiate into relevant cells. Nonetheless, the procedure to obtain them is still invasive, and has a large variability in differentiation efficiency and early senescence in *in vitro* cultures (7, 9, 10).

Human induced pluripotent stem cells (hiPSCs) have been proposed to provide an excellent alternative for both cartilage regeneration and disease modeling applications (11). Firstly, their production can be scaled, circumventing restrictions in defect size for treatments in the clinic and during disease modeling. Secondly, the use of a cell line circumvents the need for biopsies and thus repeated surgeries on patients. Finally, hiPSCs can be genetically modified to increase chondrogenic potential, introduce patient specific mutations for research purposes, and/or reduce their immunogenicity. Nonetheless, obtaining good quality neo-cartilage from hiPSCs has so far proven challenging.

Issues arise due to the strong variation in differentiation efficiencies between hiPSC lines and clones and a tendency to generate hypertrophic and fibrous matrix (7, 12). Hence, even though several protocols are available, the optimal method for the generation of chondrocytes from hiPSCs remains to be established. Some studies comparing human bone marrow-derived mesenchymal stromal cells (hBMSCs) and hiPSC-derived mesenchymal stromal cells (hiMSCs) suggest major functional and genetic differences, not only between cells but also between neo-

cartilage from both cell types (13, 14). However, in these studies, hiMSCs were generated via the formation of cell aggregates called embryoid bodies (EBs), often variable and with low efficiency (13, 14) while direct monolayer generation was shown to be more robust (15).

Alternatively, a stepwise approach could be taken to generate neo-cartilage from hiPSCs via human chondroprogenitor cells (hiCPCs) (16-18). Notably, differentiation of hiPSCs with this protocol optimizes each developmental step through anterior primitive streak formation and successive emergence of hiCPCs, diminishing variability between independent differentiations. Unfortunately, a major disadvantage of this method is the inefficiency to expand hiCPCs, mainly due to the rapid loss of their chondrogenic potential within a few passages (17).

Here, we aimed to assess upon both approaches towards consistent generation of neo-cartilage from hiPSC with characteristics similar to chondrocytes from hPACS and hBMSCs (the 'gold standard'). We therefore compared chondrocytes derived from hiMSCs and hiCPCs with hPACs and hBMSCs to outline similarities and differences between their neo-cartilage and establish their potential suitability for regenerative medicine and disease modelling.

MATERIALS AND METHODS

Tissue culture and chondrogenesis

Cell culture of hiPSCs and primary cells

Two independent control hiPSC lines were used in the current study. Approval for the generation of hiPSCs from skin fibroblasts of healthy donors is available under number P13.080. Cells were generated from skin fibroblasts of a female: LUMC0030iCTRL12 (030) and a male: LUMC0004iCTRL10 (004) by the LUMC hiPSC core facility and registered at the Human pluripotent stem cell registry. Cells were characterized according to pluripotent potential and spontaneous differentiation capacity by the hiPSC core facility (20) and were karyotyped after 15 passages in culture.

hiPSCs were maintained under standard conditions (37°C, 5% CO_2) in TeSR-E8 medium (STEMCELL Technologies) on VitronectinXF-coated plates (STEMCELL Technologies). The medium was refreshed daily and cells were passaged in aggregates using Gentle Cell Dissociation Reagent (STEMCELL Technologies) upon reaching approximately 80% confluency. Human BMSCs and hPACs were collected from OA patients undergoing joint replacement surgery as part of the RAAK study. Collection and expansion of the primary cells has been previously described (8). Cells were counted with the Nucleocounter NC-200 (Chemometec).

Differentiation of hiPSC towards hiMSCs and hiCPCs

Human iMSCs were generated using the Stemcell Technologies Mesenchymal Progenitor Kit following the manufacturers' instructions with small modifications. Following three passages using the recommended Mesencult ACF plus medium, cells were grown in DMEM high glucose (Gibco) supplemented with 10% fetal calf serum (FCS; Biowest), basic FGF (bFGF; 5ng/ml; Life Technologies), and antibiotics (100U/ml penicillin, 100µg/ml streptomycin; Gibco) until elongated and with fibroblast-like morphology. At passage 5, MSC surface markers were analyzed by flow cytometry, and the trilineage potential of the hiMSCs was determined. Generation of hiCPCs was performed as described previously (17). At day 14, analysis for cell surface markers was performed, and hiCPC aggregates were collected for chondrogenesis (**Supplementary Figure 1**).

Multilineage Differentiations

For adipogenesis, $1.5x10^4$ cells/cm^2 were seeded on tissue culture-treated 6-well plates (Cellstar), and differentiation was induced in α-MEM (Gibco) supplemented with 10% FCS, antibiotics, dexamethasone (0.25µM; Sigma-Aldrich), L-ascorbate-2-phosphate (50µg/ml; Sigma-Aldrich), insulin (100µg/ml; Sigma-Aldrich), indomethacin (50µM; Sigma-Aldrich), and 1-methyl-3-isobutylxantine (0.5mM; Sigma-Aldrich). Medium was refreshed twice a week for 21 days.

Chondrogenesis was performed in 3D cell pellets following our established protocol (21). In short, cell pellets (hBMSCs, hiMSCs, hPACs) were maintained in DMEM high glucose (Gibco) supplemented with 1% ITS-plus (Corning), dexamethasone (100nM), L-ascorbate-2-phosphate (50µg/ml), L-proline (40µg/ml; Sigma-Aldrich), sodium pyruvate (100µg/ml; Sigma-Aldrich), TGF-β1 (10ng/ml; PeproTech), and antibiotics. The medium was refreshed every 3–4 days. Chondrogenesis for hiCPCs was performed basically as described by Dicks *et al. [17]:* cell aggregates were maintained in DMEM/F-12 (Gibco) supplemented with 1% ITS-plus, 2-Mercaptoethanol (55µM; Gibco), dexamethasone (100nM), 1% non-essential amino acids (NEAA; Gibco), L-ascorbate-2-phosphate (50µg/ml), L-proline (40µg/ml), TGF-β1 (10ng/ml), and antibiotics, for 21 days while refreshing medium every 3-4 days. Note that due to their initial stem cell state, hBMSCs and hiMSCs require an extended period for chondrogenesis and deposition of mature cartilage ECM (35 days) as compared to hPACs and hiCPCs (21 days).

Osteogenesis was induced by maintaining day-21 chondrogenic pellets for an additional 14 days with α-MEM supplemented with 10% heat-inactivated FCS, dexamethasone (0.1µM), L-ascorbate-2-phosphate (50µg/ml), b-Glycerophosphate (5mM; Sigma-Aldrich), and antibiotics.

Flow cytometric analyses

Human BMSCs and hiMSCs were analyzed for the following panel of surface markers: CD31, CD45, CD73, CD90, CD105, CD146, and CD166 (BD Biosciences). Human iCPCs were analyzed for CD45, CD90, CD146, and CD166. LIVE/DEAD fixable Aqua Dead Cell stain kit (Thermofisher) was used to define dead cells, and OneComp ebeads (Thermofisher) were used to compensate for the fluorochromes. Data were obtained using the BD LSR-II Flow Cytometer and analyzed with FlowJo 6.0 software.

RNA isolation and RT-qPCR

Differentiations with hiPSC lines were performed in triplicate. For RNA isolations, two pellets were pooled, and isolation was performed as described previously (21). Total mRNA (150 ng) was processed with a first strand cDNA kit according to the manufacturer's protocol (Roche Applied Science). cDNA was further diluted five times, and preamplification with TaqMan preamp master mix (Thermo Fisher Scientific Inc.) was performed for a panel of 20 designated genes related to chondrogenesis, hypertrophy, deposition and degradation of cartilage ECM, and neo-cartilage quality (primer sequences in **Supplementary Table S1**). Gene expression was measured with a Fluidigm Biomark HD machine using a 96.96 IFC chip. Quality control of the data was performed, and non-detected values were imputed according to the minimum detected value. Unsuccessful differentiations, defined by the minimum detected expression of *COL2A1* for hPACs and hBMSCs neo-cartilage, were disregarded.

Histology and immunohistochemistry

Tissues (neo-cartilage and neo-bone) were fixed in 4% formaldehyde and embedded in paraffin. After sectioning, slides were deparaffinized and rehydrated prior to histology or immunohistochemistry.

Overall cellular and tissue structure was visualized with hematoxylin-eosin (HE) staining. Glycosaminoglycans were visualized by staining with 1% Alcian Blue 8-GX (Sigma-Aldrich) and Nuclear Fast red staining (Sigma-Aldrich). Calcium deposits were stained with 2% Alizarin Red S (Sigma-Aldrich).

To detect COL2 (MAB1330; Millipore; 1:100 in TBST/10% normal goat serum, overnight at 4°C), COL1 (ab34710; Abcam; 1:1000 in TBST/10% normal goat serum, overnight at 4°C), and COL10 (x53/2031501005; Quartett; 1:100 in TBST/10% normal goat serum, overnight at 4°C), immunohistochemistry was performed with 3-diaminobenzidine (DAB) solution (Sigma-Aldrich) and hematoxylin (Klinipath) as described before (21).

Lipid droplets were stained for 10 minutes with Oil-Red-O solution (Sigma-Aldrich) after fixation of the cells in 4% formaldehyde. To reduce the background, the following staining cells were gently washed with 60% isopropanol and distilled water.

Statistics and similarities

Relative gene expression (−ΔCt values) were calculated using levels of glyceraldehyde 3-phosphate dehydrogenase (*GAPDH*) and acidic ribosomal phosphoprotein P0 (*ARP*) as housekeeping genes. Betas, standard errors (SE), and P-values for gene expression differences across cell types were determined by applying generalized estimation equations (GEE; IBM SPSS software). P-values <0.05 were considered statistically significant.

Similarities between the different cell types and differentiations were calculated based on Pearson correlations using a panel of 20 relevant genes.

RESULTS

Generation and characterization of hiMSCs

Two independent control hiPSC lines, well-characterized by morphology, pluripotent status, spontaneous differentiation capacity, and by karyotyping, were used for this study (**Supplementary Figure S2** and Ref. (20)). Cells were differentiated towards hiMSCs and compared to hBMSCs after five passages. Expression of typical MSC surface markers as defined by the International Society of Cellular Therapy (ISCT: presence of CD73, CD90, CD105; absence of CD31, CD45 (22)) and expression of CD146 and CD166 (expressed in chondroprogenitor cells (18)) were assessed by flow cytometry (**Figure 1a-b**). Highly comparable expression was observed for CD73, CD90, CD105, and CD166 between hiMSCs and hBMSCs, while cells were negative for CD31. Significant differences, however, were found for CD146 and CD45. Both markers were expressed in a larger percentage of the hiMSC population compared to 44% and 9% in hBMSCs, respectively (CD146: for hiMSC-030 and hiMSC-004 resp. 98% and 96%, P-value=3.06×10^{-7} and 1.39×10^{-6}; CD45: for hiMSC-030 and hiMSC-004 resp. 29% and 28% with P-value=1.38×10^{-9} and 0×10^{-0}). **Figure 1c-1d** shows morphology of hiMSCs, with majority of the cells being spindle-shaped, elongated, and fibroblast-like. Importantly, hiMSCs showed tri-lineage differentiation into fat (Oil red, **Fig c'-d'**), bone (Alizarin red, **Fig c''-d''**), and cartilage (Alcian blue, **Fig c'''-d'''**), as confirmed by histology. Altogether, our analyses confirmed successful differentiation of hiPSCs into a mesenchymal stromal cell type.

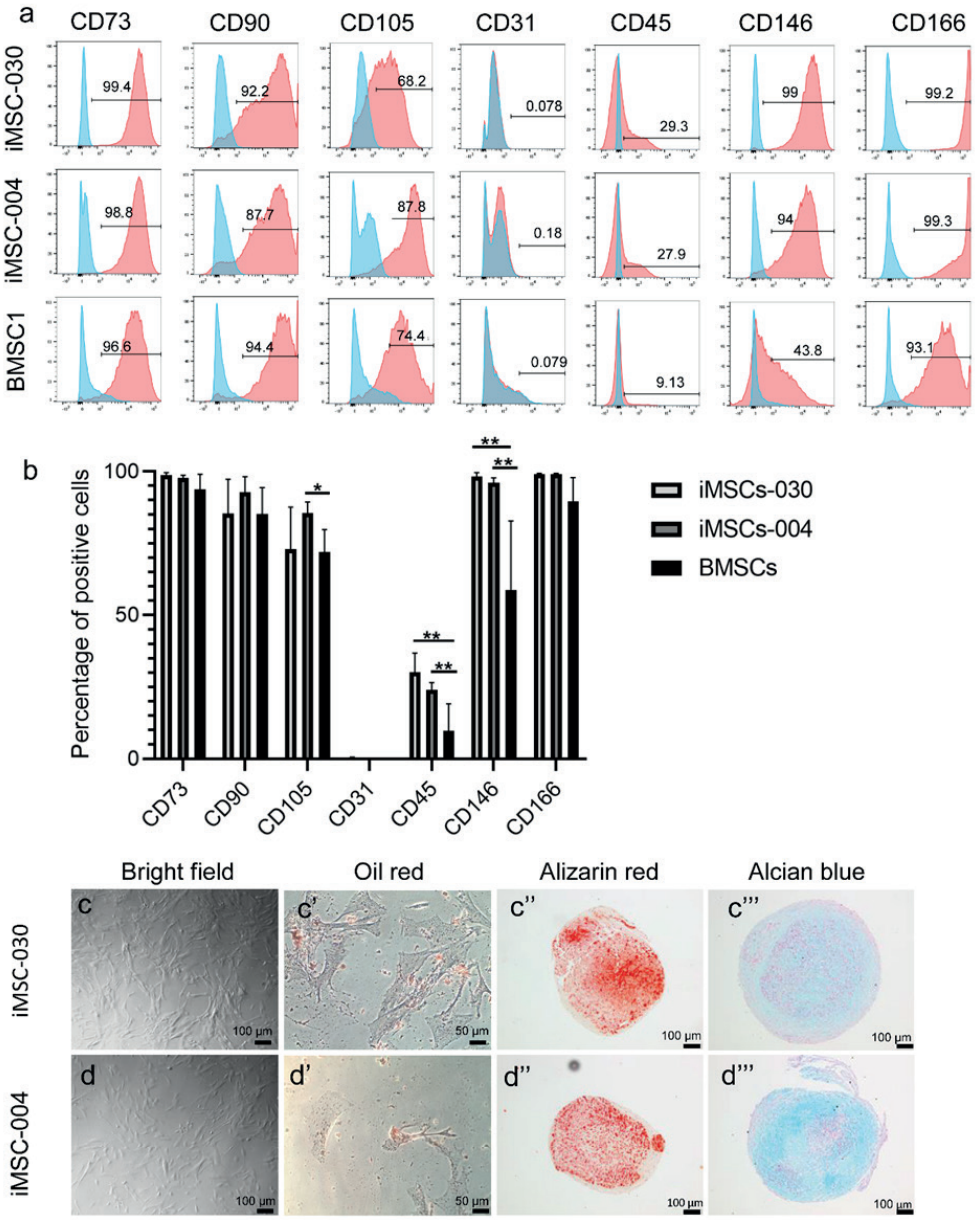

Figure 1. Characterization of hiMSCs. a-b) Flow cytometry analysis of MSC characteristic markers. The blue histogram shows unstained cells, while the red histogram shows specific marker cell staining. Results shown are the average of three independent differentiations with their standard deviation for each hiPSC line and for three hBMSC lines (hiMSC-030: CD146: **P-value= 3.06×10^{-7} and CD45, **P-value=5.93×10^{-10}; hiMSC-004: CD146, **P-value=1.39×10^{-6}; CD45, **P-value=0×10^{-0} and CD105, *P-value=4.18×10^{-4}). **c-d**) Bright field microscopy image of hiMSCs and representative images for trilineage differentiation. Human iMSCs show a fibroblastic and spindle-shaped morphology (**c-**

d); adipocytes were stained by Oil red (**c'-d'**), osteocytes by Alizarin red (**c''-d''**), and chondrocytes by Alcian blue (**c'''-d'''**).

Generation and characterization of hiCPCs

Control hiPSCs were differentiated towards hiCPCs. After 14 days, analysis of cell surface markers showed similar expression of CD45, CD90, and CD166 across both hiPSC lines (**Figure 2a-b-c**). However, CD146 was expressed within a lower percentage of hiCPC-030 as compared to hiCPC-004 (10% versus 20%, P-value=5.1×10^{-3}). Notably, overall percentages of CD90, CD146, and CD166 positive cells appeared smaller than compared to the hiMSCs, while the percentage of CD45-positive hiCPCs was relatively large (38% and 25% among hiCPCs-004 and hiCPCs-030, respectively). **Figure 2d** shows cell morphology, indicating population heterogeneity and spontaneous cell aggregation as arises during the hiCPC-generating process.

Histochemistry analysis of neo-cartilage

Prior to quantitative gene expression analyses, general neo-cartilage pellet formation and cellular structures of hiMSCs and hiCPCs was compared to that of hBMSCs and hPACs by HE and Alcian Blue staining. Following 35 days of chondrogenesis, HE staining of hiMSC neo-cartilage showed the presence of a core with higher number of cells, concurrent with less matrix as compared to hBMSC-derived neo-cartilage (**Figure 3a-f**). Yet, the presence of lacunae can be observed in the hiMSC neo-cartilage, indicating successful generation of cartilage ECM as also confirmed by the Alcian Blue staining (**Figure 3b-g**). To reduce heterogeneity of hiCPC population, 3D pellets were generated starting from cell aggregates (such as indicated in **Figure 2d-d'**). HE staining showed relatively homogeneous ECM deposition, lacunae formation, but also off-target cells on the outer surface of some hiCPC pellets (**Figure 3f'**, hiCPC-004). When comparing hiCPC- and hPAC-derived neo-cartilage, Alcian Blue staining seemed more intense and homogenous as compared to that of hiMSCs and hBMSCs (compare **Figure 3b-b''** and **3g-g''**).

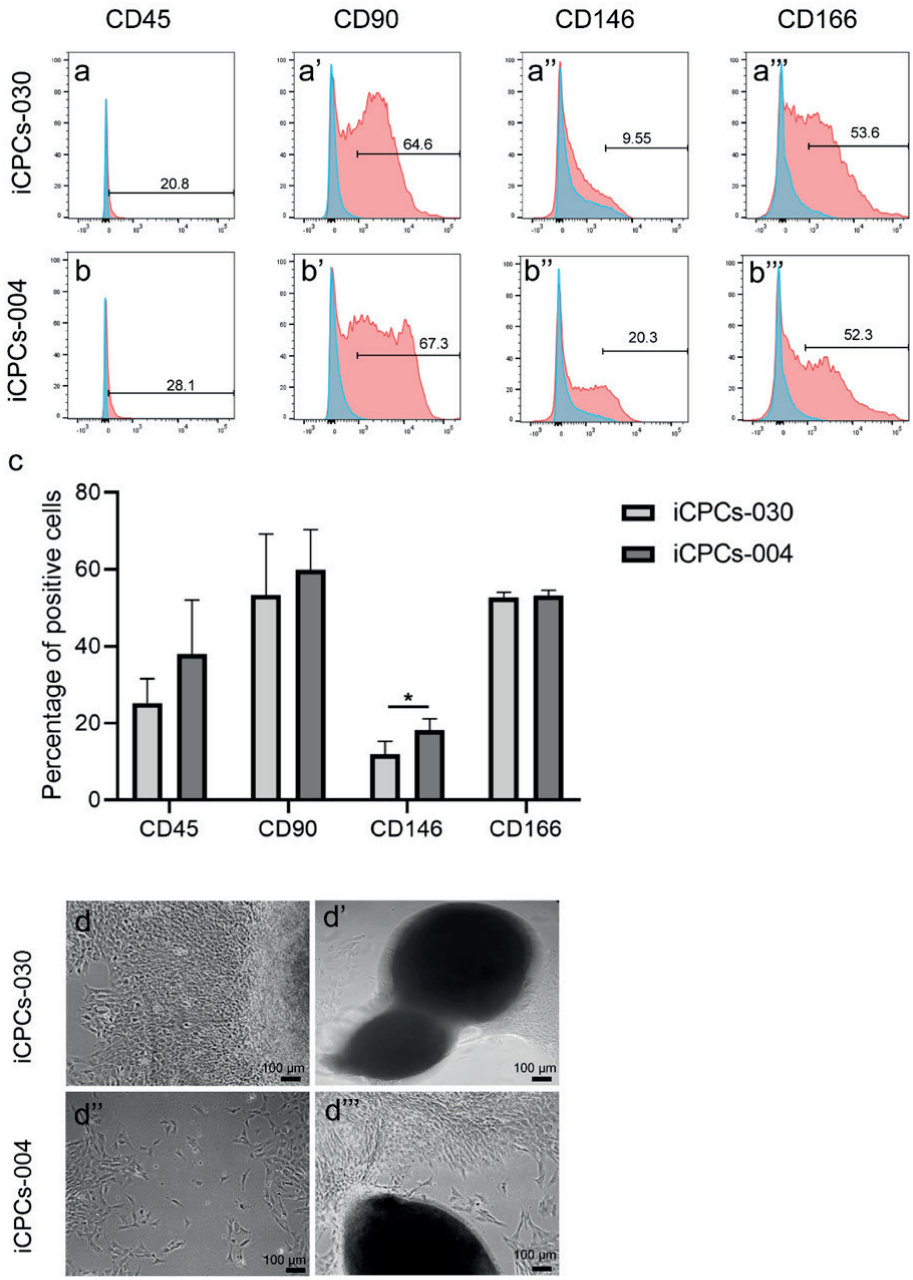

Figure 2. Characterization of hiCPCs. a, b, c) Flow cytometry analysis of CD45, CD90, CD146, and CD166 for hiCPCs. Results shown are the average of independent differentiations for each hiPSC line (n=2, *P-value=5.1x10^{-3}). **d**) Bright field microscopy image of hiCPCs showing cells growing in monolayer and cell aggregates following 14 days in differentiation.

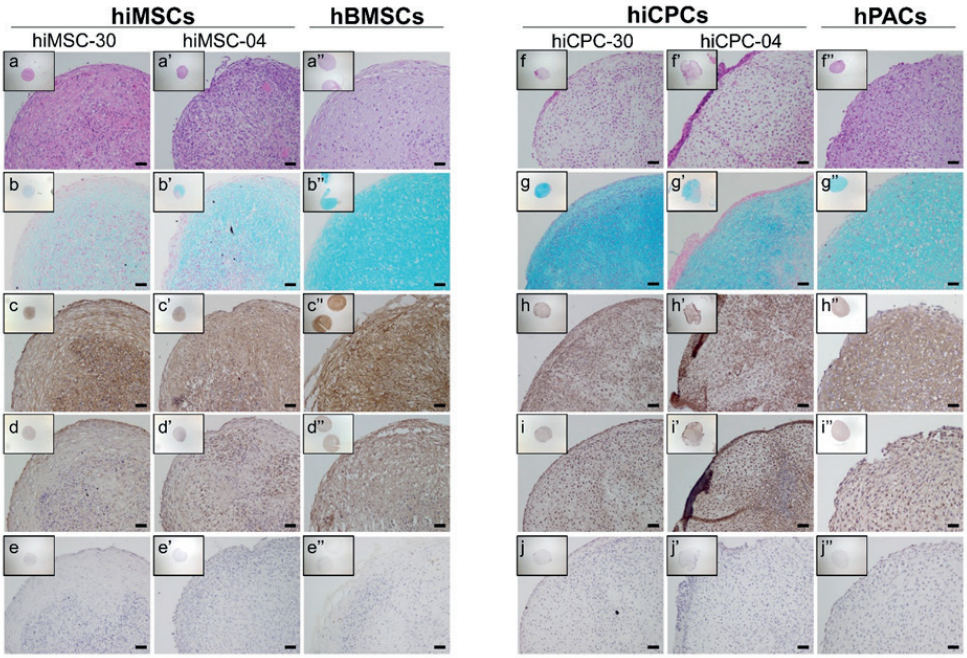

Figure 3. Histology and immunohistochemistry of neo-cartilage. Representative images of neo-cartilage generated by hiMSCs and hBMSCs after 35 days of chondrogenesis (**a-e**), or by hiCPCs and hPACs following 21 days of chondrogenesis (**f-j**), stained with H&E (**a** and **f**), Alcian Blue (**b** and **g**), COL1 (**c** and **h**), COL2 (**d** and **i**), and COL10 (**e** and **j**). Scale bars: 50 µm.

Gene expression profiles and immunohistochemistry of hiMSC-, hBMSC-, and hPAC-derived neo-cartilage

To characterize chondrogenesis efficiency, RT-qPCR was performed of hiMSC- and hBMSC-derived neo-cartilage (day 35) and hPAC-derived neo-cartilage (day 21). Fold differences were calculated for chondrocyte-specific genes relative to hBMSCs-derived neo-cartilage (**Table 1** and **Figure 4**). While the expression of *COL2A1* only showed a trend towards lower expression (FD=-17.2, P-value=9.0×10^{-2}), significantly lower levels of matrix gene *ACAN* (FD=-21.8, P-value=1.1×10^{-2}) and chondrogenic transcription factor *SOX9* (FD=-3.9, P-value=2.6×10^{-2}) were expressed in hiMSC-derived neo-cartilage compared to that from hBMSCs. Additionally, in hiMSCs-derived neo-cartilage, *EPAS1* was significantly lower (FD=-5.7, P-value=9.8×10^{-3}), and hypertrophic cartilage marker *COL10A1* was very lowly expressed (FD=-4092.3, P-value=0.0×10^{-0}).

Based on the gene expression profiles, we determined that following 35 days of chondrogenesis, neo-cartilage pellets derived from hiMSCs and hBMSCs were 53% similar (SD=16; see **Supplementary Table S2a** for complete overview

of hiMSC-hBMSC similarities). Since the similarity was not very strong, we questioned whether differentiated hiMSCs were more comparable to hPACs. However, based on the expression profile of our gene panel, we found only 39% similarity (SD=20; see **Supplementary Table S2c** for a complete overview of hiMSC-hPAC similarities). In fact, the majority of the genes here assessed (14 out of 20; **Table 2**) were significantly different expressed between hiMSC- and hPAC-derived neo-cartilage. Specifically, expression of matrix genes such as *COL2A1* (FD=-10.5, P-value=$4.2x10^{-2}$) and *ACAN* (FD=-29.5, P-value=$7.6x10^{-3}$) were lower, while catabolic and mineralization genes such as *MMP13* (FD=123.2, P-value=$1.4x10^{-3}$), *COL1A1* (FD=5.5, P-value=$1.7x10^{-3}$), and *ALPL* (FD=51.7, P-value=$1.4x10^{-3}$) were higher expressed. Altogether, this suggests that during chondrogenesis, hiMSCs deposit neo-cartilage of inferior quality as compared to that of hPACs.

Although inherently less sensitive to gene expression levels, hence less suitable for quantitative analyses, immunohistochemistry of COL1, COL2 and COL10 was performed to allow visualization of protein localization for hBMSC- and hiMSC-derived neo-cartilage. As it can be seen in **Figure 3c-c"**, COL1 in hiMSC-derived neo-cartilage seemed to be particularly localized in the surrounding of cells and at the core of the neo-cartilage pellet, while BMSC-derived neo-cartilage showed a homogeneous staining across the matrix. COL2 staining of hiMSC-derived neo-cartilage as compared to BMSC-derived neo-cartilage showed more variability, while being particularly localized, across all the different cell lines, in the cytoplasm and not in the ECM (**Figure 3d-d"**). With respect to COL10A1 protein expression, staining intensity was generally low similar to the *COL10A1* gene expression (**Figure 3e-e"**).

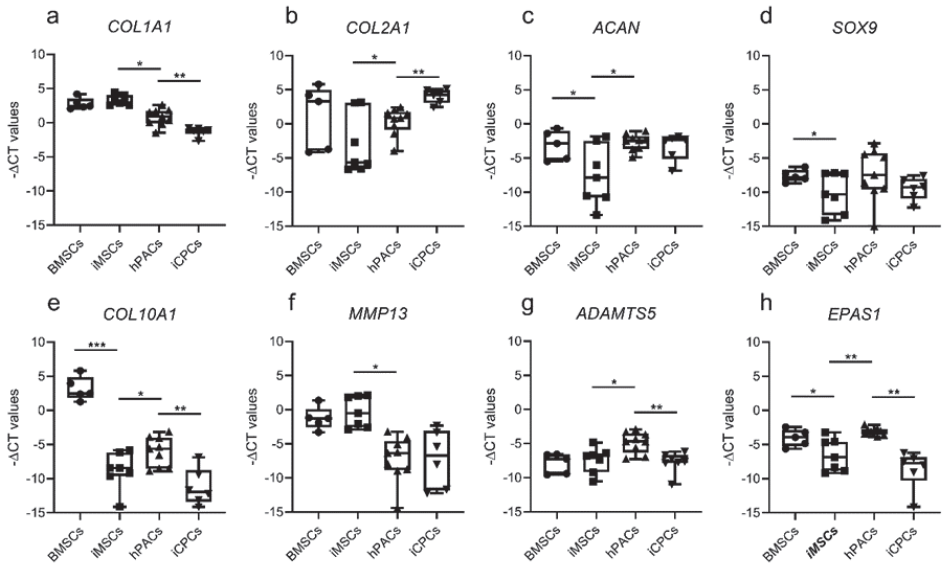

Figure 4. Boxplots for -ΔCt values of matrix, hypertrophy and chondrogenic genes (a-h) as indicated between hiMSCs and hBMSCs, hiMSCs and hiCPCs, and hiCPCs and hPACs, following 35 days (hBMSCs, hiMSCs) and 21 days (hPACs, hiCPCs) of chondrogenesis (n=5-7; * P-value< 0.05; ** P-value< 10^{-4}; *** P-value< 10^{-6}.).

Table 1. Differences in gene expression between hiMSC-and hBMSC-derived neo-cartilage at week 5. Significant data are highlighted in bold.

hiMSCs versus hBMSCs neo-cartilage				
Matrix genes	**FD**	**Beta**	**SE**	**P value**
ACAN	**-21.8**	**-4.4**	**1.7**	**$1.1x10^{-2}$**
COL2A1	-17.2	-4.1	2.4	$9.0x10^{-2}$
COL1A1	1.4	0.5	0.4	$2.7x10^{-1}$
COL10A1	**-4092.3**	**-12.0**	**1.2**	**$0.0x10^{+0}$**
Hypertrophy genes	**FD**	**Beta**	**SE**	**P value**
ADAMTS5	1.4	0.5	0.9	$5.9x10^{-1}$
MMP13	2.0	1.0	1.0	$3.5x10^{-1}$
EPAS1	**-5.7**	**-2.5**	**1.0**	**$9.8x10^{-3}$**
WWP2	-1.2	-0.3	0.3	$2.8x10^{-1}$
ALPL	-3.1	-1.6	1.3	$2.1x10^{-1}$
Chondrogenesis genes	**FD**	**Beta**	**SE**	**P value**
SOX5	-3.9	-2.0	1.3	$1.3x10^{-1}$
SOX6	-2.2	-1.1	0.9	$2.2x10^{-1}$
SOX9	**-3.9**	**-2.4**	**1.1**	**$2.6x10^{-2}$**

hiMSCs versus hBMSCs neo-cartilage				
FGFR2	**-22.0**	**-4.5**	**1.6**	**$5.9x10^{-3}$**
NOTCH1	1.5	0.6	0.8	$5.0x10^{-1}$
NOTCH3	-2.9	-1.5	0.9	$6.9x10^{-2}$
SMAD3	1.4	0.5	0.5	$3.3x10^{-1}$
SMAD7	1.0	0.0	0.5	$9.7x10^{-1}$
GDF5	1.6	0.2	0.5	$6.4x10^{-1}$
PRG4	-5.0	-0.4	0.7	$6.0x10^{-1}$
NFAT5	**-1.5**	**-0.6**	**0.3**	**$1.9x10^{-2}$**

Characterization of differences between hiCPC- and hPAC-derived neo-cartilage

Subsequently, hiCPC chondrogenesis was characterized. In contrast to hBMSCs, hiCPCs already showed a strong deposition of cartilage ECM at day 21 as determined by Alcian Blue and COL2 staining (**Figure 3g-g"** and **i-i"**). Furthermore, we noticed that, based on expression levels of *COL2A1*, 79% of all hiCPC-derived pellets passed our criterium for deposition of neo-cartilage. Among hiMSC differentiations, however, more variation was observed and fewer pellets (54%) passed the pre-set threshold for expression levels of *COL2A1*.

Gene expression analyses of hiCPC-derived neo-cartilage compared to that of hPACs (**Table 3** and **Figure 4**) demonstrated significantly higher levels of *COL2A1* (FD=13.0, P-value=$5.7x10^{-7}$) and lower expression of genes associated with cartilage hypertrophy, such as *COL10A1* (FD=-35.9, P-value=$5.7x10^{-7}$) and *COL1A1* (FD=-4.3, P-value=$7.7x10^{-6}$). In addition, levels of the catabolic gene *ADAMTS5* were significantly lower (FD=-5.2, P-value=$1.0x10^{-5}$). Together, this indicates enhanced quality of matrix deposited by hiCPCs during chondrogenesis. Comparison of the chondrocyte-specific gene panel showed 65% similarity (SD=12.5) between hiCPC- and hPAC-derived neo-cartilage (see **Supplementary Table S2b** for complete overview of hiCPC-hPAC similarities). Prolonged chondrogenesis of hiCPCs until day 35 did not further improve similarity with hPACs, while expression levels of hypertrophic and mineralization gene *ALPL* significantly increased (FD=4.0, P-value=$1.8x10^{-2}$; **Supplementary Table S3**).

To explore protein localization and matrix structure, COL1, COL2, and COL10 staining was performed for hiCPC- and hPAC-derived neo-cartilage pellets. As can be observed in **Figure 3h"** COL1 staining was consistently expressed throughout the ECM of the hPACs-derived neo-cartilage, while hiCPC-derived pellets (**Figure 3h**) showed a less uniform staining. Expression of COL2 was well-detectable in the hiCPC neo-cartilage throughout the pellets and comparable to

hPAC-derived neo-cartilage (**Figure 3i-i"**). Comparable to hBMSC- and hiMSCs-derived neo-cartilage, only faint COL10 expression in the ECM was observed (**Figure 3j** and **3j"**).

Table 2. Differences in gene expression between hiMSC- and hPAC-derived neo-cartilage at respectively week 5 and 3. Significant data are highlighted in bold.

hiMSCs versus hPACs neo-cartilage				
Matrix genes	**FD**	**Beta**	**SE**	**P value**
ACAN	**-29.5**	**-4.9**	**1.6**	**$7.6x10^{-3}$**
COL2A1	**-10.5**	**-3.4**	**1.7**	**$4.2x10^{-2}$**
COL1A1	**5.5**	**2.5**	**0.5**	**$1.7x10^{-3}$**
COL10A1	**-6.7**	**-2.8**	**1.2**	**$2.0x10^{-2}$**
Hypertrophy genes	**FD**	**Beta**	**SE**	**P value**
ADAMTS5	**-5.9**	**-2.6**	**0.8**	**$1.8x10^{-3}$**
MMP13	**123.2**	**6.9**	**1.3**	**$1.4x10^{-3}$**
EPAS1	**-10.9**	**-3.4**	**0.8**	**$4.8x10^{-5}$**
WWP2	**-2.3**	**-1.2**	**0.4**	**$2.8x10^{-3}$**
ALPL	**51.7**	**5.7**	**1.8**	**$1.4x10^{-3}$**
Chondrogenesis genes	**FD**	**Beta**	**SE**	**P value**
SOX5	**-8.2**	**-3.0**	**1.3**	**$2.3x10^{-2}$**
SOX6	-2.6	-1.4	0.9	$1.5x10^{-1}$
SOX9	-5.4	-2.4	1.7	$1.4x10^{-1}$
FGFR2	**-89.6**	**-6.5**	**1.5**	**$2.1x10^{-5}$**
NOTCH1	-1.1	-0.1	0.7	$8.6x10^{-1}$
NOTCH3	2.0	1.0	0.7	$1.7x10^{-1}$
SMAD3	**-2.4**	**-1.3**	**0.6**	**$2.5x10^{-2}$**
SMAD7	1.6	0.7	0.6	$2.1x10^{-1}$
GDF5	**-22.0**	**-0.7**	**0.2**	**$1.8x10^{-4}$**
PRG4	**-77.7**	**-1.1**	**0.1**	**$3.5x10^{-9}$**
NFAT5	-1.2	-0.2	0.3	$4.3x10^{-1}$

Table 3. Differences in gene expression levels between hiCPC- and hPAC-derived neo-cartilage at week 3 of chondrogenesis. Significant data are highlighted in bold.

hiCPCs versus hPACs neo-cartilage				
Matrix genes	**FD**	**Beta**	**SE**	**P value**
ACAN	-1.6	-0.7	0.8	$4.2x10^{-1}$
COL2A1	**13**	**3.7**	**0.7**	**$5.7x10^{-7}$**
COL1A1	**-4.3**	**-2.1**	**0.5**	**$7.7x10^{-6}$**
COL10A1	**-36**	**-5.2**	**1.2**	**$1.9x10^{-5}$**
Hypertrophy genes	**FD**	**Beta**	**SE**	**P value**
ADAMTS5	**-5.2**	**-2.4**	**0.5**	**$1.0x10^{-5}$**
MMP13	1.0	0.1	1.9	$9.7x10^{-1}$
EPAS1	**-48**	**-5.6**	**1.1**	**$2.1x10^{-7}$**
WWP2	1.0	0.0	0.5	$9.6x10^{-1}$
ALPL	1.8	0.8	1.8	$6.4x10^{-1}$
Chondrogenesis genes	**FD**	**Beta**	**SE**	**P value**
SOX5	1.4	0.5	0.4	$2.4x10^{-1}$
SOX6	-2.3	-1.2	1.4	$3.9x10^{-1}$
SOX9	-3.8	-1.9	1.5	$1.9x10^{-1}$
FGFR2	1.5	0.6	0.5	$2.8x10^{-1}$
NOTCH1	3.1	1.6	0.9	$5.7x10^{-2}$
NOTCH3	1.7	0.8	0.6	$2.1x10^{-1}$
SMAD3	**-8.7**	**-3.1**	**1.0**	**$1.2x10^{-3}$**
SMAD7	-1.9	-0.9	1.4	$5.0x10^{-1}$
GDF5	**-15.7**	**-1.3**	**0.3**	**$5.0x10^{-6}$**
PRG4	**-18.3**	**-0.8**	**0.2**	**$1.0x10^{-6}$**
NFAT5	-1.2	-0.3	0.3	$3.7x10^{-1}$

DISCUSSION

To get more insight into the consistency of frequently used neo-cartilage differentiation protocols for hiPSCs, as well as the resulting neo-cartilage quality, we here compared a stepwise protocol to generate human chondroprogenitor cells (hiCPCs) and hiPSC-derived mesenchymal stromal cells (hiMSCs), then allowed them to undergo chondrogenesis in parallel with human primary chondrocytes (hPACs) and bone marrow mesenchymal stromal cell (hBMSCs) equivalents. The results obtained with our 20-gene chondrocyte-specific gene panel showed almost 70% similarity of hiCPC neo-cartilage when compared with human primary chondrocytes. This stepwise protocol circumvented the need for intermediate cells (hiMSCs), for which we found only 39% similarity to hPACs.

In addition to the relatively high similarity, the advantages of the stepwise approach include the shorter time frame and high efficiency of chondrogenesis. Based on a pre-set threshold for expression levels of *COL2A1,* 79% of the hiCPC pellets deposited good neo-cartilage, while, in line with previous studies (14, 15), chondrogenesis with the hiMSCs was successful in 54% of the pellets. Among others, hiCPC-derived neo-cartilage showed significantly (13-fold) higher expression of *COL2A1* compared to that from hPACs, which was in accordance with the COL2 protein expression as detected with immunohistochemistry. *COL1A1* and *COL10A1* expression were 4.3-fold and 36-fold lower, respectively, than their levels in hPACs. Results of COL1 immunohistochemistry were in line with this, however, for COL10 expression we did not observe pronounced differences across the different cell sources. Furthermore, the expression level of *ADAMTS5* in hiCPC-derived neo-cartilage was found to be 5.2-fold lower than that in hPACs, which may explain the visibly higher Alcian blue intensity, indicative of s-GAG levels in the hiCPC-derived neo-cartilage. Together, our data denote that generation of hiCPC-derived neo-cartilage offers promising prospects for skeletal regenerative therapies with less hypertrophic neo-cartilage; although, further improvement in differentiation efficiency and quality may still be possible and further confirmation of applicability by *in vivo* experiments will be required.

Unfortunately, a major disadvantage of hiCPCs is the reduction of their chondrogenic potential following expansion *in vitro* (17, 18), requiring repeated chondrogenic differentiations to ensure deposition of high quality neo-cartilage. A possible culprit of this, is the generation of a diverse heterogenous hiCPC population, where neurogenic and mesenchymal lineage cells are involved (18, 23). A chondrogenic selection of this population and further optimization of differentiation factors may improve chondrogenic potential and diminish expansion problems while increasing cartilage quality. Such increase in differentiation potential has been demonstrated by Dicks *et al.* when sorting for CD146, CD166, and PDGFRβ surface marker expression or by using a GFP-*COL2A1* reporter hiPSC line. This *COL2A1* marker, however, is known to be expressed in a wide variety of tissues (24). Therefore, another option would be to use a reporter line with an earlier chondrogenic marker, such as *SOX9,* to further enhance the efficiency of the differentiation. This was recently performed for immortalized adipose-derived stem cells with stable *SOX9* overexpression, which showed enhanced chondrogenic potential (25).

Of note was the expression of CD45 in both hiCPC lines, (38% of hiCPC-004 with SD=14 and 25% of the hiCPC-030 with SD=6.3) since CD45 is a transmembrane protein tyrosine phosphatase and a known characteristic of hematopoietic cells (26). It has been found that chondrogenesis in the presence of CD45-positive cells of hematopoietic origin enhanced the expression of chondrogenic genes such as *COL2A1* and *SOX9* (27). Therefore, the CD45-expressing cells within the

mixed population of cells from different lineages that are generated with the stepwise protocol may contribute to enhancing the chondrogenic potential of the cells. This was, however, not observed for the hiMSCs.

Characterization of the hiMSCs showed that the well-known hBMSC surface markers (i.e. CD90, CD105, CD73, CD31, CD166) were similarly expressed across the various differentiations, with exception of CD45 (27% of hiMSCs with SD=6 as compared to 10% of hBMSCs with SD=9) and CD146 (97% of hiMSCs with SD=2 as compared to 59% of hBMSCs with SD=24). CD146 is a transmembrane glycoprotein that belongs to the immunoglobulin superfamily of cell adhesion molecules (CAMs), and is involved in cell adhesion and proliferation (28). Furthermore, it has been described as an excellent multipotency marker for MSCs, as compared to specialized cells (29-31), while showing a direct correlation to chondrogenic potential (32).

Comparison of hiMSC- and BMSC-derived neo-cartilage showed a 53% similarity. Although this is considerable, it should be noted that the hiMSCs from both hiPSC lines and across all differentiations performed do display high levels of heterogeneity, as shown in **Figure 3**. To compensate for this, Diederichs *et al.* suggested pre-selecting cells with high expression levels of *SOX9* after a week in culture (15). In their study, this approach increased the success rate and reduced variation. On the other hand, as also observed before (15), *COL10A1* was very lowly expressed at gene expression and protein level, which is characteristic of poor neo-cartilage ECM. Improvement may be established by modifications of the chondrogenic medium, such as by adding BMP2 or BMP4 (13). Finally, when comparing hiMSC- and hPAC-derived neo-cartilage, we can strongly conclude that matrix generated by hiMSC has a hypertrophic phenotype with a 39% similarity to neo-cartilage from primary chondrocytes. This is defined by the lower expression of *COL2A1*(-10.5 fold lower), while *COL1A1*, *ALPL,* and *MMP13* were highly upregulated (5.5, 51.7, and 123.2-fold highly, respectively). The expression of *MMP13* and *ALPL* would suggest a higher collagen degradation with a subsequent calcification, characteristic of terminal chondrogenic differentiation, endochondral ossification and OA initiation (33, 34). Quantification of MMP13 enzymatic activity could help to determine whether the gene expression upregulation also results in an increase of the activate protein (34). The observed differences in neo-cartilage were expected since neo-cartilage from BMSCs and hPAC have a low similarity, and it could be advocated that hiMSCs are an ideal candidate for studying skeletal diseases in which endochondral bone formation and hypertrophy are a driving mechanism (35, 36).

Although hPACs were collected from macroscopically unaffected regions of the articular cartilage, a potential drawback of our study is that they were collected

from patients undergoing joint replacement surgery due to end stage OA. Hence, it could be speculated that, given the higher *COL2A1* and concurrent lower *COL1A1* and *ADAMTS5* levels in hiCPC-derived neo-cartilage, hiCPCs deposit neo-cartilage that is more comparable to healthy cartilage. However, the acquisition of healthy tissue is a challenge in the field, and potential differences between hPACs from preserved and healthy cartilage remain to be determined. Additionally, the emphasis of our manuscript is on the sensitive signaling processes occurring during chondrogenesis. Consequently, further analysis of other significantly different genes and other intrinsic chondrogenic mechanisms would still need to be confirmed by protein expression and ultimately tested in an *in vivo* model.

CONCLUSION

When taking a stepwise approach for chondrogenesis from hiPSCs via chondroprogenitor cells, similarities of almost 70% to primary chondrocytes can be accomplished within 21 days of chondrogenesis. For application of regenerative therapies, this may well be very promising. On the other hand, chondrogenesis methods via hiMSCs result in lower similarity to hPACs, while levels of hypertrophic markers are higher. As such, hiMSCs may be more suitable for *in vitro* models of skeletal diseases.

Acknowledgements

The Leiden University Medical Centre has and is supporting the RAAK study, and we thank all study participants of the RAAK study. We thank Evelyn Houtman, Enrike van der Linden, Robert van der Wal, Peter van Schie, Shaho Hasan, Maartje Meijer, Daisy Latijnhouwers, Anika Rabelink-Hoogenstraaten, and Geert Spierenburg for their contribution to the collection of the joint tissues. We thank all the members of the Molecular Epidemiology Osteoarthritis group for their valuable discussion and feedback. Data is generated within the scope of the Medical Delta programs Regenerative Medicine 4D ("Generating complex tissues with stem cells and printing technology and Improving Mobility with Technology").

Funding

Research leading to these results has received funding from the Dutch Arthritis Society (DAF-16–1-406), the Dutch Scientific Research council NWO/ZonMW VICI scheme (nr 91816631/528), the National Institutes of Health grants AG15768 and AG46927, and from the European Union's Horizon 2020 research and innovation program (No 874671; the material presented and views expressed here are the responsibility of the authors only; the EU Commission takes no responsibility for any use made of the information set out).

Disclosure of potential conflicts of interest

None declared.

Data availability statement

The data that support the funding of this study are available from the corresponding author upon request.

Ethics approval and consent to participate

The Medical Ethics Committee of the LUMC gave approval for the RAAK study (P08.239) and for generation of hiPSCs from skin fibroblasts of healthy donors (P13.080). Informed consent was obtained from all donors.

REFERENCES

1. McKee TJ, Perlman G, Morris M, Komarova SV. Extracellular matrix composition of connective tissues: a systematic review and meta-analysis. Sci Rep. 2019;9(1):10542.
2. Luo Y, Sinkeviciute D, He Y, Karsdal M, Henrotin Y, Mobasheri A, et al. The minor collagens in articular cartilage. Protein Cell. 2017;8(8):560-72.
3. Krishnan Y, Grodzinsky AJ. Cartilage diseases. Matrix Biol. 2018;71-72:51-69.
4. Patel JM, Saleh KS, Burdick JA, Mauck RL. Bioactive factors for cartilage repair and regeneration: Improving delivery, retention, and activity. Acta Biomater. 2019;93:222-38.
5. Stenberg J, de Windt TS, Synnergren J, Hynsjo L, van der Lee J, Saris DB, et al. Clinical Outcome 3 Years After Autologous Chondrocyte Implantation Does Not Correlate With the Expression of a Predefined Gene Marker Set in Chondrocytes Prior to Implantation but Is Associated With Critical Signaling Pathways. Orthop J Sports Med. 2014;2(9):2325967114550781.
6. Ebert JR, Fallon M, Ackland TR, Janes GC, Wood DJ. Minimum 10-Year Clinical and Radiological Outcomes of a Randomized Controlled Trial Evaluating 2 Different Approaches to Full Weightbearing After Matrix-Induced Autologous Chondrocyte Implantation. Am J Sports Med. 2020;48(1):133-42.
7. de Windt TS, Vonk LA, Slaper-Cortenbach ICM, Nizak R, van Rijen MHP, Saris DBF. Allogeneic MSCs and Recycled Autologous Chondrons Mixed in a One-Stage Cartilage Cell Transplantion: A First-in-Man Trial in 35 Patients. Stem Cells. 2017;35(8):1984-93.
8. Bomer N, den Hollander W, Suchiman H, Houtman E, Slieker RC, Heijmans BT, et al. Neo-cartilage engineered from primary chondrocytes is epigenetically similar to autologous cartilage, in contrast to using mesenchymal stem cells. Osteoarthritis Cartilage. 2016;24(8):1423-30.
9. Fellows CR, Matta C, Zakany R, Khan IM, Mobasheri A. Adipose, Bone Marrow and Synovial Joint-Derived Mesenchymal Stem Cells for Cartilage Repair. Front Genet. 2016;7:213.
10. Barry F. MSC Therapy for Osteoarthritis: An Unfinished Story. J Orthop Res. 2019;37(6):1229-35.
11. Liu H, Yang L, Yu FF, Wang S, Wu C, Qu C, et al. The potential of induced pluripotent stem cells as a tool to study skeletal dysplasias and cartilage-related pathologic conditions. Osteoarthritis Cartilage. 2017;25(5):616-24.
12. Nakayama N, Pothiawala A, Lee JY, Matthias N, Umeda K, Ang BK, et al. Human pluripotent stem cell-derived chondroprogenitors for cartilage tissue engineering. Cell Mol Life Sci. 2020;77(13):2543-63.
13. Xu M, Shaw G, Murphy M, Barry F. Induced Pluripotent Stem Cell-Derived Mesenchymal Stromal Cells Are Functionally and Genetically Different From Bone Marrow-Derived Mesenchymal Stromal Cells. Stem Cells. 2019;37(6):754-65.
14. Diederichs S, Tuan RS. Functional comparison of human-induced pluripotent stem cell-derived mesenchymal cells and bone marrow-derived mesenchymal stromal cells from the same donor. Stem Cells Dev. 2014;23(14):1594-610.
15. Diederichs S, Klampfleuthner FAM, Moradi B, Richter W. Chondral Differentiation of Induced Pluripotent Stem Cells Without Progression Into the Endochondral Pathway. Front Cell Dev Biol. 2019;7:270.
16. Nejadnik H, Diecke S, Lenkov OD, Chapelin F, Donig J, Tong X, et al. Improved approach for chondrogenic differentiation of human induced pluripotent stem cells. Stem Cell Rev Rep. 2015;11(2):242-53.
17. Adkar SS, Wu CL, Willard VP, Dicks A, Ettyreddy A, Steward N, et al. Step-Wise Chondrogenesis of Human Induced Pluripotent Stem Cells and Purification Via a Reporter Allele Generated by CRISPR-Cas9 Genome Editing. Stem Cells. 2019;37(1):65-76.
18. Dicks A, Wu CL, Steward N, Adkar SS, Gersbach CA, Guilak F. Prospective isolation of chondroprogenitors from human iPSCs based on cell surface markers identified using a CRISPR-Cas9-generated reporter. Stem Cell Res Ther. 2020;11(1):66.

19. Ramos YF, den HW, Bovee JV, Bomer N, van der Breggen R, Lakenberg N, et al. Genes Involved in the Osteoarthritis Process Identified through Genome Wide Expression Analysis in Articular Cartilage; the RAAK Study. PLoS One. 2014;9(7):e103056.
20. Dambrot C, van de Pas S, van Zijl L, Brandl B, Wang JW, Schalij MJ, et al. Polycistronic lentivirus induced pluripotent stem cells from skin biopsies after long term storage, blood outgrowth endothelial cells and cells from milk teeth. Differentiation. 2013;85(3):101-9.
21. Bomer N, den Hollander W, Ramos YF, Bos SD, van der Breggen R, Lakenberg N, et al. Underlying molecular mechanisms of DIO2 susceptibility in symptomatic osteoarthritis. Ann Rheum Dis. 2015;74(8):1571-9.
22. Dominici M, Le Blanc K, Mueller I, Slaper-Cortenbach I, Marini F, Krause D, et al. Minimal criteria for defining multipotent mesenchymal stromal cells. The International Society for Cellular Therapy position statement. Cytotherapy. 2006;8(4):315-7.
23. Wu CL, Dicks A, Steward N, Tang R, Katz DB, Choi YR, et al. Single cell transcriptomic analysis of human pluripotent stem cell chondrogenesis. Nat Commun. 2021;12(1):362.
24. Seufert DW, Hanken J, Klymkowsky MW. Type II collagen distribution during cranial development in Xenopus laevis. Anat Embryol (Berl). 1994;189(1):81-9.
25. Katz D, Huynh N, Savadipour A, Palte I, Guilak F. An immortalized human adipose-derived stem cell line with highly enhanced chondrogenic properties. Biochemical and Biophysical Research Communications. 2020;530(1):252-8.
26. Fellows CR, Williams R, Davies IR, Gohil K, Baird DM, Fairclough J, et al. Characterisation of a divergent progenitor cell sub-populations in human osteoarthritic cartilage: the role of telomere erosion and replicative senescence. Sci Rep. 2017;7:41421.
27. Kuznetsov SA, Mankani MH, Gronthos S, Satomura K, Bianco P, Robey PG. Circulating skeletal stem cells. J Cell Biol. 2001;153(5):1133-40.
28. Buchert J, Diederichs S, Kreuser U, Merle C, Richter W. The Role of Extracellular Matrix Expression, ERK1/2 Signaling and Cell Cohesiveness for Cartilage Yield from iPSCs. Int J Mol Sci. 2019;20(17).
29. Matta C, Boocock DJ, Fellows CR, Miosge N, Dixon JE, Liddell S, et al. Molecular phenotyping of the surfaceome of migratory chondroprogenitors and mesenchymal stem cells using biotinylation, glycocapture and quantitative LC-MS/MS proteomic analysis. Sci Rep. 2019;9(1):9018.
30. Espagnolle N, Guilloton F, Deschaseaux F, Gadelorge M, Sensebe L, Bourin P. CD146 expression on mesenchymal stem cells is associated with their vascular smooth muscle commitment. J Cell Mol Med. 2014;18(1):104-14.
31. Harkness L, Zaher W, Ditzel N, Isa A, Kassem M. CD146/MCAM defines functionality of human bone marrow stromal stem cell populations. Stem Cell Res Ther. 2016;7:4.
32. Su X, Zuo W, Wu Z, Chen J, Wu N, Ma P, et al. CD146 as a new marker for an increased chondroprogenitor cell sub-population in the later stages of osteoarthritis. J Orthop Res. 2015;33(1):84-91.
33. Chen S, Fu P, Cong R, Wu H, Pei M. Strategies to minimize hypertrophy in cartilage engineering and regeneration. Genes Dis. 2015;2(1):76-95.
34. Li H, Wang D, Yuan Y, Min J. New insights on the MMP-13 regulatory network in the pathogenesis of early osteoarthritis. Arthritis Res Ther. 2017;19(1):248.
35. Kerkhofs J, Leijten J, Bolander J, Luyten FP, Post JN, Geris L. A Qualitative Model of the Differentiation Network in Chondrocyte Maturation: A Holistic View of Chondrocyte Hypertrophy. PLoS One. 2016;11(8):e0162052.
36. Dreier R. Hypertrophic differentiation of chondrocytes in osteoarthritis: the developmental aspect of degenerative joint disorders. Arthritis Res Ther. 2010;12(5):216.

Supplementary Figures

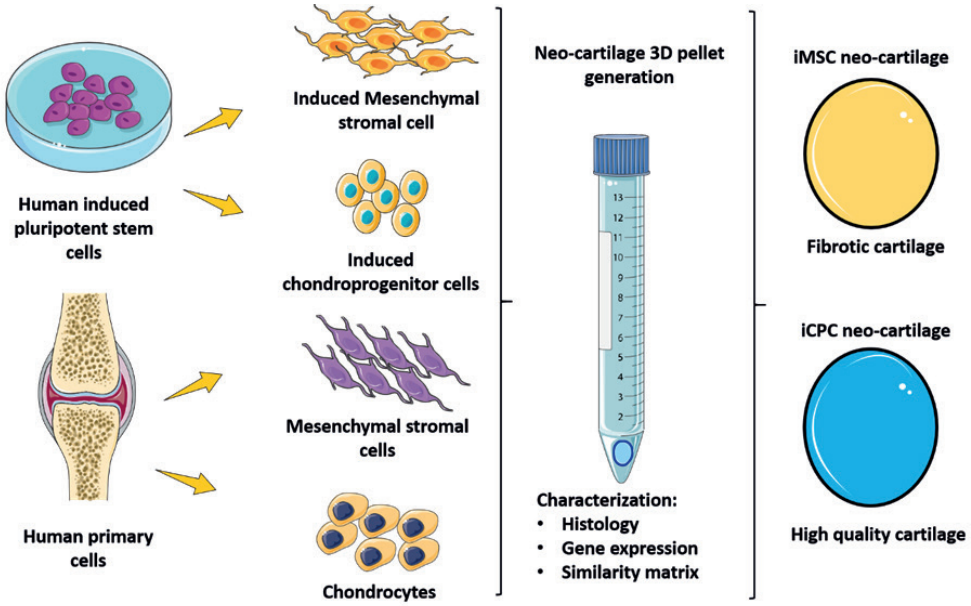

Supplementary Figure S1. Schematic representation of study set up (generated with Servier Medical ART:SMART).

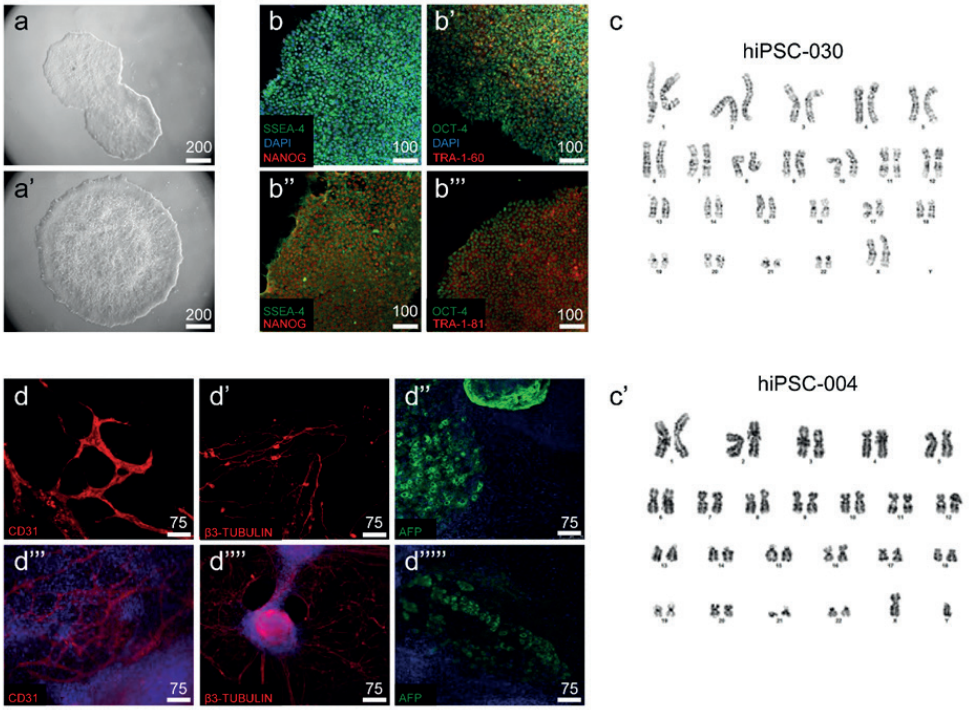

Supplementary Figure S2. Characterization of generated hiPSC control lines. a) Bright field microscopy image of hiPSC colonies. **b**) Immunofluorescent staining for NANOG, TRA-1-60, and TRA-1-81 (red), and SSEA-4 and OCT-4 (green) as indicated in the image. Nuclei are stained with Dapi (blue). **c**) Karyotype demonstrating absence of chromosomal abnormalities. **d**) Expression of CD31, b3-Tubulin, and AFP, as indicated in the image, upon spontaneous differentiation into the three different lineages (mesoderm, ectoderm, and endoderm, respectively). Control line hiPSC-004: **a'**, **b''**, **b'''**, **d'''**, **d''''**, **d'''''**; control line hiPSC-030: **a**, **b**, **b'**, **d**, **d'**, and **d''**.

Supplementary Table S1. Sequences of primers used for RT-qPCR.

	Primer Sequences	
Matrix Genes	**Fwd**	**Rvs**
ACAN	5'AGAGACTCACACAGTCGAAACAGC-3'	5'-CTATGTTACAGTGCTCGCCAGTG-3'
COL2A1	5'-CTACCCCAATCCAGCAAACGT-3'	5'-AGGTGATGTTCTGGGAGCCTT-3'
COL1A1	5' - GTGCTAAAGGTGCCAATGGT-3'	5' -ACCAGGTTCACCGCTGTTAC -3'
COL10A1	5'-GGCAACAGCATTATGACCCA-3'	5'-TGAGATCGATGATGGCACTCC-3'
Hypertrophy genes	**Fwd**	**Rvs**
ADAMTS5	5'-CGTGTACTTGGGCGATGACA-3'	5'-CTGTTGTTGCACACCCCTCT-3'
MMP13	5'-TTGAGCTGGACTCATTGTCG-3'	5'-GGAGCCTCTCAGTCATGGAG-3'
EPAS1	5'-ACAGGTGGAGCTAACAGGAC-3'	5'-CCGTGCACTTCATCCTCATG-3'
WWP2	5'-CACATGTGTCTCCTGGTCCC-3'	5'-GGCAGGGGAAGTGTGCATAT-3'
ALPL	5'-CAAAGGCTTCTTCTTGCTGGTG-3'	5'-CCTGCTTGGCTTTTCCTTCA-3'
Chondrogenesis genes	**Fwd**	**Rvs**
SOX5	5'-CCTCAAAGCCTCTGTCCCAG-3'	5'-TGCCTTGGTGACAGCATCAT-3'
SOX6	5'-AACAACGGCAGCAAATGGAC-3'	5'-TGGATCTGTTGCTGCAGGAG-3'
SOX9	5'-CCCCAACAGATCGCCTACAG-3'	5'-CTGGAGTTCTGGTGGTCGGT-3'
FGFR2	5'-TCTCTTCAACGGCAGACACC-3'	5'-AAAGCAACCTTCTCCCAGGG-3'
NOTCH1	5'-AGGACTGCAGCGAGAACATT-3'	5'-GCAGTAGAAGGAGGCCACAC-3'
NOTCH3	5'-GTGGATGGCGTCAACACCTA-3'	5'-CTGCAGCTGACACTCATCCA-3'
SMAD3	5'-GCCCCTTTCAGGTAACCGTC-3'	5'-GAAGCGGCTGATGCTCCTTA-3'
SMAD7	5'- CGAATTATCTGGCCCCTGGG-3'	5'-TCCCCACTCTCGTCTTCTCC-3'
GDF5	5'-GACATGGTCGTGGAGTCGTG-3'	5'-CCCCTCTGTGATTCCAGGAGT-3'
PRG4	5'-AAAGTCAGCACATCTCCCAAG-3'	5'-GTGTCTCTTTAGCGGAAGTAGTC-3'
NFAT5	5'-AGGCCTGCAGAGTAACTGGA-3'	5'-CCGCCAGTGTCATGTTGTTG-3'
Housekeeping genes	**Fwd**	**Rvs**
GAPDH	5'-TGCCATGTAGACCCCTTGAAG-3'	5'-ATGGTACATGACAAGGTGCGG-3'
ARP	5'-CACCATTGAAATCCTGAGTGATGT-3'	5'-TGACCAGCCGAAAGGAGAAG-3'

Supplementary Table S2. Similarity tables for the different samples included in the current study.

Similarity table BMSCs against iMSCs (a)

	BMSC1	BMSC2	BMSC3	BMSC4	BMSC5	iMSC1	iMSC2	iMSC3	iMSC4	iMSC5	iMSC6	iMSC7
BMSC1	1.0	0.9	0.7	0.9	0.8	0.4	0.3	0.3	0.6	0.6	0.6	0.7
BMSC2	0.9	1.0	0.9	0.9	0.8	0.5	0.4	0.4	0.7	0.7	0.7	0.6
BMSC3	0.7	0.9	1.0	0.7	0.9	0.6	0.6	0.6	0.8	0.5	0.6	0.8
BMSC4	0.9	0.9	0.7	1.0	0.7	0.4	0.2	0.2	0.4	0.6	0.6	0.4
BMSC5	0.8	0.8	0.9	0.7	1.0	0.6	0.4	0.5	0.7	0.4	0.4	0.8
iMSC1	0.4	0.5	0.6	0.4	0.6	1.0	0.7	0.8	0.6	0.6	0.6	0.6
iMSC2	0.3	0.4	0.6	0.2	0.4	0.7	1.0	0.8	0.7	0.7	0.7	0.7
iMSC3	0.3	0.4	0.6	0.2	0.5	0.8	0.8	1.0	0.6	0.5	0.5	0.6
iMSC4	0.6	0.7	0.8	0.4	0.7	0.6	0.7	0.6	1.0	0.5	0.6	0.8
iMSC5	0.6	0.7	0.5	0.6	0.4	0.6	0.7	0.5	0.5	1.0	1.0	0.6
iMSC6	0.6	0.7	0.6	0.6	0.4	0.6	0.7	0.5	0.6	1.0	1.0	0.6
iMSC7	0.7	0.6	0.8	0.4	0.8	0.6	0.7	0.5	0.8	0.6	0.6	1.0

Similarity table hPACs against iCPCs (b)

	hPAC1	hPAC2	hPAC3	hPAC4	hPAC5	hPAC6	hPAC7	hPAC8	hPAC9	iCPC1	iCPC2	iCPC3	iCPC4	iCPC5	iCPC6
hPAC1	1.0	0.9	0.9	0.9	0.9	0.9	0.8	0.7	0.9	0.7	0.6	0.7	0.6	0.8	0.8
hPAC2	0.9	1.0	1.0	0.7	0.8	0.7	0.6	0.6	0.8	0.6	0.5	0.5	0.5	0.7	0.8
hPAC3	0.9	1.0	1.0	0.8	0.8	0.8	0.7	0.6	0.9	0.7	0.6	0.6	0.6	0.8	0.8
hPAC4	0.9	0.7	0.8	1.0	0.9	0.9	0.9	0.9	0.9	0.8	0.6	0.7	0.7	0.8	0.8
hPAC5	0.9	0.8	0.8	0.9	1.0	0.8	0.7	0.7	0.8	0.7	0.5	0.7	0.6	0.7	0.8
hPAC6	0.9	0.7	0.8	0.9	0.8	1.0	0.8	0.8	0.9	0.6	0.5	0.7	0.5	0.7	0.7
hPAC7	0.8	0.6	0.7	0.9	0.7	0.8	1.0	1.0	0.8	0.7	0.6	0.7	0.6	0.7	0.8
hPAC8	0.7	0.6	0.6	0.9	0.7	0.8	1.0	1.0	0.7	0.7	0.6	0.7	0.6	0.7	0.7
hPAC9	0.9	0.8	0.9	0.9	0.8	0.9	0.8	0.7	1.0	0.7	0.5	0.7	0.6	0.6	0.6
iCPC1	0.7	0.6	0.7	0.8	0.7	0.6	0.7	0.7	0.7	1.0	0.9	0.8	0.7	0.9	0.9

Similarity table hPACs against iCPCs (b)

	hPAC1	hPAC2	hPAC3	hPAC4	hPAC5	hPAC6	hPAC7	hPAC8	hPAC9	iCPC1	iCPC2	iCPC3	iCPC4	iCPC5	iCPC6
iCPC2	0.6	0.5	0.6	0.6	0.5	0.5	0.6	0.6	0.5	0.9	1.0	0.8	0.7	0.9	0.8
iCPC3	0.7	0.5	0.6	0.7	0.7	0.7	0.7	0.7	0.7	0.8	0.8	1.0	0.7	0.8	0.8
iCPC4	0.6	0.5	0.6	0.7	0.6	0.5	0.6	0.6	0.6	0.7	0.7	0.7	1.0	0.7	0.6
iCPC5	0.8	0.7	0.8	0.8	0.7	0.7	0.7	0.7	0.6	0.9	0.9	0.8	0.7	1.0	0.9
iCPC6	0.8	0.8	0.8	0.8	0.8	0.7	0.8	0.7	0.6	0.9	0.8	0.8	0.6	0.9	1.0

Similarity table hPACs against iMSCs (c)

	hPAC1	hPAC2	hPAC3	hPAC4	hPAC5	hPAC6	hPAC7	hPAC8	hPAC9	iMSC1	iMSC2	iMSC3	iMSC4	iMSC5	iMSC6	iMSC7
hPAC1	1.0	0.9	0.9	0.9	0.9	0.9	0.8	0.7	0.9	0.3	0.6	0.6	0.1	0.2	0.1	0.5
hPAC2	0.9	1.0	1.0	0.8	0.8	0.7	0.6	0.6	0.8	0.2	0.5	0.5	0.1	0.2	0.1	0.4
hPAC3	0.9	1.0	1.0	0.8	0.8	0.8	0.7	0.6	0.9	0.2	0.6	0.6	0.1	0.2	0.0	0.4
hPAC4	0.9	0.8	0.8	1.0	0.9	0.9	0.9	0.9	0.9	0.5	0.7	0.7	0.3	0.4	0.3	0.6
hPAC5	0.9	0.8	0.8	0.9	1.0	0.8	0.7	0.7	0.8	0.4	0.6	0.6	0.2	0.3	0.3	0.6
hPAC6	0.9	0.7	0.8	0.9	0.8	1.0	0.8	0.8	0.9	0.4	0.5	0.5	0.2	0.4	0.2	0.6
hPAC7	0.8	0.6	0.7	0.9	0.7	0.8	1.0	1.0	0.8	0.4	0.7	0.7	0.3	0.4	0.3	0.6
hPAC8	0.7	0.6	0.6	0.9	0.7	0.8	1.0	1.0	0.7	0.5	0.7	0.7	0.4	0.5	0.4	0.6
hPAC9	0.9	0.8	0.9	0.9	0.8	0.9	0.8	0.7	1.0	0.1	0.5	0.5	0.0	0.2	0.0	0.5
iMSC1	0.5	0.2	0.2	0.5	0.4	0.4	0.4	0.5	0.1	1.0	0.6	0.6	0.7	0.9	0.8	0.7
iMSC2	0.6	0.5	0.6	0.7	0.6	0.5	0.7	0.7	0.5	0.6	1.0	1.0	0.5	0.7	0.5	0.5
iMSC3	0.6	0.5	0.6	0.7	0.6	0.5	0.7	0.7	0.5	0.6	1.0	1.0	0.6	0.7	0.5	0.5
iMSC4	0.1	0.1	0.1	0.3	0.2	0.2	0.3	0.4	0.0	0.7	0.5	0.6	1.0	0.7	0.7	0.6
iMSC5	0.2	0.2	0.2	0.4	0.3	0.4	0.4	0.5	0.2	0.9	0.7	0.7	0.7	1.0	0.8	0.7
iMSC6	0.1	0.1	0.0	0.3	0.3	0.2	0.3	0.4	0.0	0.8	0.5	0.5	0.7	0.8	1.0	0.8
iMSC7	0.5	0.4	0.4	0.6	0.6	0.6	0.6	0.6	0.5	0.7	0.5	0.5	0.6	0.7	0.8	1.0

Supplementary Table S3. Differences in gene expression between hiCPC-derived neo-cartilage at week 3 and 5. Significant differential expression depicted in bold.

hiCPCs week 3 versus week 5				
Matrix genes	**FD**	**Beta**	**SE**	**P value**
ACAN	-5.1	-2.8	1.7	$1.0x10^{-1}$
COL2A1	-4.7	-2.7	1.6	$9.3x10^{-2}$
COL1A1	-1.2	-0.3	0.8	$7.5x10^{-1}$
COL10A1	-2.4	-1.6	1.1	$1.5x10^{-1}$
Hypertrophy genes	**FD**	**Beta**	**SE**	**P value**
ADAMTS5	-3.4	-2.1	1.3	$9.4x10^{-2}$
MMP13	-1.2	-0.3	2.0	$8.9x10^{-1}$
EPAS1	-5.0	-2.8	1.7	$1.1x10^{-1}$
WWP2	-1.1	-0.2	0.4	$5.4x10^{-1}$
ALPL	**4.3**	**2.5**	**1.1**	**$1.8x10^{-2}$**
Chondrogenesis genes	**FD**	**Beta**	**SE**	**P value**
SOX5	-1.5	-0.7	0.5	$1.7x10^{-1}$
SOX6	2.0	1.2	1.4	$3.7x10^{-1}$
SOX9	-1.1	-0.2	0.8	$8.0x10^{-1}$
FGFR2	-1.4	-0.6	0.7	$3.4x10^{-1}$
NOTCH1	1.0	0.0	0.6	$9.6x10^{-1}$
NOTCH3	1.4	0.5	0.3	$6.5x10^{-2}$
SMAD3	1.5	0.7	1.0	$4.4x10^{-1}$
SMAD7	3.2	2.0	1.4	$1.5x10^{-1}$
GDF5	-1.4	-0.6	1.2	$6.2x10^{-1}$
PRG4	-1.3	-0.4	0.7	$5.0x10^{-1}$
NFAT5	-1.3	-0.5	0.4	$2.1x10^{-1}$

CHAPTER 4

Mutation in the CCAL1 locus accounts for bidirectional process of human subchondral bone turnover and cartilage mineralization

Alejandro Rodríguez Ruiz[1§], Marcella van Hoolwerff[1§], Sara Sprangers[2], Eka Suchiman[1], Ton Schoenmaker[2,3], Petra Dibbets-Schneider[4], Johan L. Bloem[4], Rob GHH Nelissen[7], Christian Freund[5,6], Christine Mummery[5,6], Vincent Everts[2], Teun J. de Vries[3], Yolande FM Ramos[1*#], and Ingrid Meulenbelt[1*]

[1]Dept. Biomedical Data Sciences, Section Molecular Epidemiology, Leiden University Medical Center, Leiden (LUMC), The Netherlands; [2]Dept. Oral Cell Biology, [3]Dept. Periodontology, Academic Centre for Dentistry Amsterdam (ACTA), University of Amsterdam (UvA) and Vrije University (VU) Amsterdam, 1081 LA Amsterdam, The Netherlands; [4]Dept. Radiology, LUMC; [5]Dept. Anatomy, LUMC; [6]LUMC iPSC Core Facility. [7]Dept. Orthopedics LUMC, Leiden, The Netherlands.

[§]Contributed equally.
[*]Shared last.

Rheumatology (Oxford). 2022;00:1-13

ABSTRACT:

Objectives: To study the mechanism by which the readthrough mutation in *TNFRSF11B*, encoding osteoprotegerin (OPG) with additional 19 amino acids at its C-terminus (OPG-XL), causes the characteristic bidirectional phenotype of subchondral bone turnover accompanied by cartilage mineralization in chondrocalcinosis patients.

Methods: OPG-XL was studied by human induced pluripotent stem cells expressing OPG-XL and two isogenic CRISPR/Cas9-corrected controls in cartilage and bone organoids. Osteoclastogenesis was studied with monocytes from OPG-XL carriers and matched healthy controls followed by gene expression characterization. DEXA scans, and MRI analyses were used to characterize the phenotype of carriers and non-carriers of the mutation.

Results: Human OPG-XL carriers relative to sex- and age-matched controls showed, after an initial delay, large active osteoclasts with high number of nuclei. By employing hiPSCs expressing OPG-XL and isogenic CRISPR/Cas9-corrected controls to established cartilage and bone organoids, we demonstrated that expression of OPG-XL resulted in excessive fibrosis in cartilage and high mineralization in bone accompanied by marked downregulation of *MGP* and upregulation of *DIO2* gene expression, respectively.

Conclusions: The readthrough mutation at CCAL1 locus in *TNFRSF11B* identifies an unknown role for OPG-XL in subchondral bone turnover and cartilage mineralization in humans via DIO2 and MGP functions. Previously, OPG-XL was shown to affect binding between RANKL and heparan sulphate (HS) resulting in loss of immobilized OPGXL. Therefore, effects may be triggered by deficiency in the immobilization of OPG-XL Since the characteristic bidirectional pathophysiology of articular cartilage calcification accompanied by low subchondral bone mineralization is also a hallmark of OA pathophysiology, our results are likely extrapolated to common arthropathies.

Key messages:

- OPG-XL mutation directly affects chondrocyte and osteoblast states towards matrix mineralization mediated by respectively MGP and DIO2.
- Expression of OPG-XL drives accumulation of large active osteoclasts with high number of nuclei.
- Interference with OPG–RANKL–heparan sulphate underlying concurrent cartilage calcification and subchondral bone loss likely extrapolates to common arthropathies.

INTRODUCTION

Joint tissue degeneration during osteoarthritis (OA) is a complex multistep process characterized by pathogenic bidirectional process of subchondral bone turnover and cartilage mineralization (1, 2). It has been suggested that this characteristic inverse mineralization process has shared mechanisms with the frequently observed concurrent pathogenic bone turnover and vasculature mineralization (2, 3). Key proteins likely involved are osteoprotegerin (OPG), a decoy receptor of osteoclastogenesis (4) and matrix Gla protein (MGP), a vitamin K dependent inhibitor of ectopic bone formation (5) since overexpression or knockdown of these genes in murine models results in such inverse pathological mineralization process (6-8). The inverse causal role of dysfunctional OPG in human joint tissue mineralization was demonstrated by identification of a readthrough mutation (c1205A=T; p.Stop402Leu) in *TNFRSF11B* encoding OPG at the chondrocalcinosis locus 1 (CCAL1) (9) in multiple families worldwide (10-12). In these families CCAL1 phenotype is defined by early onset OA with different levels of articular cartilage calcification i.e. chondrocalcinosis (13) and low subchondral bone mineralization (12).

OPG is a well-known soluble decoy receptor competing with receptor activator of nuclear factor (RANK) expressed at osteoclasts for binding to nuclear factor kB ligand (RANKL) (14). Binding of RANKL to RANK is driving osteoclastogenesis hence bone turnover, while binding to OPG inhibits this process (15). Pleiotropic functions of OPG and RANKL were more recently suggested by showing that RANKL stimulates osteoclast fission to produce transcriptionally distinct osteomorphs which in turn recycle towards large multinucleated osteoclasts or polykaryons by fusion under tight control of OPG (15). Although binding of OPG to RANKL, established by N-terminal domains of OPG, is frequently studied, less is known about the interaction of OPG via its C-terminus with membrane bound heparan sulphate (HS) on osteoblasts (16). A binding that appears indispensable for RANKL mediated inhibition of osteoclastogenesis due to immobilization of secreted OPG on the osteoblast membrane and formation of a stable HS-OPG-RANKL complex (16, 17). In line with this, the CCAL1 readthrough mutation, adding an additional 19 amino acids to the C-terminus of OPG, denoted OPG-XL, has been shown to hamper OPG-HS binding hence permitting osteoclastogenesis and bone turnover (11). This explains characteristic low subchondral bone density in affected CCAL1 family members (12) and sporadic cases (18).

The mechanism by which OPG-XL results in cartilage calcification remains, however, elusive. In fact, a robust role of *TNFRSF11B* and its ligand *TNFSF11* encoding RANKL particularly in cartilage (patho)physiology has been highlighted by transcriptome wide studies. Herein, *TNFRSF11B* and *TNFSF11* but not *TNFRSF11A* encoding RANK show high expression and are robustly responsive to OA cartilage pathophysiology as marked by consistent high upregulation in

human OA affected relative to preserved (19-21) or healthy (22) cartilage. In contrast, differential expression of *TNFRSF11B* or *TNSF11* in subchondral bone underlying preserved and lesioned areas of OA cartilage was not observed (23). Other than that, with *TNFSF11* being a robust OA risk gene identified in the largest genome-wide association study to date (24), aberrant function of OPG/RANKL also underlies common OA aetiopathology.

Here, we set out to functionally characterize the effects of OPG-XL in joint tissues by employing mutated and control human primary chondrocytes, as well as human induced pluripotent stem cells (hiPSCs) from affected CCAL1 family members and CRISPR/Cas9 repaired hiPSCs isogenic controls, to established *in vitro* organoid models of cartilage and bone (25). Additionally, to study the effect of OPG-XL in human osteoclastogenesis, monocytes isolated from blood of carriers of the mutation were compared to monocytes of age- and sex-matched controls in osteoclastogenesis assays. Altogether, we aimed to decipher effects of OPG-XL on joint tissue mineralization that could explain the CCAL1 phenotype of articular cartilage calcification in concurrence with low subchondral bone mineralization. Given that subchondral bone turnover and cartilage calcification are general hallmarks of OA pathophysiology and at the molecular level involve *TNFRSF11B* and *TNFSF11,* our results are likely of relevance to common OA.

MATERIALS AND METHODS

Study participants

Within the Familial early-onset Osteoarthritis (FOA) study, 13 family members were incorporated (six females and seven males aged 23-62 years with mean age 47 years; **Supplementary Table S1**). Cartilage samples were collected within the ongoing Research Arthritis and Articular Cartilage (RAAK) study from five common OA patients and one family member undergoing total joint replacement surgery (RAAK: two females and three males aged 50–87 years with mean age 73 years; FOA: female aged 61).

Genotyping and radiographic analyses

FOA family members were genotyped with in-house genetic test developed by Department of Clinical Genetics to determine presence or absence of previously identified readthrough mutation in *TNFRSF11B* (OPG-XL; **Figure 1A**), (9) and were characterized by dual energy X-ray absorptiometry (DEXA) as well as radiographs and magnetic resonance imaging (MRI) of the knees to respectively determine BMD and OA severity, (dual energy X-ray absorptiometry) as well as radiographs and MRI (magnetic resonance imaging) of the knees to respectively determine bone mineral density (BMD) and OA severity (**Supplementary Table S2** and

S3; **Figure 1B**). DEXA scans of 253 controls were used to compare results to the general population. OA features were scored based on semi quantitative MRI OA knee score (MOAKS(1)) highlighting different characteristics (e.g. bone marrow lesions, osteophytes, cysts, and loss of cartilage full thickness) at 14 articular subregions in the knee.

Generation, characterization and CRISPR/Cas9 correction of OPG-XL patient hiPSCs

Human iPSCs were generated by the LUMC iPSC core facility as described before (26) from skin fibroblasts of a FOA participant, carrier of the mutation resulting in expression of OPG-XL (line LUMC0103iOPG). Pluripotency and spontaneous differentiation were assessed, and cells were karyotyped after 15 passages (**Supplementary Figure S1A-C**). Cells were maintained under standard conditions (37°C, 5% CO_2) in TeSR-E8 medium (STEMCELL Technologies).

To obtain two independent isogenic hiPSC controls without the mutation (lines B89 and C81), CRISPR/Cas9 correction of the mutation was performed for the OPG-XL hiPSCs (LUMC0103iOPG). sgRNAs were designed by *in silico* tools (Rgenome.net and MultiCrispr.net) and selected based on predicted highest specificity and least off-target effects: gRNA1 (5'-AAAAATAAGCTGCTTATTACTGG-3'), and gRNA2 (5'-AAGCTGCTTATTA CTGGAAATGG-3'). The sgRNAs were cloned into a CRISPR/Cas9 plasmid carrying sequences for expression of green fluorescent protein (PX458), and co-transfected using Lipofectamine Stem Reagent (Thermo Fisher Scientific Inc) with a single-stranded oligo donor repair template (ssODN 5'-CACTGAAAGCCTCAAGTGCCTGAGAAACAGTTTACTCATCCATGGGATCTCGC-CAATTGTGAGGAAACAGCTCAATGGCGATTTCGAGTTATAAGCAGCTTATTTTTACT-GATTGGACCTGGTTACC-3') to achieve homologous directed repair (HDR). Twenty-four hours after transfection of gRNAs and ssODN, single-cell-sorting for green fluorescent protein positive cells was performed with FACSAria-I (BD Biosciences), and hiPSCs were seeded at low density (270 cells/cm^2) for clonal expansion. After eight days, colonies were collected and reseeded as single-cells in 96-well plates with TESR-E8 and CloneR (STEMCELL Technologies). DNA was obtained from single colonies using Quick Extract (Lucigen). Region of interest was amplified with PCR and screening for homozygous CRISPR/Cas9-corrected colonies (wt) was done by restriction with PsiI (New England Biolabs). Two homozygous clones (B89 and C81 from gRNA2 and gRNA1, respectively) were identified and repair of the readthrough mutation was confirmed by Sanger sequencing (**Supplementary Figure S1D-F**).

Human primary chondrocytes

Human primary chondrocytes were collected from OA patients (RAAK study; N=5 donors) and carrier of OPG-XL (FOA study; N=1 donor) undergoing joint replacement surgery. Collection, expansion, and deposition of cartilage extracellular matrix of primary chondrocytes has been previously described (20).

Chondrogenesis and osteogenesis of iPSCs

Mesenchymal stromal cells were generated from hiPSC (hiMSCs) of the OPG-XL hiPSCs (LUMC0103iOPG) and of the two thereof derived CRISPR/Cas9 isogenic control hiPSCs (B89 and C81) using Stemcell Technologies' Mesenchymal Progenitor Kit following the manufacturer's instructions. Chondrogenesis and osteogenesis was performed in organoids following our established protocol employing 750000 cells per organoid as described before (25). Cells were counted with the Nucleocounter NC-200 (Chemometec).

Isolation of blood cells and osteoclastogenesis

Peripheral blood mononuclear cells (PBMCs) were isolated from whole blood of six FOA members with mutation and six sex- and age- matched controls (characteristics of donors in **Supplementary Table S4**) using Ficoll density gradient centrifugation as previously described (27). CD14-positive monocytes were collected by negative selection using magnetic MACS microbeads according to the manufacturer's instructions. Cells were then seeded onto slices of human tibia bone of healthy individuals and cultured in medium composed of α-MEM supplemented with 10% fetal calf serum (HyClone I, Thermo Fisher Scientific Inc) and antibiotics following pre-treatment with 10 ng/ml macrophage colony-stimulating factor (M-CSF, R&D Systems) for three days. Osteoclastogenesis was induced by addition of 2 ng/ml RANKL (R&D Systems) in the presence of 10 ng/ml M-CSF. Cultures were maintained at 37°C and 5% CO2 with medium refreshed twice weekly.

CTX-1 measurement and resorption-pit assay

Concentration of C-terminal telopeptide of type 1 collagen (CTX-1) in conditioned media following 14 or 21 days culture on slices of human tibia bone was determined with ELISA (Immunodiagnostic System, Inc) according to the manufacturer's protocol. Measurements were performed for osteoclastogenesis assays of three FOA participants expressing OPG-XL and matched healthy controls. Relative activity per osteoclast was calculated by dividing the concentration of CTX-1 by the total number of osteoclasts. Bone resorption was analyzed in cell cultures of two FOA participants expressing OPG-XL and matched healthy controls as previously described (28) with Coomassie Brilliant Blue (Sigma-Aldrich). Pre-defined areas of

each bone slice, covering approximately one fifth of the total area, were analyzed with Image Pro-Plus software (Media Cybernetics).

Histology and immunohistochemistry

Histology was performed as previously described (4). Overall cellular and tissue structure was visualized with hematoxylin-eosin (H&E) staining. Glycosaminoglycans were visualized by staining with 1% Alcian Blue 8-GX (Sigma-Aldrich) and Nuclear Fast red (Sigma-Aldrich). Calcium deposits were visualized with 2% Alizarin Red S (Sigma-Aldrich).

Formation of osteoclasts was assessed after 14 and 21 days of culture on plastic. Osteoclasts were fixed in 4% formaldehyde for 10 min at ambient temperature and stained for tartrate resistant acid phosphatase (TRAcP) using a commercial kit (Leukocyte acid phosphatase kit, Sigma–Aldrich) according to the manufacturer's instructions. Nuclei were visualized with 4'6-diamidino-2-phenylindole dihydrochloride (DAPI, Sigma-Aldrich). Only cells with three or more nuclei were considered osteoclasts. Results are presented as osteoclasts per cm^2 or in nuclei per osteoclast.

Gene expression analysis

For osteoclast assays, RNA was extracted from the different cultures at day 7, 14 and 21. For each individual RNA isolation of neo-cartilage and neo-bone, we pooled two organoids for either OPG-XL or CRISPR/Cas9 repaired (wt) from several independent rounds of differentiations. This generated for neo-cartilage of OPG-XL a total of 5 to 7 datapoints and for wt a total of 9 to 12 datapoints in the gene expression plots. For neo-bone, this generated for OPG-XL and wt a total of respectively 10 to 16 and 7 to 14 datapoints.

A total of 150 ng mRNA was processed with first strand cDNA kit according to manufacturer's protocol (Roche Applied Science). Genes of interest were determined by preamplification with TaqMan preamp master mix (Thermo Fisher Scientific Inc) and subsequent RT-qPCR in triplicate with BiomarkTM 96.96 Dynamic Arrays (Fluidigm) and integrated fluidic circuit (IFC) chip. Quality control of the data was performed as previously described (4). Unsuccessful differentiation experiments defined by the minimum detected expression of *COL2A1* for human primary chondrocytes and BMSCs neo-cartilage, were disregarded. Relative gene expression (−ΔCt-values) was calculated using levels of glyceraldehyde 3-phosphate dehydrogenase (*GAPDH*) and acidic ribosomal phosphoprotein P0 (*ARP*) as housekeeping genes. The RT-qPCR primers are listed in **Supplementary Table S5**.

Statistical analysis

Generalized estimating equations (GEE) (30) as implemented in IBM SPSS 25.0 software was applied to analyze association between phenotype and genotype. GEE methodology provides a method of analyzing correlated data that otherwise could not be modeled in a generalized linear model. By applying this method, we were able to effectively adjust for familial dependencies of included participants to obtain Betas, standard errors (SE) and P-values for gene expression differences across neo-cartilage and neo-bone (2).

Differences between osteoclast categories defined by the number of nuclei and gene expression were tested using two-way ANOVA and Sidak's multiple comparison test (GraphPad Prism 6.0 software). P-values <0.05 were considered statistically significant.

RESULTS

Carriers of OPG-XL are characterized by severe OA and osteopenia

TNFRSF11B was genotyped in study participants, identifying seven carriers and six non-carriers of OPG-XL among thirteen members of a family with early-onset OA (FOA; **Figure 1**; **Supplementary Table S1**). Whole body DEXA scans showed that bone mineral density (BMD) of non-carriers was similar to that of the general population (**Figure 1C**; **Supplementary Table S2A**). In contrast, carriers of OPG-XL had significantly lower BMD specifically of the femoral neck, narrow neck and total hips, confirming incidence of osteopenia (**Figure 1C**; **Supplementary Table S2B**). No significant difference, however, was observed for lumbar spine BMD. Furthermore, OA features were scored for FOA members based on the semi quantitative MRI OA knee score (MOAKS). This showed that severe osteophytosis, bone marrow lesions (BML), and cysts have significant higher prevalence in carriers of the mutation than in non-carriers (**Supplementary Table S3**). Analysis of the knee radiographs confirmed presence of chondrocalcinosis in three participants expressing OPG-XL. Altogether, this demonstrated that the CCAL1 phenotype in the FOA family is characterized by low BMD and severe cartilage loss, osteophyte formation, and presence of cysts and BML. High mineralization of cartilage was also observed in knee joint of a carrier of the mutation undergoing joint replacement surgery (**Figure 1D**, specific regions with calcified cartilage indicated with dashed line).

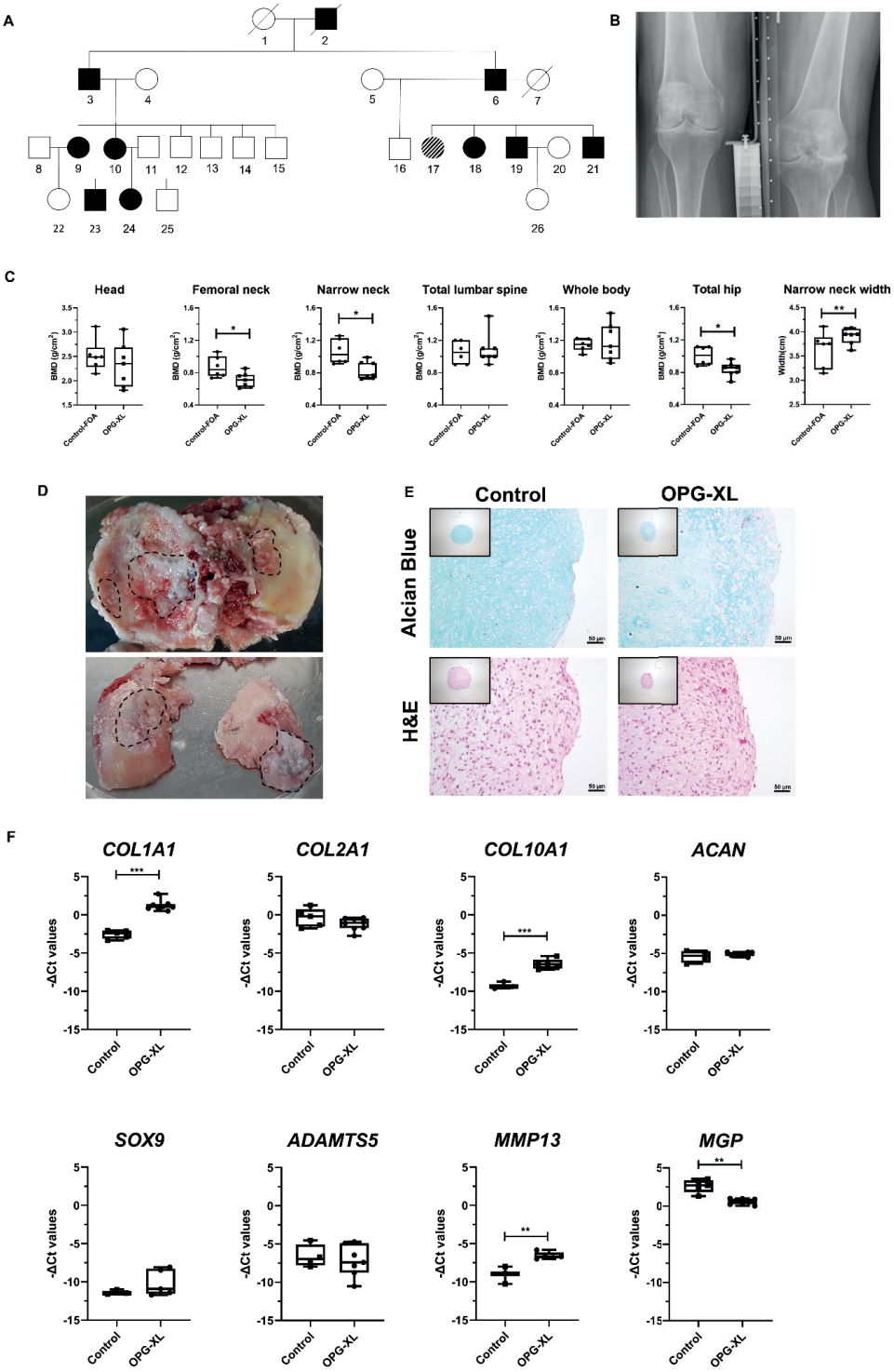
A
B
C
Head
Femoral neck
Narrow neck
Total lumbar spine
Whole body
Total hip
Narrow neck width
BMD (g/cm²)
Width (cm)
Control-FOA
OPG-XL
D
E
Control
OPG-XL
Alcian Blue
H&E
50 µm
F
COL1A1
COL2A1
COL10A1
ACAN
SOX9
ADAMTS5
MMP13
MGP
-ΔCt values
Control
OPG-XL

Figure 1. Characterization of early-onset osteoarthritis family. A) Pedigree of early-onset osteoarthritis family (FOA) with the *TNFRSF11B* readthrough mutation (OPG-XL). Squares represent males and circles females (black symbols represent affected individuals; diagonal lines indicate deceased family members). **B**) Knee radiograph of individual no. 9 from the family tree, with severe articular surface destruction. **C**) BMD of family members with and without the OPG-XL mutation as determined by dual energy X-ray absorptiometry scans and corrected for sex, age and BMI (N= 7 OPG-XL family members, N = 6 healthy family members). **D**) Knee joint from patient that underwent replacement surgery (indicated with dashed line regions with severely calcified cartilage). **E**) Alcian blue and H&E staining of neo-cartilage organoids derived from primary chondrocytes of common OA patients and of OPG-XL carrier (day 21 of chondrogenesis; scale bars: 50 mm). **F**) Boxplots for DCt values of matrix genes in neo-cartilage of common OA patients (N = 5 patients, n = 1) and of OPG-XL carrier (N = 1 FOA, n = 8). P-values determined with generalized estimation equation while including every independent gene as dependent variable, BMD as dependent variable, and age, sex, BMI and mutation status as covariate (*P < 0.05; **P < 104 ; ***P < 106). *ACAN*: aggrecan; *ADAMTS5*: a disintegrin and metalloproteinase with thrombospondin motifs; H&E: haematoxylin and eosin; *MGP*: matrix Gla protein; *MMP13*: matrix metallopeptidase 13; OPG-XL: C-terminal extended osteoprotegerin encoded by *TNFRSF11B* readthrough mutation; *SOX9*: SRY-box transcription factor 9.

Primary chondrocytes with OPG-XL deposit hypertrophic neo-cartilage with low glycosaminoglycan content

We first examined, in an established 3D *in vitro* chondrogenesis model of human primary chondrocytes (29) of a carrier of the OPG-XL mutation (N=1 patient, n=8 replicates), formation of neo-cartilage in comparison to primary chondrocytes from participants of the RAAK study undergoing joint replacement surgery (N=5 patients, n=1 replicate). As shown in **Figure 1E**, Alcian blue staining in neo-cartilage with OPG-XL appeared less homogeneous as compared to neo-cartilage deposited by RAAK chondrocytes. Furthermore, H&E staining showed less dense matrix deposition towards the edges of the organoid. Gene expression of common extracellular matrix (ECM) genes and degradation markers highlighted significantly higher expression of *COL1A1*, *COL10A1* and *MMP13* (**Figure 1F**; **Supplementary Table S6**.). Moreover, low MGP expression indicated a higher mineralization in the OPG-XL neo-cartilage organoids. Together, these data indicated deposition of low quality neo-cartilage matrix with a fibrotic (*COL1A1*) and/or hypertrophic (*COL10A1*) and mineralized (*MGP*) phenotype in the presence of OPG-XL.

Neo-cartilage and neo-bone expressing OPG-XL exhibit altered mineralization and fibrotic phenotype

To study effects of OPG-XL on deposition of extracellular matrix in the joint, patient hiPSCs carrying the mutation were generated from skin fibroblasts (**Supplementary Figure S1**), and both neo-cartilage as well as -bone organoids were created from these hiPSCs and two independent isogenic, CRISPR/Cas9-corrected control (wt) hiPSCs. Structure of deposited neo-cartilage ECM was visualized by histological staining with Alcian blue and H&E (**Figure 2A**;

Supplementary Figure S2). This showed ECM deposition across both groups. Matrix however, was more homogeneous in the two isogenic control organoids as compared to organoids from hiPSCs expressing OPG-XL. Additionally, H&E staining visualized fibrotic ECM particularly towards the outer rim of the OPG-XL neo-cartilage organoids.

In line with the histological observations, quantitative gene expression analysis showed no difference between the two isogenic controls (**Figure 2B**, grey- and purple-filled circles in wt boxes). Therefore, samples were analyzed together in comparison to OPG-XL samples which revealed no significant differences in expression levels of *TNFSF11* encoding RANKL, *TNFRSF11A* encoding RANK, nor in expression levels of *TNFRSF11B* in neo-cartilage in the presence of OPG-XL. Fibrotic character of neo-cartilage deposited in presence of OPG-XL was confirmed by significantly higher expression of *COL1A1* and lower expression of the cartilage specific *COL2A1* and aggrecan (*ACAN*). Concurrently, strong upregulation of alkaline phosphatase (*ALPL*) and osteoblast characteristic RUNX family transcription factor 2 (*RUNX2*) were detected together with significantly lower expression of SRY-Box Transcription Factor 9 (*SOX9*). Notably, lower expression of *MGP* was highly significant which was also observed in neo-cartilage deposited by primary chondrocytes with OPG-XL (**Figure 1F**). These data indicated a strong shift in cartilage metabolism towards mineralization and transdifferentiation towards osteoblasts. This was in contrast with lower expression levels of Secreted Phosphoprotein 1 (*SPP1*) and matrix metallopeptidase 13 (*MMP13*).

Structure of deposited neo-bone ECM was visualized by histological staining with Alizarin red and H&E **(Figure 2A**; **Supplementary Figure S2)**. Alizarin red staining was more intense and more homogeneously distributed in the OPG-XL organoids compared to isogenic controls. In the control group, H&E showed a higher concentration of cells within the core of the organoid and an outer rim characterized by fibrosis.

In line with the findings in cartilage organoids, quantitative gene expression analysis of neo-bone showed no significant differences in levels of *TNFRSF11B* and *TNFRSF11A* expression. Unlike neo-cartilage, neo-bone carrying the OPG-XL mutation did show lower expression of *TNFSF11* (**Figure 2B**; **Table 1**; **Supplementary Figure S3**). Moreover, neo-bone expressing OPG-XL had significantly higher expression of *COL1A1* and *COL10A1*, but particularly of *DIO2*. Altogether, results indicate that both neo-cartilage and neo-bone ECM in the presence of OPG-XL is characterized by increased fibrosis and strong mineralization, respectively, indicating a modulatory role for OPG in cartilage and bone formation.

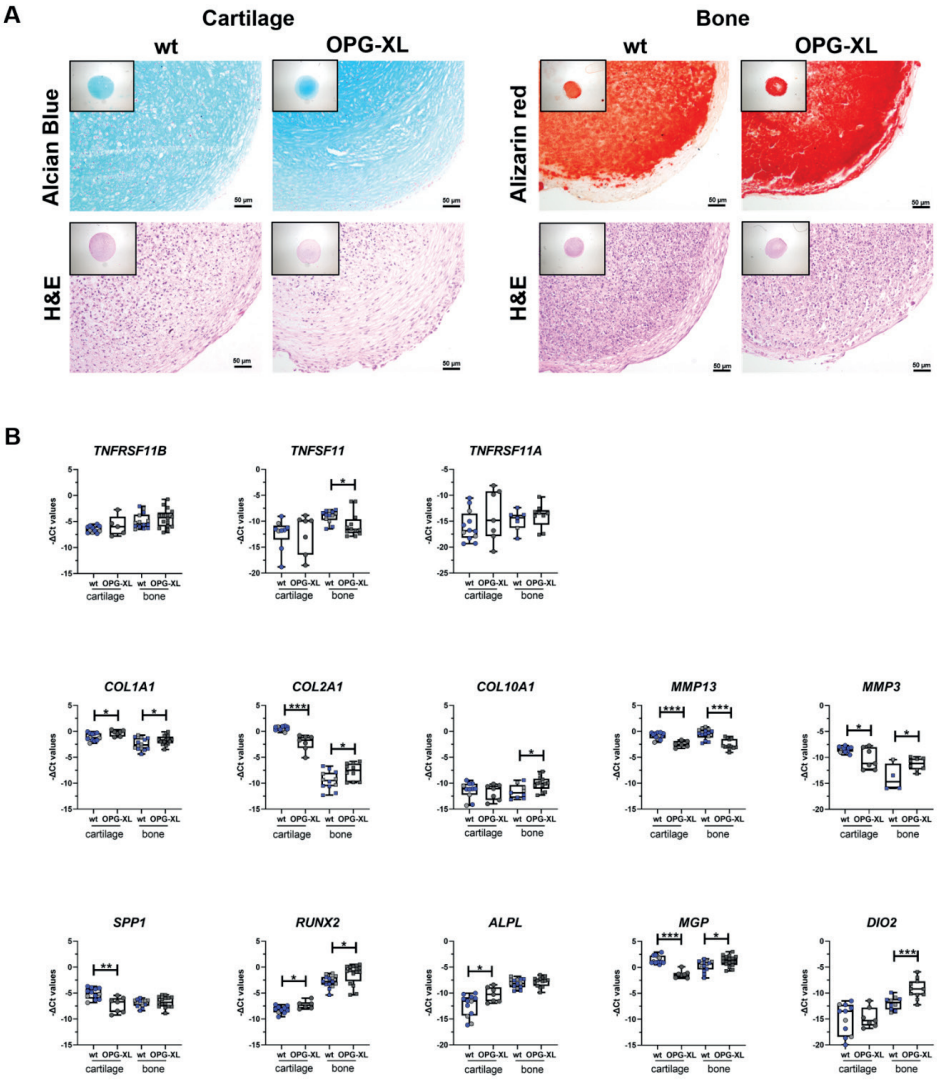

Figure 2. Characterization of OPG-XL neo-cartilage and neo-bone organoids. Alcian blue, Alizarin red and H&E staining of neo-cartilage and neo-bone. **B**) Boxplots for -ΔCt values of relevant genes for CRISPR/Cas9 control (WT) and OPG-XL organoids following 6 weeks of chondrogenesis with additional 2 weeks of osteogenesis to generate neo-bone (scale bars: 50 mm; neo-cartilage: WT n = 9–12 and OPG-XL n = 5–7 samples; neo-bone: WT n = 7–14 and OPG-XL n = 10–16 samples). P-values determined with generalized estimation equation while including every independent gene as dependent variable, and mutation status as covariate (*P < 0.05; **P < 104 ; ***P < 106). *ALPL*: alkaline phosphatase; *DIO2*: type 2 deiodinase; H&E: haematoxylin and eosin; *MGP*: matrix Gla protein; *MMP3*: matrix metallopeptidase 3; *MMP13*: matrix metallopeptidase 13; OPG-XL: C-terminal extended osteoprotegerin encoded by *TNFRSF11B* readthrough mutation; *RUNX2*: RUNX family transcription factor 2; *SPP1*: secreted phosphoprotein 1; *TNFSF11*: gene encoding RANK ligand; *TNFRSF11A*: gene encoding RANK; *TNFRSF11B*: gene encoding osteoprotegering or OPG.

Table 1. Gene expression analyses of neo-cartilage and neo-bone organoids.

Neo-Cartilage									
Extracellular matrix					Mineralization				
Genes	**FD**	**Beta**	**SE**	**P value[a]**	**Genes**	**FD**	**Beta**	**SE**	**P value[a]**
COL1A1	**1.7**	**0.8**	**0.3**	**$7.4x10^{-3}$**	**SPP1**	**-4.6**	**-2.2**	**0.6**	**$2.0x10^{-4}$**
COL2A1	**-6.7**	**-2.8**	**0.5**	**$3.9x10^{-7}$**	**RUNX2**	**1.9**	**0.9**	**0.4**	**$1.0x10^{-2}$**
COL10A1	-1.2	-0.3	0.7	$6.4x10^{-1}$	**ALPL**	**4.4**	**2.1**	**0.8**	**$5.9x10^{-3}$**
MMP13	**-2.4**	**-1.6**	**0.3**	**$1.4x10^{-8}$**	**MGP**	**-7.1**	**-2.8**	**0.3**	**$1.6x10^{-17}$**
MMP3	**-3.4**	**-1.8**	**0.7**	**$1.5x10^{-2}$**	POSTN	1.1	0.2	0.3	$5.2x10^{-1}$
TNFRSF11B	1.6	0.7	0.8	$4.0x10^{-1}$	ASPN	1.0	0.0	0.3	$9.5x10^{-1}$
TNFRSF11A	1.8	2.0	1.9	$2.9x10^{-1}$	DIO2	1.2	0.3	1.1	$8.0x10^{-1}$
TNFRSF11	1.0	0.1	1.6	$9.7x10^{-1}$	ANKH	-1.2	-0.2	0.5	$6.9x10^{-1}$
ACAN1	**-3.9**	**-2.0**	**0.8**	**$1.5x10^{-2}$**					
SOX9	**-2.0**	**-1.0**	**0.3**	**$4.5x10^{-3}$**					
COMP	-1.2	-0.3	0.2	$1.8x10^{-1}$					
ADAMTS5	1.6	0.6	1.1	$5.6x10^{-1}$					
SMAD3	**-2.7**	**-1.4**	**0.4**	**$4.0x10^{-4}$**					
Neo-bone									
Extracellular matrix					Mineralization				
Genes	**FD**	**Beta**	**SE**	**P value[a]**	**Genes**	**FD**	**Beta**	**SE**	**P value[a]**
COL1A1	**1.7**	**0.7**	**0.4**	**$3.9x10^{-2}$**	SPP1	1.1	0.2	0.3	$5.8x10^{-1}$
COL2A1	**3.3**	**1.7**	**0.7**	**$1.2x10^{-2}$**	**RUNX2**	**2.8**	**1.5**	**0.6**	**$7.7x10^{-3}$**
COL10A1	**4.8**	**1.5**	**0.6**	**$5.6x10^{-3}$**	ALPL	1.2	0.3	0.3	$3.4x10^{-1}$
MMP13	**-3.3**	**-2.1**	**0.4**	**$7.8x10^{-9}$**	**MGP**	**1.9**	**0.9**	**0.4**	**$1.2x10^{-2}$**
MMP3	**-14.9**	**2.6**	**1.2**	**$2.8x10^{-2}$**	POSTN	-1.4	-0.5	0.5	$3.14x10^{-1}$
TNFRSF11B	1.5	0.6	0.6	$3.3x10^{-1}$	**ASPN**	**-3.6**	**-1.8**	**0.5**	**$1.4x10^{-4}$**
TNFRSF11A	1.8	0.9	1.0	$3.8x10^{-1}$	**DIO2**	**6.6**	**2.7**	**0.7**	**$3.5x10^{-5}$**
TNFSF11	**-3.2**	**-1.7**	**0.7**	**$2.0x10^{-2}$**	IL11	1.6	0.7	0.5	$1.8x10^{-1}$
					SOST	**2.9**	**1.5**	**0.7**	**$3.5x10^{-2}$**

Results presented are the average of seven samples for neo-cartilage and 16 samples for neo-bone in OPG-XL carriers compared with 12 samples for neo-cartilage and 14 samples for neo-bone in CRISPR/Cas9-corrected controls (WT) at week 6 following chondrogenesis and additional 2 weeks following osteogenesis. P-values determined with generalized estimation equation while including every independent gene as dependent variable, and mutation status as covariate (P-values >0.05 are indicated in bold). FD: fold difference.

Restrained osteoclastogenesis and large polykaryons of monocytes from FOA patients expressing OPG-XL

Given that OPG plays a key role in osteoclast formation, osteoclastogenesis assays were performed with monocytes from six carriers of OPG-XL mutation and six healthy controls (**Figure 3A**). The number of osteoclasts and their respective nuclei were determined at day 14 and day 21 of culture (**Supplementary Table S7**). As shown in **Figure 3B** and **Supplementary Table S7**, the total number of osteoclasts (cells with >3 nuclei) formed at day 14 in OPG-XL (n=90) is delayed relative to controls (n=296). At day 21, however, we showed a significant accumulation of osteoclasts with high number of nuclei formed in OPG-XL (39% >6 nuclei) compared to controls (15% >6 nuclei; **Figure 3C**; **Supplementary Table S7**). Together, these data indicate that after initial restrained osteoclastogenesis, a relative larger fraction of osteoclasts with large number of nuclei accumulate in the presence of OPG-XL as compared to controls.

A

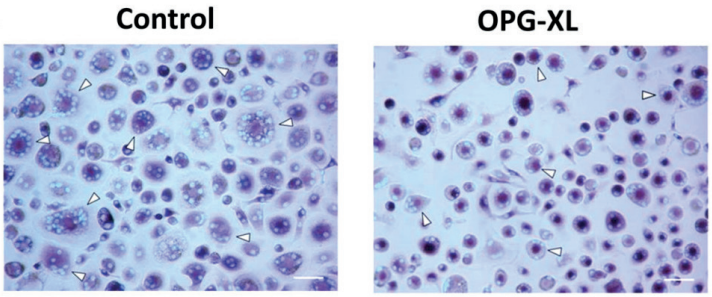

B

TRAcP positive cells/cm² at day 14			
Nuclei/osteoclast [a]	**Controls [b]**	**OPG-XL [b]**	**P value [c]**
3-5	263 (89%)	86 (96%)	5.9×10^{-2}
6-10	30 (10%)	4 (4%)	9.5×10^{-2}
10-20	3 (1%)	0	ND
>20	0	0	ND
Total	296	90	

TRAcP positive cells/cm² at day 21			
Nuclei/osteoclast [a]	**Controls [b]**	**OPG-XL [b]**	**P value [c]**
3-5	644 (85%)	290 (61%)	2.5×10^{-21}
6-10	94 (12%)	114 (24%)	1.1×10^{-7}
10-20	13 (2%)	53 (11%)	6.8×10^{-13}
>20	6 (1%)	16 (3%)	1.2×10^{-3}
Total	757	473	

[a] Strata of osteoclasts according to the number of nuclei per osteoclast. [b] Average number of osteoclasts from N = 6 OPG-XL carriers and N = 6 sex- and age-matched controls; 2–3 replicates each were counted. [c] *P*-value for each stratum was determined with $\chi 2$ test relative to total number of osteoclasts in all other strata.

Figure 3. Characterization of osteoclastogenesis. A) Representative TRAcP staining of osteoclasts generated from monocytes of OPG-XL carriers and sex- and agematched controls after 21 days of culture with M-CSF and RANKL (Scale bar = 200 μm). **B**) Osteoclasts were counted and separated according to the number of nuclei per osteoclast at day 14 and day 21. OPG-XL: C-terminal extended osteoprotegerin encoded by *TNFRSF11B* readthrough mutation; RANKL: RANK ligand; TRAcP: Tartrate-resistant acid phosphatase.

Osteoclasts expressing OPG-XL display similar bone resorptive activity as compared to controls

Following morphological characterization of osteoclasts, resorptive activity was assessed. To that end, formation of resorption pits by osteoclasts generated from controls and from carriers of OPG-XL was determined. As shown in **Figure 4**, despite lower numbers of osteoclasts in the presence of OPG-XL, overall bone resorption was comparable, with at least equal surface areas of resorption pits after 21 days (**Figure 4A**) and amounts of CTX-I released at days 7, 14, and 21 (**Figure 4B-D**). These data indicate that, despite the fact that less osteoclasts develop in the presence of OPG-XL, the total bone resorption activity was comparable to controls.

Finally, well-known markers of osteoclast bone resorption activity were analyzed by RT-qPCR. As shown in **Figure 4E** and **Table 2**, at day 21 OPG-XL-expressing osteoclasts showed significantly higher levels of *NFATc1* (Nuclear factor of activated T-cells, cytoplasmic 1), *CTSK* (Cathepsin K), *TRAcP* (Tartrate-resistant acid phosphatase) and *DC-STAMP* (Dendrocyte Expressed Seven Transmembrane Protein). This suggests that monocytes carrying the OPG-XL mutation, despite an initial delay in osteoclastogenesis, are prone to differentiate towards osteoclasts with potential for higher bone resorption activity based on gene expression levels.

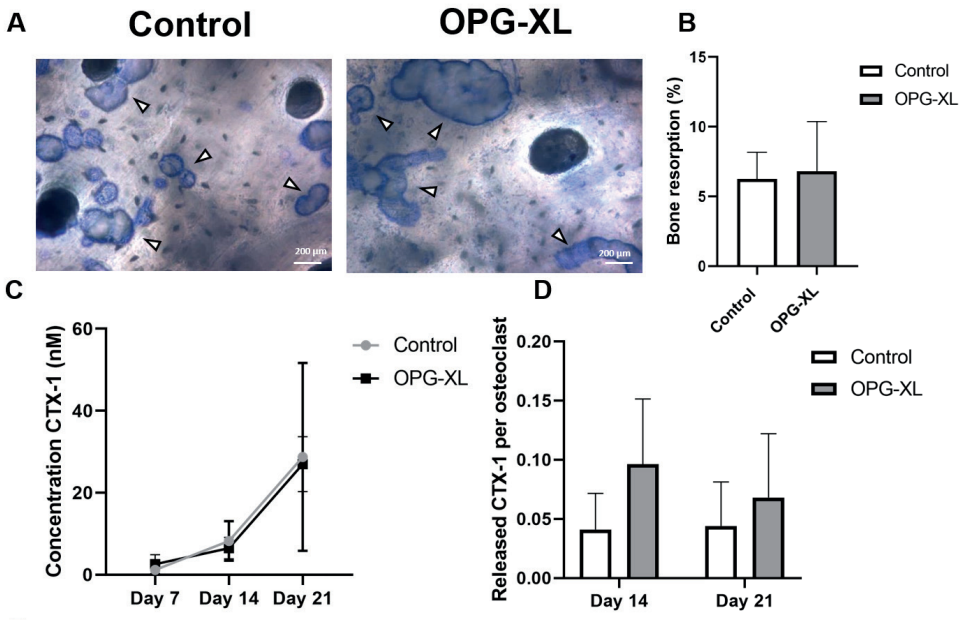

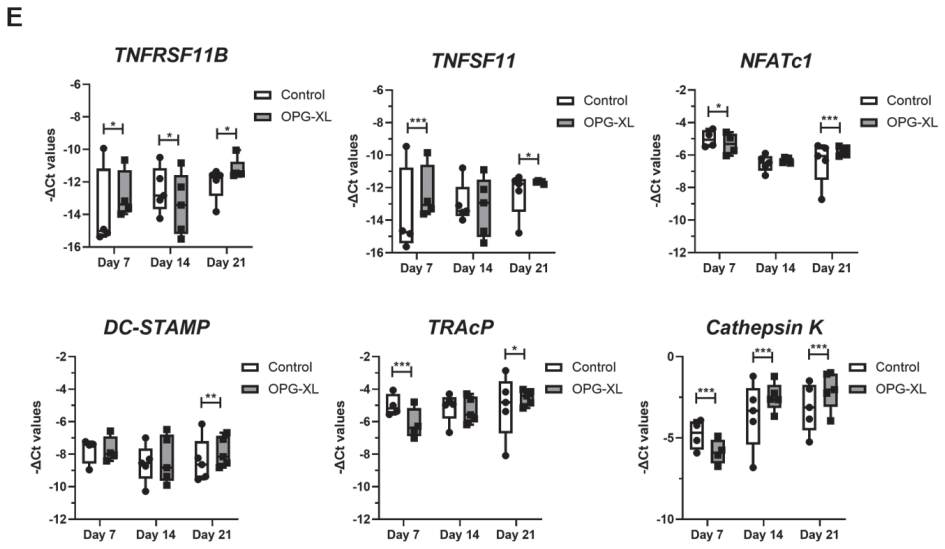

Figure 4. Bone resorption and gene expression for osteoclasts from controls and OPG-XL carriers. **A**) Representative image of bone resorption pits formed by osteoclasts from control and OPG-XL carrier on slices of human tibia bone after 21 days of culture (scale bars: 200 μm). **B**) Percentage of bone resorption for controls (N = 2) and OPG-XL carriers (N = 2). **C**) Concentration of CTX-1 (nM) in conditioned medium after 7, 14 and 21 days of culture (controls and OPG-XL carriers N = 3). **D**) CTX-1 release in conditioned medium per osteoclast at 14 and 21 days of culture (controls N = 3 and OPG-XL carriers N = 3). **E**) Boxplots for -ΔCt values of genes related to osteoclast formation and activity (n = 2–3 replicates from 4–5 controls and OPG-XL carriers). P-values determined with two-way ANOVA with Sidak's multiple comparison analysis (*$P < 0.05$; **$P < 10^{-4}$; ***$P < 10^{-6}$). *CTX-1*: C-terminal telopeptide of type 1 collagen; *DC-STAMP*: endrocyte Expressed Seven Transmembrane Protein; *NFATc1*: Nuclear factor of activated T-cells, cytoplasmic 1; OPG-XL: C-terminal extended osteoprotegerin encoded by *TNFRSF11B* readthrough mutation; *TNFSF11*: gene encoding RANK ligand; *TNFRSF11B*: gene encoding osteoprotegerin or OPG; *TRAcP*: Tartrate-resistant acid phosphatase.

Table 2. Gene expression analyses of osteoclasts from OPG-XL carriers and sex- and age-matched controls.

Markers of osteoclast activity					
	FD	**P value**		**FD**	**P value**
TNFRSF11B			***DC-STAMP***		
Day 7	**2.0**	**$1.7x10^{-2}$**	Day 7	1.0	$9.9x10^{-1}$
Day 14	**-1.9**	**$1.5x10^{-2}$**	Day 14	1.2	$9.5x10^{-2}$
Day 21	**1.8**	**$2.8x10^{-2}$**	**Day 21**	**1.5**	**$1.0x10^{-4}$**
TNFSF11			**TRAcP**		
Day 7	**2.4**	**$1.0x10^{-4}$**	**Day 7**	**-2.2**	**$1.0x10^{-4}$**
Day 14	-1.2	$6.4x10^{-1}$	Day 14	-1.1	$5.7x10^{-1}$
Day 21	**1.6**	**$1.6x10^{-2}$**	**Day 21**	**1.5**	**$6.2x10^{-3}$**
NFATc1			***CTSK***		
Day 7	**-1.3**	**$1.2x10^{-2}$**	**Day 7**	**-2.1**	**$1.0x10^{-4}$**
Day 14	1.1	$1.2x10^{-1}$	**Day 14**	**2.2**	**$1.0x10^{-4}$**
Day 21	**1.6**	**$1.0x10^{-4}$**	**Day 21**	**2.1**	**$1.0x10^{-4}$**

[a]Results presented are the average of $n = 2–3$ replicates from $N = 4–5$ OPG-XL carriers compared with age- and sex-matched controls. *P*-values determined with two-way ANOVA with Sidak's multiple comparison analysis (P-values > 0.05 are indicated in bold). FD: fold difference; OPG-XL: C-terminal extended osteoprotegerin encoded by *TNFRSF11B* readthrough mutation.

DISCUSSION

In the current study we explored the mechanism by which OPG-XL causes the characteristic bidirectional phenotype of subchondral bone turnover accompanied by cartilage mineralization in CCAL1 patients. Notably, OPG-XL displaying 19 additional amino acids at the C-terminal end, was previously found to hamper the formation of a stable HS-OPG-RANKL complex on the osteoblast membrane, (17) permitting RANKL mediated osteoclastogenesis in a murine model (11). Here we show that human osteoclastogenesis with monocytes from OPG-XL carriers relative to sex- and age-matched controls after an initial delay, indeed have enhanced osteoclastogenesis towards prominent large and active osteoclasts. By further characterization of OPG-XL by employing hiPSCs from a carrier of the mutation and two isogenic CRISPR/Cas9-corrected controls in cartilage and bone organoids, we demonstrated for the first time that, likely due to interference with RANKL-HS-OPG, the mutation at the CCAL1 locus directly affects healthy osteoblast and chondrocyte states towards mineralization via respectively *DIO2* and *MGP* functions. The fact that OPG/RANKL as well as *DIO2* (29) and *MGP* (2, 31) are intrinsically involved in joint tissue (patho)physiology might indicate a link to common age-related osteoarthritis.

The hiPSC-derived neo-cartilage tissue deposited by OPG-XL chondrocytes, relative to isogenic controls, revealed a fibrotic histological phenotype with marked downregulation of *COL2A1:COL1A1* ratio and most notable, downregulation of *MGP* expression. *MGP* is a well-known inhibitor of ectopic bone formation (5) and a robust OA risk gene (24, 31) with the risk allele associated towards lower gene expression levels (2, 31). Hence, our data, showing lower expression of *MGP* in OPG-XL neo-cartilage organoids, suggest that OPG-XL directly affects propensity of chondrocytes to enter a mineralized OA state. On a different note, we showed that in OPG-XL neo-cartilage organoids the OPG/RANKL/RANK triad was not changed.

Neo-osseous tissue deposited by osteoblasts from hiPSCs carrying the mutation relative to their isogenic controls did display high calcification as reflected by the prominent Alizarin red staining concurrent with notable high expression of *DIO2*. *DIO2*, encoding type 2 deiodinase enzyme, is essentially facilitating bone formation and mineralization (32). Together, results of our human OPG-XL cartilage and bone organoids demonstrates that the mutation directly affects chondrocyte and osteoblast gene expression profiles marking matrix mineralization processes. We hypothesize that this is due to the impaired binding of OPG with HS, likely in interaction with RANKL as recently shown (11). Since the prominent Alizarin red staining of neo-osseous tissue, concurrent with *DIO2* upregulation could explain the extensive phenotypic foci of calcified cartilage observed in affected articular cartilage tissue of CCAL1 family members, we hypothesize that the chondrocalcinosis observed in OPG-XL carriers is likely not preceding OA onset in cartilage but arises merely during ongoing OA pathophysiology i.e. when chondrocytes have a tendency to undergo trans-differentiation to osteoblast (33).

By performing osteoclastogenesis assays of OPG-XL carriers relative to age- and sex-matched controls we showed that, although significantly lower in number, osteoclastogenesis in OPG-XL carriers resulted in high nucleated osteoclasts (**Figure 3**). These multi-nuclear osteoclasts appear at least equally active as controls as demonstrated by the comparable resorbed bone surface and released levels of CTX-I (**Figure 4**). The fact that we were able to quantify the resorption pits only for 2 donors and controls has likely resulted in limited statistical power to detect small differences. This hypothesis could hence explain the bidirectional phenotype of the OPG-XL carriers characterized by higher cartilage mineralization and osteopenia. A similar case was previously reported by Zhang et al (34), where MGP knock out mice have a characteristic phenotype of premature bone mineralization and osteopenia. Since RANKL was found to induce osteoclast fusion whereas OPG blocked fusion of highly mobile osteomorphs, (15) it is tempting to link the role of immobilized OPG on

the surface of osteoblasts to *in vivo* recycling of osteoclasts (35). Nevertheless, our study does not allow to distinguish whether the OPG-XL mutation results in highly nucleated and active osteoclasts due to enhanced RANKL availability or due to dysfunctional blocking of osteomorph fusion.

Among genes significantly changed in the presence of OPG-XL we observed that *MMP13* was higher in the primary chondrocytes while it was lower in the iPSC-derived chondrocytes. This suggests that *MMP13* itself is not directly related to the changes resulting from OPG-XL, but rather, that the effect results from individual variation and/or differences in the maturity of neo-cartilage derived from hiPSCs as compared to that of primary chondrocytes.

By precise genetic engineering of hiPS cells derived from affected CCAL1 family members, while applying established differentiation protocols towards human biomimetic cartilage and osseous organoids, (36) we could study in multiple biological replicates how expression of OPG-XL could result in the characteristic bidirectional phenotype of subchondral bone turnover accompanied by cartilage mineralization. Strength of using isogenic controls is that this allows to study unbiased effects of the mutation, independent of variation between family members such as genetics, sex or age. As such, we are confident that our approach was able to create reliable data highly translating to human *in vivo* situation while complying to the societal need to reduce animal studies (37, 38). A potential drawback of our study is that we were not able to model direct interaction between cells populating cartilage and bone; chondrocytes, osteoblast and osteoclasts. In this context, using the isogenic pairs of our patient-derived hiPSCs in human joint-on-chip models, currently being developed, could further address the molecular mechanism underlying the bi-directional effect OPG on hard and soft tissues (39, 40).

In conclusion, our data demonstrated that expression of OPG-XL in human cartilage and bone is not only enhancing RANKL-induced osteoclastogenesis but also directly affecting chondrocyte and osteoblast states towards matrix mineralization via functions of respectively *MGP* and *DIO2*. We advocate that the bidirectional phenotype of subchondral bone turnover accompanied by cartilage mineralization is a characteristic process that occurs in CCAL1 patients at early ages but which can be extrapolated to common age related OA patients. Vice versa, our data suggest that in cartilage, proper binding of OPG to HS on chondrocytes intrinsically contributes to a healthy unmineralized tissue state while in bone it supports the steady state turnover with adaptive activity involving osteoblasts and osteoclasts.

Acknowledgements

We thank members of the early-onset family and all the participants of the RAAK study. The LUMC has and is supporting the RAAK study. We thank all the members of our group for valuable discussion and feedback. We also thank Enrike van der Linden, Demiën Broekhuis, Peter van Schie, Shaho Hasan, Maartje Meijer, Daisy Latijnhouwers and Geert Spierenburg for collecting the RAAK material, and Luuk Ciere and Ankita Das for their support in the disease model generation. We thank Valeria Orlova for expert suggestions regarding differentiation of hiPSCs, and the Sequence Analysis Support Core (SASC) of the Leiden University Medical Center for their support.

Funding

Research leading to these results has received funding from the Dutch Arthritis Society (DAF-16-1-406 and DAF-16-1-405), and the Dutch Scientific Research council NWO/ZonMW VICI scheme (nr 91816631/528). This work was partly supported by grants from Marie Curie Initial Training Network (Euroclast, FP7-People-2013-ITN: #607447). Data is generated within the scope of the Medical Delta programs Regenerative Medicine 4D and Improving Mobility with Technology.

Disclosure of potential conflicts of interest

None declared.

Data availability statement

The data that support the funding of this study are available from the corresponding author upon request.

Ethics approval and consent to participate

The Medical Ethics Committee of the LUMC gave approval for the RAAK study (P08.239 and P19.013), the familial OA (FOA) study (P12-256), and for generation of hiPSCs from skin fibroblasts of healthy donors (P13.080). Informed consent was obtained from all participants and donors in our manuscript.

REFERENCES

1. Findlay DM, Kuliwaba JS. Bone-cartilage crosstalk: a conversation for understanding osteoarthritis. Bone Res. 2016;4:16028-40.
2. Houtman E, Coutinho de Almeida R, Tuerlings M, Suchiman HED, Broekhuis D, Nelissen R, et al. Characterization of dynamic changes in Matrix Gla Protein (MGP) gene expression as function of genetic risk alleles, osteoarthritis relevant stimuli, and the vitamin K inhibitor warfarin. Osteoarthritis Cartilage. 2021;29(8):1193-1202.
3. Vassalle C, Mazzone A. Bone loss and vascular calcification: A bi-directional interplay? Vascul Pharmacol. 2016;86:77-86.
4. Bucay N, Sarosi I, Dunstan CR, Morony S, Tarpley J, Capparelli C, et al. osteoprotegerin-deficient mice develop early onset osteoporosis and arterial calcification. Genes Dev. 1998;12(9):1260-8.
5. Luo G, Ducy P, McKee MD, Pinero GJ, Loyer E, Behringer RR, et al. Spontaneous calcification of arteries and cartilage in mice lacking matrix GLA protein. Nature. 1997;386(6620):78-81.
6. Theoleyre S, Wittrant Y, Tat SK, Fortun Y, Redini F, Heymann D. The molecular triad OPG/RANK/RANKL: involvement in the orchestration of pathophysiological bone remodeling. Cytokine Growth Factor Rev. 2004;15(6):457-75.
7. Kiechl S, Werner P, Knoflach M, Furtner M, Willeit J, Schett G. The osteoprotegerin/RANK/RANKL system: a bone key to vascular disease. Expert Rev Cardiovasc Ther. 2006;4(6):801-11.
8. Tschiderer L, Willeit J, Schett G, Kiechl S, Willeit P. Osteoprotegerin concentration and risk of cardiovascular outcomes in nine general population studies: Literature-based meta-analysis involving 26,442 participants. PLOS ONE. 2017;12(8):e0183910.
9. Ramos YF, Bos SD, van der Breggen R, Kloppenburg M, Ye K, Lameijer EW, et al. A gain of function mutation in *TNFRSF11B* encoding osteoprotegerin causes osteoarthritis with chondrocalcinosis. Ann Rheum Dis. 2015;74(9):1756-62.
10. Baldwin CT, Farrer LA, Adair R, Dharmavaram R, Jimenez S, Anderson L. Linkage of early-onset osteoarthritis and chondrocalcinosis to human chromosome 8q. Am J Hum Genet. 1995;56(3):692-7.
11. Mitton-Fitzgerald E, Gohr CM, Williams CJ, Ortiz A, Mbalaviele G, Rosenthal AK. Effects of the *TNFRSF11B* Mutation Associated With Calcium Pyrophosphate Deposition Disease in Osteoclastogenesis in a Murine Model. Arthritis & Rheumatology. 2021;73(8):1543-9.
12. Williams CJ, Qazi U, Bernstein M, Charniak A, Gohr C, Mitton-Fitzgerald E, et al. Mutations in osteoprotegerin account for the CCAL1 locus in calcium pyrophosphate deposition disease. Osteoarthritis Cartilage. 2018;26(6):797-806.
13. Meulenbelt I, Bijkerk C, Breedveld FC, Slagboom PE. Genetic linkage analysis of 14 candidate gene loci in a family with autosomal dominant osteoarthritis without dysplasia. J Med Genet. 1997;34(12):1024-7.
14. Boyce BF, Xing L. Functions of RANKL/RANK/OPG in bone modeling and remodeling. Arch Biochem Biophys. 2008;473(2):139-46.
15. McDonald MM, Khoo WH, Ng PY, Xiao Y, Zamerli J, Thatcher P, et al. Osteoclasts recycle via osteomorphs during RANKL-stimulated bone resorption. Cell. 2021;184(5):1330-47.e13.
16. Li M, Yang S, Xu D. Heparan Sulfate Regulates the Structure and Function of Osteoprotegerin in Osteoclastogenesis. The Journal of biological chemistry. 2016;291(46):24160-71.
17. Li M, Xu D. Antiresorptive activity of osteoprotegerin requires an intact heparan sulfate-binding site. Proceedings of the National Academy of Sciences. 2020;117(29):17187-94.
18. Abhishek A, Doherty S, Maciewicz R, Muir K, Zhang W, Doherty M. Association between low cortical bone mineral density, soft-tissue calcification, vascular calcification and chondrocalcinosis: a case-control study. Ann Rheum Dis. 2014;73(11):1997-2002.
19. Coutinho de Almeida R, Ramos YFM, Mahfouz A, den Hollander W, Lakenberg N, Houtman E, et al. RNA sequencing data integration reveals an miRNA interactome of osteoarthritis cartilage. Ann Rheum Dis. 2019;78(2):270-7.

20. Ramos YF, den Hollander W, Bovee JV, Bomer N, van der Breggen R, Lakenberg N, et al. Genes involved in the osteoarthritis process identified through genome wide expression analysis in articular cartilage; the RAAK study. PLoS One. 2014;9(7):e103056.
21. den Hollander W, Ramos YF, Bomer N, Elzinga S, van der Breggen R, Lakenberg N, et al. Transcriptional associations of osteoarthritis-mediated loss of epigenetic control in articular cartilage. Arthritis Rheumatol. 2015;67(8):2108-16.
22. Ijiri K, Zerbini LF, Peng H, Otu HH, Tsuchimochi K, Otero M, et al. Differential expression of GADD45beta in normal and osteoarthritic cartilage: potential role in homeostasis of articular chondrocytes. Arthritis Rheum. 2008;58(7):2075-87.
23. Tuerlings M, van Hoolwerff M, Houtman E, Suchiman E, Lakenberg N, Mei H, et al. RNA Sequencing Reveals Interacting Key Determinants of Osteoarthritis Acting in Subchondral Bone and Articular Cartilage: Identification of IL11 and CHADL as Attractive Treatment Targets. Arthritis Rheumatol. 2021;73(5):789-99.
24. Boer CG, Hatzikotoulas K, Southam L, Stefánsdóttir L, Zhang Y, Coutinho de Almeida R, et al. Deciphering osteoarthritis genetics across 826,690 individuals from 9 populations. Cell. 2021;184(18):4784-818.e17.
25. Rodriguez Ruiz A, Dicks A, Tuerlings M, Schepers K, van Pel M, Nelissen R, et al. Cartilage from human-induced pluripotent stem cells: comparison with neo-cartilage from chondrocytes and bone marrow mesenchymal stromal cells. Cell Tissue Res. 2021;386(2):309-320.
26. Dambrot C, van de Pas S, van Zijl L, Brandl B, Wang JW, Schalij MJ, et al. Polycistronic lentivirus induced pluripotent stem cells from skin biopsies after long term storage, blood outgrowth endothelial cells and cells from milk teeth. Differentiation. 2013;85(3):101-9.
27. Sprangers S, Schoenmaker T, Cao Y, Everts V, de Vries TJ. Different Blood-Borne Human Osteoclast Precursors Respond in Distinct Ways to IL-17A. J Cell Physiol. 2016;231(6):1249-60.
28. de Vries TJ, Schoenmaker T, Beertsen W, van der Neut R, Everts V. Effect of CD44 deficiency on in vitro and in vivo osteoclast formation. J Cell Biochem. 2005;94(5):954-66.
29. Bomer N, denHollander W, Ramos YF, Bos SD, van der Breggen R, Lakenberg N, et al. Underlying molecular mechanisms of DIO2 susceptibility in symptomatic osteoarthritis. Ann Rheum Dis. 2015;74(8):1571-9.
30. Zeger SL, Liang KY. Longitudinal data analysis for discrete and continuous outcomes. Biometrics. 1986;42(1):121-30.
31. den Hollander W, Boer CG, Hart DJ, Yau MS, Ramos YFM, Metrustry S, et al. Genome-wide association and functional studies identify a role for matrix Gla protein in osteoarthritis of the hand. Ann Rheum Dis. 2017;76(12):2046-53.
32. Bassett JH, Boyde A, Howell PG, Bassett RH, Galliford TM, Archanco M, et al. Optimal bone strength and mineralization requires the type 2 iodothyronine deiodinase in osteoblasts. Proc Natl Acad Sci U S A. 2010;107(16):7604-9.
33. Zhou X, von der Mark K, Henry S, Norton W, Adams H, de Crombrugghe B. Chondrocytes transdifferentiate into osteoblasts in endochondral bone during development, postnatal growth and fracture healing in mice. PLoS genetics. 2014;10(12):e1004820.
34. Zhang Y, Zhao L, Wang N, Li J, He F, Li X, et al. Unexpected Role of Matrix Gla Protein in Osteoclasts: Inhibiting Osteoclast Differentiation and Bone Resorption. Mol Cell Biol. 2019;39(12).
35. Jansen ID, Vermeer JA, Bloemen V, Stap J, Everts V. Osteoclast fusion and fission. Calcif Tissue Int. 2012;90(6):515-22.
36. Takahashi K, Tanabe K, Ohnuki M, Narita M, Ichisaka T, Tomoda K, et al. Induction of pluripotent stem cells from adult human fibroblasts by defined factors. Cell. 2007;131(5):861-72.
37. Bédard P, Gauvin S, Ferland K, Caneparo C, Pellerin È, Chabaud S, et al. Innovative Human Three-Dimensional Tissue-Engineered Models as an Alternative to Animal Testing. Bioengineering (Basel). 2020;7(3):115-55.
38. Goldstein DB, Allen A, Keebler J, Margulies EH, Petrou S, Petrovski S, et al. Sequencing studies in human genetics: design and interpretation. Nat Rev Genet. 2013;14(7):460-70.

39. Ma H-P, Deng X, Chen D-Y, Zhu D, Tong J-L, Zhao T, et al. A microfluidic chip-based co-culture of fibroblast-like synoviocytes with osteoblasts and osteoclasts to test bone erosion and drug evaluation. R Soc Open Sci. 2018;5(9):180528-40.
40. Wu Q, Liu J, Wang X, Feng L, Wu J, Zhu X, et al. Organ-on-a-chip: recent breakthroughs and future prospects. Biomed Eng Online. 2020;19(1):9-28.

Supplementary figures:

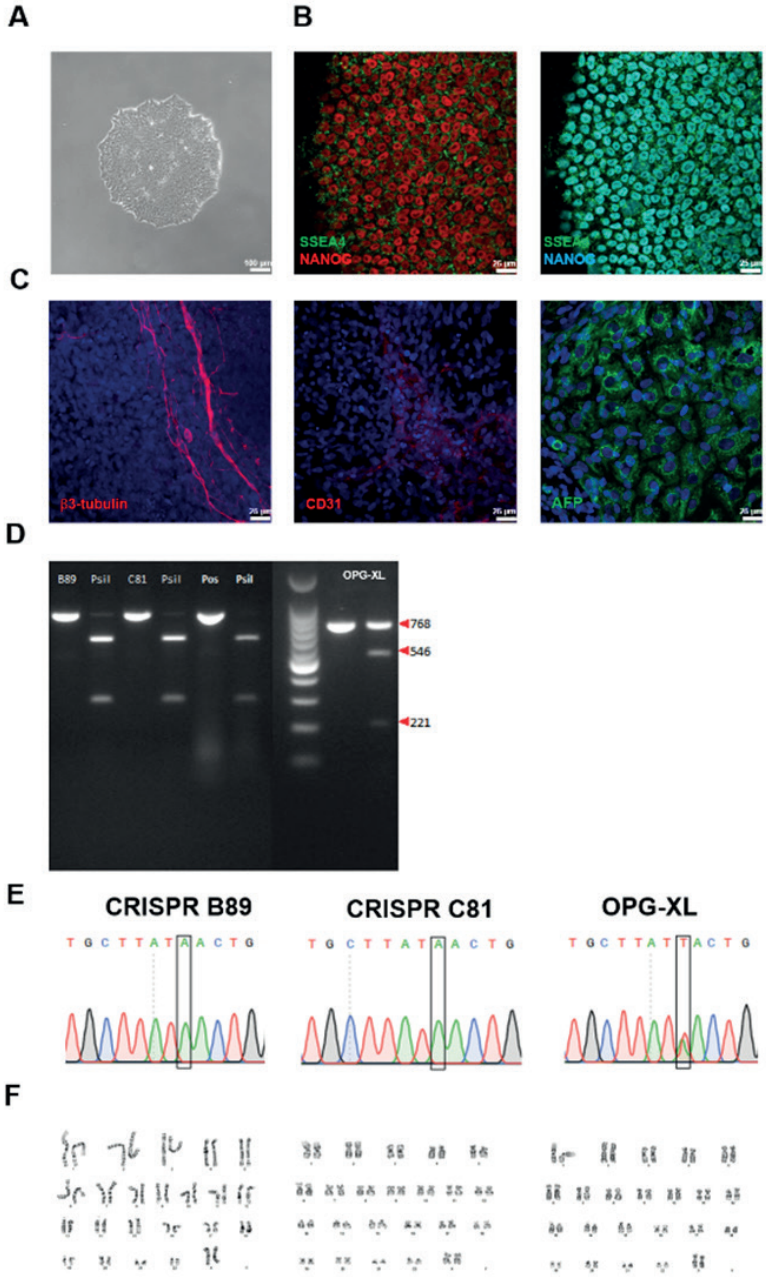

Supplementary Figure S1. Characterization of generated OPG-XL hiPSCs and CRISPR/Cas9-corrected clonal screening. A) Bright field microscopy image of a representative OPG-XL mutated hiPSC colony. **B**) Immunofluorescent staining for NANOG, SSEA-4, and OCT3/4 confirming pluripotency. **C**) Expression of β3-Tubulin, CD31, and AFP upon spontaneous differentiation into

the three different lineages (ectoderm, mesoderm and endoderm, respectively). Nuclei are stained with Dapi (blue). **D**) Clonal screening for OPG-XL repaired mutation by genomic PCR followed by PsiI digestion. Patient DNA shows three bands after PsiI digestion, whereas repaired clones B89 (gRNA1) and C81 (gRNA2) together with the positive control show two bands. **E**) Sanger sequencing and **F**) karyotyping of 2 corrected clones and OPG-XL hiPSC line.

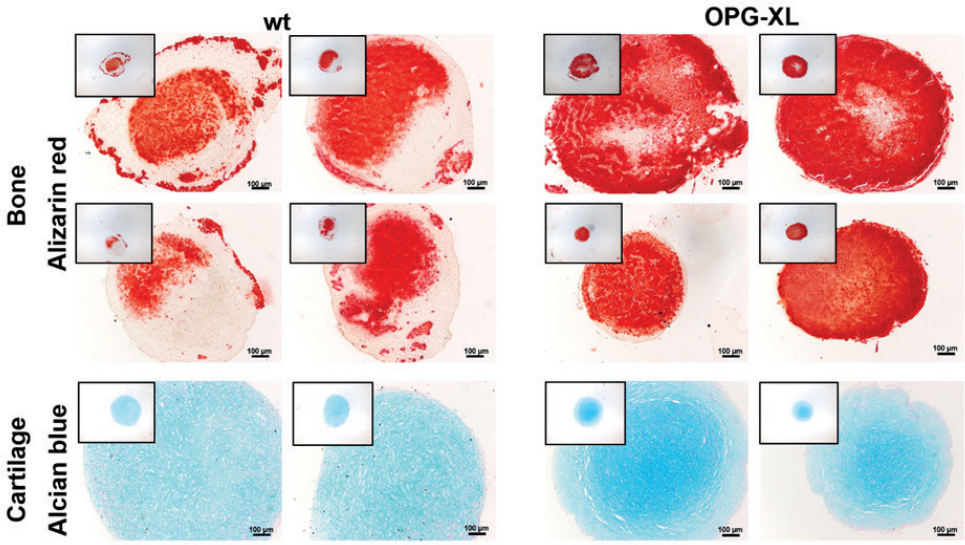

Supplementary Figure S2. Alcian Blue and Alizarin red staining of different neo-cartilage and neo-bone organoids. Histology of organoids resulting from different experiments at day 42 of chondrogenesis stained with Alcian Blue (n=2 independent differentiations) and day 14 of osteogenesis (n=4 independent differentiations) stained with Alizarin red (scale bars: 100µm).

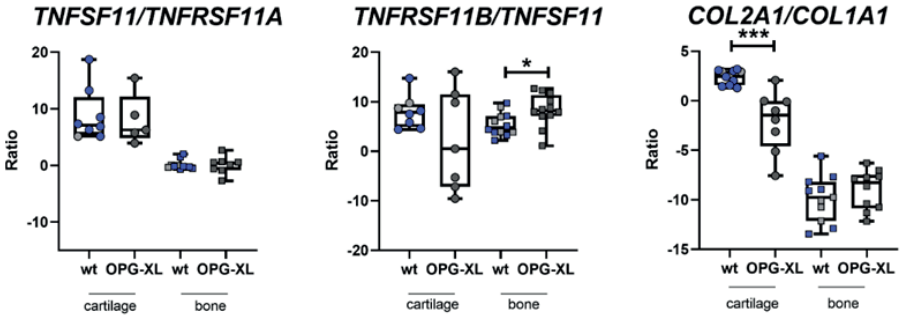

Supplementary Figure S3. Ratios of *TNFSF11/TNFRSF11A*, *TNFRSF11B/TNFSF11* and *COL2A1/COL1A1* in neo-cartilage and neo-bone of the OPG-XL mutation and CRISPR/Cas9-corrected samples. Results shown are at day 42 of chondrogenesis and day 14 of osteogenesis (neo-cartilage: n=9-12 for CRISPR-corrected control and n=5-7 for OPG-XL samples; neo-bone: n=7-14 for CRISPR-corrected control and n=10-16 for OPG-XL samples.; *P-value<0.05; **P-value<10^{-4}; ***P-value<10^{-6}).

Supplementary tables:

Supplementary Table S1. Characteristics of FOA participants.

	OPG-XL non-carriers	OPG-XL carriers
Sex (%)		
Male	66.7	42.9
Female	33.3	57.1
Age (years)		
Minimum	23.1	32.5
Maximum	60.5	61.6
Average	41.7 ± 14.3	51.7 ± 12.3
BMI (Kg/m^2)		
Minimum	22.3	24.9
Maximum	29.1	30.1
Average	24.8 ± 3	27.0 ± 1.9

OPG-XL: high impact readthrough mutation in *TNFRSF11B* at CCAL1 locus.

Supplementary Table S2. Skeletal characteristics of participants determined with DEXA scans at different regions of the skeleton.

A

DEXA	OPG-XL non-carriers	Healthy controls
BMD (g/cm2)		
Skull	2.5 ± 0.3	2.5 ± 0.3
Femoral neck	0.9 ± 0.1	0.9 ± 0.1
Narrow neck	1.1 ± 0.2	1.1 ± 0.1
Lumbar spine	1.1 ± 0.2	-
Total body	1.1 ± 0.2	1.2 ± 0.1
Total hips	1.0 ± 0.1	1.0 ± 0.1
Narrow neck width (cm)	3.6 ± 0.4	3.5 ± 0.4

Results presented are the average of OPG-XL non-carriers (N=7) versus non-related healthy controls (N=253).

B

DEXA	OPG-XL non-carriers	OPG-XL carriers	P value [a]
BMD (g/cm²)			
Skull	2.5 ± 0.3	2.3 ± 0.5	$4.3x10^{-1}$
Femoral neck	0.9 ± 0.1	0.7 ± 0.1	**$1.8x10^{-2}$**
Narrow neck	1.1 ± 0.2	0.8 ± 0.1	**$4.5x10^{-3}$**
Lumbar spine	1.1 ± 0.2	1.1 ± 0.2	$8.8x10^{-1}$
Total body	1.1 ± 0.2	1.2 ± 0.2	$1.8x10^{-1}$
Total hips	1.0 ± 0.1	0.8 ± 0.1	**$7.2x10^{-3}$**
Narrow neck width (cm)	3.6 ± 0.4	3.9 ± 0.2	**$4.1x10^{-4}$**
T-score			
Hips	-0.1 ± 1.4	-1.4 ± 0.6	**$1.2x10^{-2}$**
Lumbar spine	-0.1 ± 1.5	0.2 ± 1.8	$8.8x10^{-1}$
MOAKS			
BML and Cysts (#)	0.3 ± 0.5	18.6 ± 14.1	**$2.4x10^{-5}$**

Results presented are the average of FOA members (7 carriers versus 6 non-carriers of the OPG-XL mutation; # number).

[a]P-value was determined by performing a generalized estimation equation (GEE), with BMD, Narrow neck, T-score, and BML and cysts as dependent variable, and age, sex and BMI as covariate.

OPG-XL: high impact readthrough OPG mutation at CCAL1 locus.

Supplementary Table S3. MOAKS grading of knee joints.

MOAKS	Grades			
Osteophytes (Size)	**0**	**1**	**2**	**3**
OPG-XL non-carrier (%)	95.8 ± 5.3	4.2 ± 5.3	0	0
OPG-XL carrier (%)	30.0 ± 23.3	31.7 ± 13.4	21.7 ± 9.0	16.7 ± 17.7
P value [a]	**$6.8x10^{-4}$**	**$2.3x10^{-4}$**	**$3.4x10^{-4}$**	**$1.7x10^{-3}$**
BML & Cyst (Size)	**0**	**1**	**2**	**3**
OPG-XL non-carrier (%)	98.9 ± 1.7	1.1 ± 1.7	0	0
OPG-XL carrier (%)	57.3 ± 19.6	30.0 ± 7.1	5.3 ± 6.1	7.3 ± 8.3
P value [a]	**$1.7x10^{-10}$**	**$1.0x10^{-30}$**	**$2.0x10^{-2}$**	**$2.4x10^{-2}$**
BML & Cyst (%)	**0**	**1**	**2**	**3**
OPG-XL non-carrier (%)	99.4 ± 1.4	0	0	0.6 ± 1.4
OPG-XL carrier (%)	63.3 ± 17.0	4.7 ± 6.5	4.7 ± 7.3	26.0 ± 7.6
P value [a]	**$2.0x10^{-9}$**	$1.0x10^{-1}$	**$7.3x10^{-2}$**	**$0.0x10^{-30}$**
Cartilage (%)	**0**	**1**	**2**	**3**
OPG-XL non-carrier (%)	91.8 ± 8.1	5.8 ± 5.8	3.0 ± 3.6	0.9 ± 1.5
OPG-XL carrier (%)	56.4 ± 19.3	7.6 ± 4.3	4.4 ± 2.1	33.1 ± 17.3
P value [a]	**$3.7x10^{-4}$**	$7.8x10^{-1}$	$3.6x10^{-1}$	**$4.5x10^{-10}$**

Results presented are the average of FOA members (5 carriers versus 6 non-carriers of the OPG-XL mutation; 2 carriers were excluded due to knee prosthetics).
[a]P-value was determined by performing a generalized estimation equation (GEE), with osteophyte (size), BML and cysts size and percentage, and cartilage percentage as dependent variable, and age, sex and BMI as covariate.
OPG-XL: high impact readthrough OPG mutation at CCAL1 locus.

Supplementary Table S4. Osteoclastogenesis assay of OPG-XL family members against age- and sex-matched controls.

Pair	Participant	Sex	Age
1	Control	Male	49
	OPG-XL	Male	39
2	Control	Female	53
	OPG-XL	Female	62
3	Control	Female	60
	OPG-XL	Female	60
4	Control	Male	65
	OPG-XL	Male	48
5	Control	Male	54
	OPG-XL	Male	59
6	Control	Female	57
	OPG-XL	Female	61

OPG-XL: individual with familial early-onset osteoarthritis, carrier of high impact readthrough mutation in *TNFRSF11B* at CCAL1 locus.

Supplementary Table S5. Matrix, mineralization, osteoclastogenesis and housekeeping primer sequences.

Matrix Genes	**Fwd**	**Rvs**
ADAMTS5	5′-CGTGTACTTGGGCGATGACA-3′	5′-CTGTTGTTGCACACCCCTCT-3′
ACAN1	5′AGAGACTCACACAGTCGAAACAGC-3′	5′-CTATGTTACAGTGCTCGCCAGTG-3′
COL10A1	5′-GGCAACAGCATTATGACCCA-3′	5′-TGAGATCGATGATGGCACTCC-3′
COL1A1	5′-GTGCTAAAGGTGCCAATGGT-3′	5′-ACCAGGTTCACCGCTGTTAC -3′
COL2A1	5′-CTACCCCAATCCAGCAAACGT-3′	5′-AGGTGATGTTCTGGGAGCCTT-3′
COMP	5′-ACAATGACGGAGTCCCTGAC-3′	5′-TCTGCATCAAAGTCGTCCTG-3′
MMP13	5′-TTGAGCTGGACTCATTGTCG-3′	5′-GGAGCCTCTCAGTCATGGAG-3′
SOX9	5′-CCCCAACAGATCGCCTACAG-3′	5′-CTGGAGTTCTGGTGGTCGGT-3′
SMAD3	5′-GCCCCTTTCAGGTAACCGTC-3′	5′-GAAGCGGCTGATGCTCCTTA-3′
MMP3	5′-GAGGCATCCACACCCTAGGTT-3′	5′-TCAGAAATGGCTGCATCGATT-3′
Mineralization genes	**Fwd**	**Rvs**
ALPL	5′-CAAAGGCTTCTTCTTGCTGGTG-3′	5′-CCTGCTTGGCTTTTCCTTCA-3′
ASPN	5′-ACACGTTTTGGAAATGAGTGC-3′	5′-GAACACCGTCACCCCTTCAA-3′
MGP	5′-CGCCCCCAGATTGATAAGTA-3′	5′-TCTCCTTTGACCCTCACTGC-3′
POSTN	5′-TACACTTTGCTGGCACCTGT-3′	5′-TTTAAGGAGGCGCTGATCCA-3′
RUNX2	5′-CAATTTCCTCCTTGCCCCTCA-3′	5′-TCGGATCTACGGGAATACGCA-3′
SPP1	5′-GCCAGTTGCAGCCTTCTCA-3′	5′-AAAAGCAAATCACTGCAATTCTCA-3′
TNFRSF11A	5′-GAAGCTCAGCCTTTTGCTCA-3′	5′-GGGAACCAGATGGGATGTCG-3′
TNFRSF11B	5′-TTGATGGAAAGCTTACCGGGA-3′	5′-TCTGGTCACTGGGTTTGCATG-3′
TNFSF11	5′-CAACAAGGACACAGTGTGCAA-3′	5′-AGGTACAGTTGGTCCAGGGT-3′
DIO2	5′-TTCCAGTGTGGTGCATGTCTC-3′	5′-AGTCAAGAAGGTGGCATGTGG-3′
IL11	5′-CTCTACAGCTCCCAGGTGTGC-3′	5′-AGGTAGGACAGTAGGTCCGCT-3′
SOST1	5′-GAGCTGGAGAACAACAAGACCA-3′	5′-AGCTGTACTCGGACACGTCTTTG-3′
Osteoclastogenesis genes	**Fwd**	**Rvs**
NFATc1	5′-AGCAGAGCACGGACAGCTATC-3′	5′-GGTCAGTTTTCGCTTCCATCTC-3′
DC-STAMP	5′-ATTTTCTCAGTGAGCAAGCAGTTTC-3′	5′-AGAATCATGGATAATATCTTGAGTTCCTT-3′
TRAcP	5′-CACAATCTGCAGTACCTGCAAGAT-3′	5′-CCCATAGTGGAAGCGCAGATA-3′
Cathepsin K	5′-CCATATGTGGGACAGGAAGAGAGTT-3′	5′-TGCATCAATGGCCACAGAGA-3′
Housekeeping genes	**Fwd**	**Rvs**
GAPDH	5′-TGCCATGTAGACCCCTTGAAG-3′	5′-ATGGTACATGACAAGGTGCGG-3′
ARP	5′-CACCATTGAAATCCTGAGTGATGT-3′	5′-TGACCAGCCGAAAGGAGAAG-3′

Supplementary Table S6. Gene expression analyses of primary chondrocytes of an OPG-XL carrier compared against healthy controls.

Extracellular matrix genes				
Genes	**FD**	**Beta**	**SE**	**P value [a]**
COL1A1	**13.8**	**3.8**	**0.3**	**$1.0x10^{-30}$**
COL2A1	-1.8	-0.8	0.6	$1.3x10^{-1}$
COL10A1	**6.9**	**2.8**	**0.3**	**$8.6x10^{-16}$**
ACAN	1.2	0.3	0.4	$4.7x10^{-1}$
SOX9	2.4	1.2	0.7	$7.8x10^{-2}$
ADAMTS5	-1.5	-0.6	1.0	$5.4x10^{-1}$
MMP13	**5.6**	**-2.5**	**0.6**	**$1.0x10^{-5}$**

Results presented are the average of one carrier of the OPG-XL mutation (8 replicates) versus five independent OA patients that underwent joint replacement surgery following three weeks of chondrogenesis.

[a]P-value was determined by performing a generalized estimation equation (GEE) of -ΔCT values, with every independent gene as a dependent variable, and mutation condition as covariate.

Supplementary Table S7. Number of osteoclasts (>3 nuclei) formed in osteoclastogenesis.

Cells/cm² at 14 days	Patient 1		Patient 2		Patient 3		Patient 4		Patient 5		Patient 6		Average	
Nuclei/cell	**Control**	**OPG-XL**	**Control**	**OPG-XL**	**Control**	**OPG-XL**	**Control**	**OPG-XL**	**Control**	**OPG-XL**	**Control**	**OPG-XL**	**Control**	**OPG-XL**
3-5	353.2	123.4	110.9	46.9	134.4	57.8	337.5	62.5	339	125	210.9	100	263	86
6-10	70.3	4.7	4.7	1.6	21.9	0	31.3	3.1	29.7	6.3	20.3	7.8	30	4
11-20	4.7	0	0	0	4.7	0	1.6	0	3.1	0	4.7	0	3	0
> 20	0	0	0	0	0	0	0	0	0	0	0	0	0	0
Total	428.1	128.1	115.6	48.4	160.9	57.8	370.3	65.6	371.9	131.3	235.9	107.8	295	90
Cells/cm² at 21 days	**Patient 1**		**Patient 2**		**Patient 3**		**Patient 4**		**Patient 5**		**Patient 6**		**Average**	
Nuclei/cell	**Control**	**OPG-XL**	**Control**	**OPG-XL**	**Control**	**OPG-XL**	**Control**	**OPG-XL**	**Control**	**OPG-XL**	**Control**	**OPG-XL**	**Control**	**OPG-XL**
3-5	656.3	484.4	551.6	189.1	545.3	253.1	689.1	365.6	854.7	165.6	578.1	284.4	644	290
6-10	134.4	171.9	120.3	198.4	81.3	43.8	59.4	109.4	92.2	109.4	114.1	53.15	94	114
11-20	6.3	71.9	25	65.6	4.7	0	4.7	37.5	23.4	73.4	14.1	67.2	13	53
> 20	4.7	15.6	9.4	31.3	7.8	1.6	4.7	12.5	3.1	23.4	4.7	12.5	6	16
Total	801.6	743.8	706.3	484.4	639.1	298.4	757.8	525	973.4	371.9	710.9	417.2	758	473

Results are presented for each participant (FOA members expressing OPG-XL and age- and sex-matched controls) stratified for number of nuclei per osteoclast and counted in triplicate at day 14 and at day 21.
OPG-XL: high impact readthrough mutation in *TNFRSF11B* at CCAL1 locus.

CHAPTER 5

General discussion

GENERAL DISCUSSION AND FUTURE PERSPECTIVES

SUMMARY

Osteoarthritis disease management is hampered by a lack of translation of robust genetic findings to underlying disease mechanisms, drug target discovery and testing. In this thesis we established sustainable and reliable human 3D *in vitro* organoid models of cartilage and bone for in-depth study of *TNFRSF11B* encoding osteoprotegerin (OPG) in OA pathophysiology. OPG is a decoy receptor binding to the receptor activator of nuclear KB factor ligand (RANKL) to inhibit osteoclastogenesis. It is highly expressed in cartilage and subchondral bone, and was previously found to be consistently upregulated in transcriptome wide studies of OA affected cartilage while no specific function for OPG in cartilage was known. Additionally, a high impact mutation at the CCAL1 locus was identified by our group (1) resulting in a 19 amino acid elongation of OPG and referred to as OPG-XL. The CCAL1 phenotype is characterized by early onset osteoarthritis with different degrees of articular cartilage calcification (chondrocalcinosis), while low subchondral bone mineralization was reported in other identified CCAL1 families (2). Together, by applying next generation human organoid models of cartilage and bone we here set out to study how dysfunctional OPG is associated to OA pathophysiology and particularly for OPG-XL with respect to the bi-directional pathogenic phenotype of bone loss and articular cartilage calcification.

In **Chapter 2** we mimicked OA related expression of *TNFRSF11B* in a 3D *in vitro* model of primary chondrocytes to investigate its role in OA pathophysiology. Hereto, chondrocytes obtained from the Research Arthritis and Articular Tissue (RAAK) study were modified to overexpress *TNFRSF11B*. RNA sequencing data of preserved and lesioned cartilage from the RAAK study was used to identify differentially expressed genes correlating with *TNFRSF11B* expression. This allowed us to study a co-expression network of this gene with its associated genes in OA pathophysiology. Our study showed that *TNFRSF11B* upregulation affects chondrocytes to undergo trans-differentiation to osteoblasts.

In **Chapter 3**, we used human induced pluripotent stem cell (hiPSC) technology for an efficient directed differentiation into neo-cartilage organoids. Particularly, we focused on characterizing neo-cartilage generated from two differentiation protocols: a step-wise protocol towards generation of chondroprogenitors (hiCPCs), and a commercial protocol, following an initial transition to mesenchymal stromal cells (hiMSCs). Subsequently, neo-cartilage generated from both protocols was compared to human neo-cartilage from chondrocytes (hPACs) and bone marrow mesenchymal stromal cells (hBMSCs). Based on a set of 20 relevant genes, this showed a 65% and 53% similarity, respectively. Although still with potential to increase the similarities, our observations are

highly encouraging for the field of cartilage regeneration starting with a stable cell source such as hiPSCs.

In Chapter 4 we set out to perform in depth clinical phenotyping of OPG-XL carriers highlighting on one hand severe cartilage degeneration accompanied with severe foci of calcified cartilage, and on the other hand osteopenic subchondral bone phenotype. To obtain stable and sustainable isogenic cell sources for our model, we generated hiPSCs from an OPG-XL family member and applied CRISPR/Cas9 to repair the OPG-XL mutation. Upon employing our established OPG-XL hiPS cells and isogenic control hiPS cells to established organoid models of neo-cartilage and neo-bone tissue, the underlying disease mechanisms of OPG-XL resulting in familial early-onset OA (FOA) phenotype could be studied in detail. By doing so, we demonstrated that OPG-XL in chondrocytes resulted in excessive cartilage fibrosis marked by downregulation of *MGP*, while OPG-XL in osteoblasts showed high mineralized osseous tissue, accompanied by upregulation of *DIO2* gene expression. By differentiating monocytes from family members with OPG-XL and healthy aged matched controls to osteoclasts, and subsequently culturing them on bone, we showed a delayed osteoclastogenesis with a trend towards more active osteoclast formation in OPG-XL carriers.

Together, our studies demonstrated that generating neo-cartilage from an hiPSC source is possible and, depending on the protocol, this can result in neo-cartilage highly similar to primary chondrocytes or neo-cartilage with more hypertrophic characteristics. This highlights the strength of hiPSC technology not only for regenerative therapies but also for modelling cartilage diseases. Additionally, identified OPG co-expression network can now be exploited to further follow-up on possible novel routes underlying OA pathophysiology. Moreover, by studying the OPG-XL mutation and the common functions of OPG, we can now certainly emphasize that OA, a disease traditionally defined by cartilage loss, is heavily driven by an interplay of chondrocytes, osteoblasts and osteoclasts. The pleiotropy that OPG-XL showed in each cell indicates how OA treatments can be beneficial for one tissue while detrimental for another one. This makes OPG a double-edged sword in OA development that should be carefully monitored when treating this disease.

OSTEOPROTEGERIN; A ROLE IN COMMON OSTEOARTHRITIS

TNFRSF11B encoding for osteoprotegerin (OPG) is one of the most consistent and highly upregulated genes in lesioned OA cartilage (2, 3). Additionally, a readthrough mutation in this gene introducing 19 extra amino acids in OPG (OPG-XL) was found in an early onset OA family characterized by chondrocalcinosis.

High impact causal mutations in extended families with an early onset disease phenotype are especially relevant since they can direct towards underlying pathways that might be sharing the same etiology, hence translating its insights into common OA phenotypes (4-7).

Effects of increased OPG expression in cartilage matrix

By measuring changes of conventional matrix homeostasis and mineralization genes in **Chapter 2** we showed that upregulation of *TNFRSF11B* resulted in an increase in cartilage anabolism as measured by the higher expression of *COL1A1* and *COL2A1* while the fact that *COL10A1* was not increased suggested absence of hypertrophy (8). Nonetheless, a high *MMP13* expression combined with high *RUNX2*, *POSTN*, *ASPN* and *OGN* indicated a likely chondrocyte to osteoblast transition, commonly observed in OA pathophysiology (9, 10). We also showed that, in cartilage, the well-known *TNFRSF11B*, *TNFRSF11* and *TNFSF11A* triad is not responsive to upregulation of *TNFRSF11B.* This, together with the fact that *TNFSF11* is actually lowly expressed in cartilage and we did not find high correlation, determined by values higher than $r \geq 0.75$, between *TNFRSF11B* with *TNFRSF11A* or *TNFSF11* expression in cartilage, suggests that the interaction among the triad in cartilage may not play the same role as in bone.

This is in line with the finding of Komuro *et al* (11) and Tat *et al* (12), showing no alterations in RANK and OPG expression upon adding exogenous RANKL to chondrocytes. Interestingly, *TNFSF11* was revealed as an OA susceptibility gene in the largest OA GWAS to date (13), but this was not the case of *TNFRSF11B* and *TNFRSF11A*. This confirmed once more that the three partners of the triad have additional independent functions. Nevertheless, a higher expression of *TNFRSF11B* and of *TNFSF11* is associated with a worsening of OA status, while *TNFSF11* is one of the higher co-expressed genes to *TNFRSF11B* in OA bone (14).

Gene expression profiling with co-expression analysis has previously been used as a powerful method to identify novel co-expression networks of genes (15). This allows to determine unknown relations between shared pathways that might be of high relevance to the studied gene and to better study complex diseases such as OA (16). Moreover, these signature pathways can serve as potential candidates for diagnosis and the development of novel therapies against biological processes that might be impaired in the diseased condition (15). In our RNA sequencing data, we found 51 genes that highly correlated with *TNFRSF11B* ($r \geq 0.75$), representing the co-expression network of *TNFRSF11B* in OA pathophysiology. From this network, the expression of 30 genes was compared between control hPACs and hPACs overexpressing *TNFRSF11B*. Despite the high correlations with *TNFRSF11B*, notably only eight genes (27%) were found to be responsive to *TNFRSF11B* upregulation in our *in vitro* model (*CDON*, *BMP6*, *CDH19*,

P3H2, WNT16, SLC16A7, SLC15A3 and *FITM2*). This may be explained partly by the fact that some of the genes are upstream of *TNFRSF11B*. Alternatively, genes may be correlated to *TNFRSF11B* as a general result of ongoing OA disease processes, since *TNFRSF11B* is one of the highest upregulated genes in lesioned OA cartilage (3). This illustrates that *in vitro* models are representative for the *in vivo* situation, but also have their limitations.

Notable among the *TNFRSF11B* correlated and highly responsive genes was *BMP6*. *BMP6* encodes the bone morphogenetic protein 6 and is a member of the transforming growth factor superfamily. It is known to have a pleiotropic role that ranges from increasing chondrogenic differentiation potential and proteoglycan deposition, chondrocyte maturation, osteoclast inhibition, induction of bone ECM deposition, and OA development (17-22). By performing our unique co-expression approach we were able to show that BMP6 is strongly upregulated in our model. Given the known functions of *BMP6* in bone formation we hence hypothesize that it might play a role in driving OA by enhancing chondrocyte to osteoblast transition. This highlights the strong potential of our approach to detect novel target genes that otherwise would go unnoticed, and addresses BMP6 and the other osteogenic markers as possible cartilage OA therapeutic targets.

In conclusion, the particularly high upregulation of *MMP13* in combination with the upregulation of characteristic osteogenic genes *RUNX2, POSTN, BMP6, ASPN,* and *OGN* and in absence of differential expression of the hypertrophic and mineralization markers *COL10A1* and *ALPL,* demonstrated that *TNFRSF11B* affects OA pathophysiology by advancing late stage terminal maturation (23). This would urge for novel therapies aiming at directly reducing undesired osteogenic transitions, such as vitamin K supplementation. For that matter, the use of vitamin K antagonist as anticoagulation therapy has shown an increase in progression of hip and knee OA, highlighting the importance that vitamin K pathways can have in OA (24). Therefore, it could be speculated that vitamin K may also be considered as a possible treatment in the OPG-XL family members, since the function of MGP is dependent on this vitamin. Likewise, these highly OPG responding genes might arise as attractive targets for researching its molecular effect and bring into play novel drug treatments. On the other hand, we were not able to visualize a mineralization effect at immunohistochemistry or histology levels. This might be due to the selected early timepoint (day 7) for evaluating chondrocyte neo-cartilage deposition towards mineralization of the ECM (25). A later timepoint might have shown a stronger mineralization at protein level (23, 26). An alternative approach would be to upregulate of *TNFRSF11B* in MSCs (27) with subsequent generation of neo-cartilage. This would likely show an even stronger mineralization effect including matrix calcification. Ultimately, the lack of changes in expression in the *TNFRSF11B* triad in cartilage suggests it functions differently as in bone, highlighting more research is needed to understand their function in cartilage.

hiPSC TECHNOLOGY IN CARTILAGE REGENERATION AND DISEASE MODELING

hiPSCs provide sustainable and reliable OA relevant tissue organoids while reduce dependence on joint tissue availability. Additionally, they address the societal need to reduce, refine and replace the use of animals models (28). When combined with CRISPR/Cas9 genetic engineering, we can precisely repair or introduce disease mutations and generate isogenic controls with identical genetic background to study their particular effect. Nonetheless, hiPSCs have also shown challenges due to the strong variation in differentiation efficiencies between lines and a tendency to generate hypertrophic and fibrous matrix (29-31). In **Chapter 3** we therefore first assessed the efficiency of hiPSCs neo-cartilage organoid production as well as its quality as compared to the autologous tissue by following a step-wise protocol to generate chondrocytes from human iPSC-derived chondroprogenitor cells (hiCPCs) (32) and a commercial protocol via human iPSC-derived mesenchymal stromal cells (hiMSCs).

By prioritizing on *COL2A1* neo-cartilage gene expression (33), we observed a 79% success rate for the step-wise protocol via hiCPCs and a 54% success rate for the commercial protocol via hiMSCs. For that matter, hiMSCs displayed high levels of heterogeneity in cell morphology and proliferation with respect to each other whereas classical hBMSC characterization markers associated to trilineage differentiation potential did not correlate to chondrogenesis success. Although a 79% success rate is considerable, more research is necessary to improve expansion of hiCPCs. It could be questioned if prioritization for *COL2A1* was the optimal strategy since *COL2A1* is a late chondrogenic marker also expressed in a wide variety of cells (33).

Next, we compared the quality of the neo cartilage deposited by hiCPCs relative to human primary chondrocytes (hPACs) and of hiMSCs relative to human bone marrow mesenchymal stromal cell (hBMSCs) based on a similarity panel of 20 genes related to chondrogenesis, hypertrophy and degradation of cartilage ECM. For hiCPCs relative to hPAC neo-cartilage we observed a 65% similarity. For the hiMSCs relative to hBMSCs we observed a similarity of 53%.

These results suggest that the matrix generated by hiMSCs had a hypertrophic phenotype defined by a high gene expression of *COL1A1*, *ALPL,* and *MMP13* and low *COL2A1*. The expression of *MMP13* and *ALPL* would suggest a higher collagen degradation with a subsequent calcification, characteristic of terminal chondrogenic differentiation and endochondral ossification (34, 35). A follow-up strategy could be based on the selection of an earlier chondrogenic marker such as *SOX9*. This was recently performed for immortalized adipose-derived stem cells resulting in an enhanced chondrogenic potential in these cells

accompanied with low hypertrophy (36, 37). Hence, at its current state, it could be advocated that hiMSCs are an ideal candidate for studying skeletal diseases in which endochondral bone formation and hypertrophy are driving mechanisms (38, 39). Nonetheless, for obtaining high quality neo-cartilage an improvement of this protocol is still required.

With respect to the step-wise protocol, we can certainly claim that hiCPCs are an excellent tool for efficiently (79%) producing high quality neo-cartilage (65%). The main differences between hPAC and hiCPC neo-cartilage are based on a higher expression of chondrogenic markers and lower hypertrophy in the hiCPCs. This would make them suitable candidates for production of neo-cartilage implants as regenerative therapy and drug testing applications. To have a further translation into the clinic, neo-cartilage generated from hiCPCs should be initially tested by implantation in animal models (40), and subsequently translated into humans. Nevertheless, the lack of expansion capacity of hiCPCs arises an issue that urgently needs to be solved for further translational applications.

Neo-cartilage generation with the current hiMSCs differentiation protocol requires an optimization of the initial chondrogenic selection process. In this respect, we observed that during the experiments of **Chapter 4**, higher concentrations of cells (750000 cells/pellet) resulted in a more stable cartilage deposition, similarly to results observed by Diederichs et al (37). Hence, we advocate that high quality neo-cartilage deposition from hiMSCs requires a higher cell density (41). Another decisive factor to determine chondrogenic potential was the cell proliferation rate. This parameter was not quantitatively measured in our study. Yet, when analyzing the time frame required for cell passaging, we observed that fast proliferating cells generated a more homogenous neo-cartilage deposition (unpublished data). This was similar to results shown by Dexheimer et al (42) and Mareddy et al (43) in BMSCs. Finally, several compounds can be administered to enhance mesodermal differentiation and improve successful chondrogenesis yield (44). For instance, Kreuser et al (45) noticed that an initial WNT/β-catenin pulse by CHIR99021, an essential process for primitive streak induction, strongly enhanced ECM-related gene expression markers and chondrogenic pellet formation. On the other hand, WNT inhibition during hiPSC derived-chondrogenesis showed a better cartilage deposition (46), altogether, suggesting the timing of activation and inhibition is key. Due to other hiMSC characteristics such as expansion capacity and trilineage and immunoregulatory potential, their applications in the regenerative medicine field will quickly develop. A summary of the different advantages and disadvantages in hiCPC and hiMSC differentiation and improvement strategies can be found in **Table 1**. In the meantime, by virtue of their predisposition for hypertrophy and endochondral ossification, hiMSCs were selected in this thesis to generate neo-cartilage from the OPG-XL carriers.

Table 1. Summary of iMSC and iCPC advantages and disadvantages for regenerative medicine and disease modeling, and strategies to improve them.

Model	Advantages	Disadvantages	Strategies to improve models	References
iMSCs	Differentiation potential into chondrocytes, osteoblasts and adipocytes	Cell heterogeneity	Higher cell density in neo-cartilage organoids	(37)
	Higher expansion capacity	Longer differentiation protocol	Step-wise iMSC generation: Wnt/B-catenin	(45)
	Cell storage	Hypertrophic cartilage	Chondrogenic protocol adaptation to iMSCs (Wnt inhibition)	(46)
	Immunoregulatory potential		Optimization of a defined step-wise protocol; for instance with an early chondrogenic reporter line	(37)
	Exosome applicabilities		Selection of highly chondrogenic-osteogenic markers on iMSCs based on for instance cell proliferation capacity	(43)
			Selection of highly chondrogenic-osteogenic gene expression markers during chondrogenesis and osteogenesis	(47)
iCPCs	Direct and highly reproducible chondrogenic differentiation	Low expansion capacity	Improvement of iCPC maintenance protocol	(33)
	Similar neo-cartilage to primary chondrocytes neo-cartilage	Quick loss of chondrogenic potential	Filter aggregates depending on size	
		Inability to be stored	Use of an early chondrogenic reporter line to select for chondrogenic lineages	(32)
		Heterogeneity in visual aggregate selection and cell generation	Low cell heterogeneity might be beneficial for chondrogenesis generation	

EMPLOYING DISEASE MODELLING USING AN EARLY ONSET OA MUTATION

In **Chapter 4** we applied hiPS-cell derived cartilage and osseous organoid modelling and CRISPR/Cas9 technology to study the underlying disease mechanism of a high impact mutation at the CCAL1 locus resulting in a 19 amino acid elongation of the C-terminal end of OPG (OPG-XL). Specifically, we focused on the bidirectional pathogenic phenotype of bone loss and articular cartilage calcification observed in carriers of the mutation (1, 2).

Clinical examination by DEXA scans of the OPG-XL carriers confirmed osteopenia while MRI revealed a severe OA phenotype characterized by different degrees of chondrocalcinosis, osteophytosis, bone marrow lesions and cysts. In order to explain the bidirectional effect of OPG-XL, osteoclastogenesis was performed with monocytes from six OPG-XL carriers and matched controls. This revealed a delayed osteoclast primed state with a tendency towards increased bone resorption activity in time. Due to the rarity of the mutation, primary chondrocytes and osteoblasts are not easily obtained, demanding other strategies to investigate OPG-XL in these cells. For this, hiPSCs were generated from a carrier of the OPG-XL mutation by the LUMC iPSC core facility. Subsequently, hiPSCs were differentiated into hiMSCs and further towards chondrocytes to explore neo-cartilage deposition or towards osteoblast for neo-bone formation. Results were further confirmed in neo-cartilage of hPACs derived from a carrier of the mutation that during the course of this thesis had a joint replacement surgery, thus serving as a validation of our hiPSC model.

OPG-XL effect in neo-cartilage and neo osseous organoids

hiPSC-derived neo-cartilage tissue formed by OPG-XL chondrocytes, relative to isogenic controls, showed a fibrotic histological phenotype without obvious mineralization but with marked downregulation of *COL2A1* and, most notable, of *MGP* gene expression. As *MGP* is an inhibitor of ectopic bone formation (48) and a robust OA risk gene (13, 49) our data demonstrated that OPG-XL directly affects propensity of chondrocytes to enter a mineralized OA state. hiPSC-derived neo-osseous tissue formed by OPG-XL mutated osteoblasts relative to isogenic controls displayed a high calcification as reflected by the prominent Alizarin red staining concurrent with notable high gene expression of *DIO2* and low of *TNFSF11* encoding for RANKL. *DIO2*, encoding type 2 deiodinase enzyme, is essentially facilitating bone formation and mineralization (50), while the lower expression of *TNFSF11* indicates a direct interaction between OPG-XL and RANKL in bone which is missing in chondrocytes. By performing RNA sequencing between lesioned and preserved subchondral bone in our lab (14), *TNFSF11* was shown as one of the genes with highest correlated with *TNFRSF11B*. This was confirmed in our OPG-XL model. The strong Alizarin red staining of neo-osseous tissue, concurrent with *DIO2* and *MGP* upregulation could therefore explain the extensive phenotypic foci of calcified cartilage observed in OPG-XL carriers. This would suggest that chondrocalcinosis arises during ongoing OA pathophysiology (51).

OPG-XL effect in osteoclasts

By studying the effects of the OPG-XL mutation in our osteoclast assay, a strong reduction in osteoclasts with few nuclei in the OPG-XL group was observed. Nevertheless, when osteoclasts were cultured for longer periods, they showed a

trend towards an increase in the number of nuclei per cell. Despite the significantly lower number of osteoclasts with few nuclei, a similar bone resorption activity was described, hence suggesting a higher osteoclast activity. This was also supported by expression levels of known osteoclast markers *NFATc1*, *CTSK*, *TRAcP* and DC-*STAMP*. Nevertheless, CTX-1 expression per osteoclast did not show differences between both groups. These data would confirm an initial priming state of OPG-XL that would delay osteoclast generation, and a tendency to increase osteoclast activity over time.

In addition to the fact that osteoclastogenesis data demonstrated important modulatory effects of OPG expression during maturation of monocytes to osteoclasts, we could link the role of OPG-XL to a dysfunctional *in vivo* recycling of osteoclasts via fission of polykaryons and fusion of the recently discovered osteomorphs during bone resorption (52). In this cycle, osteomorphs are mobile cells formed after fission of osteoclasts, whereas osteoclasts can be formed by (re-)fusion of such cells. Importantly, RANKL was found to induce osteoclast fission, whereas OPG blocked fusion of osteomorphs (53) that upon withdrawal results in their fusion and a higher osteoclast activity. Hence, it could be speculated that the higher amount of RANKL due to a dysfunctional binding of RANKL-HS-OPG-XL would result in a higher osteoclast formation and fission as observed in the lower numbers of osteoclasts during initial timepoints of osteoclastogenesis. Consequently, and as a feedback mechanism, RANKL would decrease, as observed in the neo-osseus organoids, allowing osteomorphs to fuse. At the same time, dysfunctional OPG-XL would result in a lower inhibition of osteomorph fusion which would generate osteoclasts with a higher activity and more nuclei, as observed in our data **(Figure 1)**.

Pleiotropy of OPG-XL

Here, we clearly showed the pleiotropy of OPG-XL in different tissues: cartilage, bone and osteoclasts. The priming effects caused in osteoclastogenesis and the lack of response of RANK and RANKL in chondrocytes indicate that OPG has a broader role than only the well-known common bone resorption processes. This is highlighted by the contradicting results of OA therapies promoting OPG overexpression such as strontium ranelate and the data shown in this thesis. Altogether this suggests a double-edged sword effect of OPG. A coculture with hiPSC derived osteoblasts, chondrocytes and osteoclasts in a model that allows crosstalk between the different cells would be essential to understand its function in the joint tissue. Moreover, a characterization of its binding properties to HS-RANKL should be investigated.

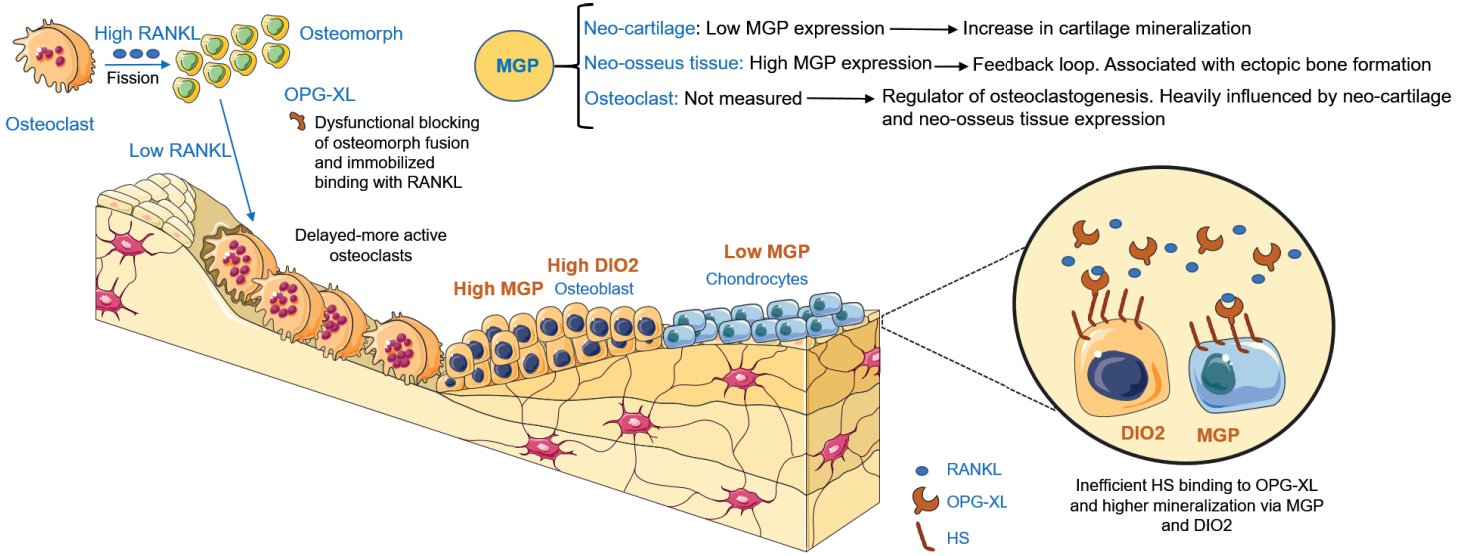

Figure 1. Proposed mechanism of OPG-XL in neo-cartilage, neo-osseus tissue and osteoclasts. Osteoclasts undergo a strong fission into osteomorphs and posteriorly accumulate for longer time periods after high RANKL expression due to inefficient OPG-XL-HS binding. Upon RANKL decrease as a feedback mechanism, and dysfunctional OPG-XL fusion blocking, osteoclast fusion resumes with a higher activity. *MGP* differences in expression in cartilage and bone through defective OPG-XL-HS binding result in a higher mineralization in cartilage and ectopic bone formation. Moreover *MGP* produced by both tissues deeply controls osteoclast activity, contributing to higher bone resorption.

With respect to osteoclastogenesis, accumulation of osteomorphs likely contribute to the FOA phenotype. A better understanding of these cells, together with a proper characterization of their markers is essential to understand their role in bone resorption in common OA and more specifically in the FOA family members. The here described characteristics of OPG are very similar to those of MGP and appear to be mediated via this protein. Therefore, in addition to further study OPG, we also propose to investigate the role of MGP in relation to osteomorph function and more specifically in other systems where MGP is involved such as in the vasculature system of the OPG-XL carriers. In the meantime, the robust MGP changes and its contribution to controlling mineralization and osteoclast generation indicate the potential suitability of this protein as a therapeutic target for the FOA family members.

FUTURE PERSPECTIVES

During the development of this thesis, hiPSC applicability into disease modeling and regenerative therapies has seen a sharpen rise. An increase of our understanding of hiPSC nature, clonal heterogeneity, and tissue differentiation is further developing by studying these cells and their differentiation potential at the single cell transcriptomic and epigenetic level (31, 54). Genetic studies of risk disease genes, especially in GWAS, offer a direct application when combined with hiPSC technology and genetic engineering strategies such as CRISPR/Cas9. Hence, particular risk SNPs could be further studied in big cohorts of hiPSC libraries with defined genetic make-up and translated from *in silico* approaches towards *in vitro* strategies (55). Nevertheless, when studying disease models, we should take into account the tissue immaturity that would have to be addressed for studying ageing diseases such as OA (56). Particularly here, the integration of environmental factors associated with OA, such as mechanical loading, should be researched (57). Moreover, a novel sense of disease perception in OA is necessary. As such, OA, a traditionally cartilage degenerative disease, is gradually progressing to be considered a whole joint disease where an interplay with osteoblasts and osteoclasts can play a pivotal role in its development. This thesis clearly shows this by studying OPG and its readthrough mutation. The effects shown in the likely chondrocyte to osteoblast transdifferentiation and OA development upon OPG overexpression are in contrast with positive results observed upon administering strontium ranelate. Additionally, the readthrough mutation identified in the OPG-XL family members clearly indicated an interplay between chondrocytes, osteoblasts and osteoclasts where vitamin K treatments arise as a possible treatment option. This highlights the need in future research for complex disease models, in which chondrocytes, osteoblasts, osteoclast and synovial cells can properly interact.

REFERENCES

1. Ramos YF, Bos SD, van der Breggen R, Kloppenburg M, Ye K, Lameijer EW, et al. A gain of function mutation in *TNFRSF11B* encoding osteoprotegerin causes osteoarthritis with chondrocalcinosis. Ann Rheum Dis. 2015;74(9):1756-62.
2. Williams CJ, Qazi U, Bernstein M, Charniak A, Gohr C, Mitton-Fitzgerald E, et al. Mutations in osteoprotegerin account for the CCAL1 locus in calcium pyrophosphate deposition disease. Osteoarthritis Cartilage. 2018;26(6):797-806.
3. Coutinho de Almeida R, Ramos YFM, Mahfouz A, den Hollander W, Lakenberg N, Houtman E, et al. RNA sequencing data integration reveals an miRNA interactome of osteoarthritis cartilage. Ann Rheum Dis. 2019;78(2):270-7.
4. Wu L, Schaid DJ, Sicotte H, Wieben ED, Li H, Petersen GM. Case-only exome sequencing and complex disease susceptibility gene discovery: study design considerations. J Med Genet. 2015;52(1):10-6.
5. Do R, Kathiresan S, Abecasis GR. Exome sequencing and complex disease: practical aspects of rare variant association studies. Hum Mol Genet. 2012;21(R1):R1-9.
6. Skarp S, Kamarainen OP, Wei GH, Jakkula E, Kiviranta I, Kroger H, et al. Whole exome sequencing in Finnish families identifies new candidate genes for osteoarthritis. PLoS One. 2018;13(8):e0203313.
7. Auer PL, Lettre G. Rare variant association studies: considerations, challenges and opportunities. Genome Med. 2015;7(1):16.
8. Fukui N, Ikeda Y, Ohnuki T, Tanaka N, Hikita A, Mitomi H, et al. Regional differences in chondrocyte metabolism in osteoarthritis: a detailed analysis by laser capture microdissection. Arthritis Rheum. 2008;58(1):154-63.
9. Bomer N, den HW, Ramos YF, Bos SD, van der Breggen R, Lakenberg N, et al. Underlying molecular mechanisms of DIO2 susceptibility in symptomatic osteoarthritis. Ann Rheum Dis. 2014.
10. Enochson L, Stenberg J, Brittberg M, Lindahl A. GDF5 reduces MMP13 expression in human chondrocytes via DKK1 mediated canonical Wnt signaling inhibition. Osteoarthritis Cartilage. 2014;22(4):566-77.
11. Komuro H, Olee T, Kuhn K, Quach J, Brinson DC, Shikhman A, et al. The osteoprotegerin/receptor activator of nuclear factor kappaB/receptor activator of nuclear factor kappaB ligand system in cartilage. Arthritis Rheum. 2001;44(12):2768-76.
12. Tat SK, Pelletier JP, Velasco CR, Padrines M, Martel-Pelletier J. New perspective in osteoarthritis: the OPG and RANKL system as a potential therapeutic target? Keio J Med. 2009;58(1):29-40.
13. Boer CG, Hatzikotoulas K, Southam L, Stefánsdóttir L, Zhang Y, Coutinho de Almeida R, et al. Deciphering osteoarthritis genetics across 826,690 individuals from 9 populations. Cell. 2021;184(18):4784-818.e17.
14. Tuerlings M, van Hoolwerff M, Houtman E, Suchiman E, Lakenberg N, Mei H, et al. RNA sequencing reveals interacting key determinants of osteoarthritis acting in subchondral bone and articular cartilage. Arthritis Rheumatol. 2020.
15. Zhang J, Nie Q, Si C, Wang C, Chen Y, Sun W, et al. Weighted Gene Co-expression Network Analysis for RNA-Sequencing Data of the Varicose Veins Transcriptome. Front Physiol. 2019;10:278.
16. Sundarrajan S, Arumugam M. Weighted gene co-expression based biomarker discovery for psoriasis detection. Gene. 2016;593(1):225-34.
17. Deng ZH, Li YS, Gao X, Lei GH, Huard J. Bone morphogenetic proteins for articular cartilage regeneration. Osteoarthritis Cartilage. 2018;26(9):1153-61.
18. Cheng H, Jiang W, Phillips FM, Haydon RC, Peng Y, Zhou L, et al. Osteogenic activity of the fourteen types of human bone morphogenetic proteins (BMPs). J Bone Joint Surg Am. 2003;85(8):1544-52.

19. van der Kraan PM, Blaney Davidson EN, van den Berg WB. Bone morphogenetic proteins and articular cartilage: To serve and protect or a wolf in sheep clothing's? Osteoarthritis Cartilage. 2010;18(6):735-41.
20. Kuo WJ, Digman MA, Lander AD. Heparan sulfate acts as a bone morphogenetic protein coreceptor by facilitating ligand-induced receptor hetero-oligomerization. Mol Biol Cell. 2010;21(22):4028-41.
21. Nims RJ, Pferdehirt L, Ho NB, Savadipour A, Lorentz J, Sohi S, et al. A synthetic mechanogenetic gene circuit for autonomous drug delivery in engineered tissues. Sci Adv. 2021;7(5).
22. Huntley R, Jensen E, Gopalakrishnan R, Mansky KC. Bone morphogenetic proteins: Their role in regulating osteoclast differentiation. Bone Rep. 2019;10:100207.
23. Aghajanian P, Mohan S. The art of building bone: emerging role of chondrocyte-to-osteoblast transdifferentiation in endochondral ossification. Bone Res. 2018;6:19.
24. Boer CG, Szilagyi I, Nguyen NL, Neogi T, Meulenbelt I, Ikram MA, et al. Vitamin K antagonist anticoagulant usage is associated with increased incidence and progression of osteoarthritis. Ann Rheum Dis. 2021;80(5):598-604.
25. Yu H, de Vos P, Ren Y. Overexpression of osteoprotegerin promotes preosteoblast differentiation to mature osteoblasts. Angle Orthod. 2011;81(1):100-6.
26. Cieslar-Pobuda A, Knoflach V, Ringh MV, Stark J, Likus W, Siemianowicz K, et al. Transdifferentiation and reprogramming: Overview of the processes, their similarities and differences. Biochim Biophys Acta Mol Cell Res. 2017;1864(7):1359-69.
27. Aghajanian P, Xing W, Cheng S, Mohan S. Epiphyseal bone formation occurs via thyroid hormone regulation of chondrocyte to osteoblast transdifferentiation. Sci Rep. 2017;7(1):10432.
28. Liu H, Yang L, Yu FF, Wang S, Wu C, Qu C, et al. The potential of induced pluripotent stem cells as a tool to study skeletal dysplasias and cartilage-related pathologic conditions. Osteoarthritis Cartilage. 2017;25(5):616-24.
29. de Windt TS, Vonk LA, Slaper-Cortenbach ICM, Nizak R, van Rijen MHP, Saris DBF. Allogeneic MSCs and Recycled Autologous Chondrons Mixed in a One-Stage Cartilage Cell Transplantion: A First-in-Man Trial in 35 Patients. Stem Cells. 2017;35(8):1984-93.
30. Nakayama N, Pothiawala A, Lee JY, Matthias N, Umeda K, Ang BK, et al. Human pluripotent stem cell-derived chondroprogenitors for cartilage tissue engineering. Cell Mol Life Sci. 2020;77(13):2543-63.
31. Volpato V, Webber C. Addressing variability in iPSC-derived models of human disease: guidelines to promote reproducibility. Dis Model Mech. 2020;13(1).
32. Adkar SS, Wu CL, Willard VP, Dicks A, Ettyreddy A, Steward N, et al. Step-Wise Chondrogenesis of Human Induced Pluripotent Stem Cells and Purification Via a Reporter Allele Generated by CRISPR-Cas9 Genome Editing. Stem Cells. 2019;37(1):65-76.
33. Dicks A, Wu CL, Steward N, Adkar SS, Gersbach CA, Guilak F. Prospective isolation of chondroprogenitors from human iPSCs based on cell surface markers identified using a CRISPR-Cas9-generated reporter. Stem Cell Res Ther. 2020;11(1):66.
34. Chen S, Fu P, Cong R, Wu H, Pei M. Strategies to minimize hypertrophy in cartilage engineering and regeneration. Genes Dis. 2015;2(1):76-95.
35. Li H, Wang D, Yuan Y, Min J. New insights on the MMP-13 regulatory network in the pathogenesis of early osteoarthritis. Arthritis Res Ther. 2017;19(1):248.
36. Katz D, Huynh N, Savadipour A, Palte I, Guilak F. An immortalized human adipose-derived stem cell line with highly enhanced chondrogenic properties. Biochemical and Biophysical Research Communications. 2020;530(1):252-8.
37. Diederichs S, Klampfleuthner FAM, Moradi B, Richter W. Chondral Differentiation of Induced Pluripotent Stem Cells Without Progression Into the Endochondral Pathway. Front Cell Dev Biol. 2019;7:270.

38. Kerkhofs J, Leijten J, Bolander J, Luyten FP, Post JN, Geris L. A Qualitative Model of the Differentiation Network in Chondrocyte Maturation: A Holistic View of Chondrocyte Hypertrophy. PLoS One. 2016;11(8):e0162052.
39. Dreier R. Hypertrophic differentiation of chondrocytes in osteoarthritis: the developmental aspect of degenerative joint disorders. Arthritis Res Ther. 2010;12(5):216.
40. Csobonyeiova M, Polak S, Nicodemou A, Zamborsky R, Danisovic L. iPSCs in Modeling and Therapy of Osteoarthritis. Biomedicines. 2021;9(2).
41. Zhao Q, Gregory CA, Lee RH, Reger RL, Qin L, Hai B, et al. MSCs derived from iPSCs with a modified protocol are tumor-tropic but have much less potential to promote tumors than bone marrow MSCs. Proc Natl Acad Sci U S A. 2015;112(2):530-5.
42. Dexheimer V, Frank S, Richter W. Proliferation as a requirement for in vitro chondrogenesis of human mesenchymal stem cells. Stem Cells Dev. 2012;21(12):2160-9.
43. Mareddy S, Crawford R, Brooke G, Xiao Y. Clonal isolation and characterization of bone marrow stromal cells from patients with osteoarthritis. Tissue Eng. 2007;13(4):819-29.
44. Xu M, Shaw G, Murphy M, Barry F. Induced Pluripotent Stem Cell-Derived Mesenchymal Stromal Cells Are Functionally and Genetically Different From Bone Marrow-Derived Mesenchymal Stromal Cells. Stem Cells. 2019;37(6):754-65.
45. Kreuser U, Buchert J, Haase A, Richter W, Diederichs S. Initial WNT/beta-Catenin Activation Enhanced Mesoderm Commitment, Extracellular Matrix Expression, Cell Aggregation and Cartilage Tissue Yield From Induced Pluripotent Stem Cells. Front Cell Dev Biol. 2020;8:581331.
46. Wu CL, Dicks A, Steward N, Tang R, Katz DB, Choi YR, et al. Single cell transcriptomic analysis of human pluripotent stem cell chondrogenesis. Nat Commun. 2021;12(1):362.
47. Chan CKF, Gulati GS, Sinha R, Tompkins JV, Lopez M, Carter AC, et al. Identification of the Human Skeletal Stem Cell. Cell. 2018;175(1):43-56.e21.
48. Luo G, Ducy P, McKee MD, Pinero GJ, Loyer E, Behringer RR, et al. Spontaneous calcification of arteries and cartilage in mice lacking matrix GLA protein. Nature. 1997;386(6620):78-81.
49. den Hollander W, Boer CG, Hart DJ, Yau MS, Ramos YFM, Metrustry S, et al. Genome-wide association and functional studies identify a role for matrix Gla protein in osteoarthritis of the hand. Ann Rheum Dis. 2017;76(12):2046-53.
50. Bassett JH, Boyde A, Howell PG, Bassett RH, Galliford TM, Archanco M, et al. Optimal bone strength and mineralization requires the type 2 iodothyronine deiodinase in osteoblasts. Proc Natl Acad Sci U S A. 2010;107(16):7604-9.
51. Zhou X, von der Mark K, Henry S, Norton W, Adams H, de Crombrugghe B. Chondrocytes transdifferentiate into osteoblasts in endochondral bone during development, postnatal growth and fracture healing in mice. PLoS genetics. 2014;10(12):e1004820.
52. Jansen ID, Vermeer JA, Bloemen V, Stap J, Everts V. Osteoclast fusion and fission. Calcif Tissue Int. 2012;90(6):515-22.
53. McDonald MM, Khoo WH, Ng PY, Xiao Y, Zamerli J, Thatcher P, et al. Osteoclasts recycle via osteomorphs during RANKL-stimulated bone resorption. Cell. 2021;184(7):1940.
54. Efrat S. Epigenetic Memory: Lessons From iPS Cells Derived From Human beta Cells. Front Endocrinol (Lausanne). 2020;11:614234.
55. Warren CR, O'Sullivan JF, Friesen M, Becker CE, Zhang X, Liu P, et al. Induced Pluripotent Stem Cell Differentiation Enables Functional Validation of GWAS Variants in Metabolic Disease. Cell Stem Cell. 2017;20(4):547-57 e7.
56. Mertens J, Reid D, Lau S, Kim Y, Gage FH. Aging in a Dish: iPSC-Derived and Directly Induced Neurons for Studying Brain Aging and Age-Related Neurodegenerative Diseases. Annu Rev Genet. 2018;52:271-93.
57. Aisenbrey EA, Bilousova G, Payne K, Bryant SJ. Dynamic mechanical loading and growth factors influence chondrogenesis of induced pluripotent mesenchymal progenitor cells in a cartilage-mimetic hydrogel. Biomater Sci. 2019;7(12):5388-403.

ADDENDUM

English Summary
Nederlandse Samenvatting
List of Publications
Curriculum Vitae
Acknowledgements

English summary

Osteoarthritis (OA) is a degenerative disease of the joints characterized by degradation of cartilage, subchondral bone remodeling, osteophyte formation and synovial inflammation. Clinically OA is marked by chronic pain, joint stiffness and disability of patients. OA generally affects hands, hips and knees and can be influenced by multiple risk factors such as body mass index (BMI), bone mineral density (BMD), injury and genetics. Currently in the Netherlands there are approximately 1.2 million people affected by OA and this number is only expected to increase. As such, the world health organization expects that by 2050, 15% of the worldwide population over 60 years old will suffer from OA. As of yet, joint replacement is the only effective therapy, however this is a very costly procedure that does not guarantee complete recovery. As a result, it is estimated that 1-2.5% of gross national products is spent in OA related treatments.

To advance development of effective disease modifying OA treatments, a better understanding of its pathophysiological mechanisms is necessary. By studying a family with early onset OA and high cartilage mineralization, a likely causal mutation in the TNF receptor superfamily member 11b (*TNFRSF11B*) encoding for osteoprotegerin (OPG) was identified. This mutation causes a 19 amino acid extension in the C-terminal domain of OPG (OPG-XL). OPG is a decoy receptor that competes with receptor activator of the nuclear KB factor (RANK) for the binding of nuclear factor KB ligand (RANKL). This triad is known for regulating the formation of osteoclasts, hence playing a critical role in bone remodeling. Given that *TNFRSF11B* is also one of the highest upregulated genes in OA lesioned cartilage as compared to preserved, this gene is likely underlying OA development and progression but its implication in cartilage homeostasis is as of yet unknown.

To explore the role of *TNFRSF11B* in development of OA, in **Chapter 2**, *TNFRSF11B* was overexpressed in an *in vitro* cell culture model of neo-cartilage deposited by chondrocytes of nine patients that underwent joint replacement surgery due to OA. Subsequently, characteristic markers of OA development and bone formation were measured. This revealed an upregulation of genes commonly associated with OA development and matrix turnover, such as *MMP13*, *COL2A1* and *COL1A1*. Additionally, the consistent higher expression of genes associated with osteoblast formation and mineralization such as *RUNX2*, *ASPN* and *OGN*, suggested a chondrocyte to osteoblast transition. Of note, neo-cartilage showed no changes in expression of the other two members of the: *TNFSF11* (RANKL) and *TNFRSF11A* (RANK), indicating a difference in the OPG mechanism in cartilage when compared to its bone counterpart.

To obtain more information about the intrinsic mechanism of OPG in OA development, we proceeded to further study the OPG-XL family. For this, we used induced pluripotent stem cells (iPSCs). iPSCs are embryonic stem cell-like cells able to differentiate into different tissues, while maintaining the genetic background of the donor. This makes them an excellent approach for disease modeling and regenerative therapies. In this thesis, we applied iPSC technology to generate a stem cell line from skin fibroblasts of a carrier of the OPG-XL mutation. Since access to cartilage and bone tissue of members of this family is rare, availability of the iPSCs allowed us to have a renewable source of neo-cartilage and neo-osseous tissue carrying this mutation for further studies.

Several protocols to generate neo-cartilage from human iPSCs were available. These protocols followed different developmental routes either by mesenchymal stromal cell (hiMSC) formation or by generating chondroprogenitor cells (hiCPC). Yet, the quality of the generated neo-cartilage was unknown. As such, to determine the best method for neo-cartilage generation for our OPG-XL model, in **Chapter 3** we compared the neo-cartilage generated from both protocols to neo-cartilage deposited by respectively bone marrow mesenchymal stromal cells (hBMSCs) and human primary articular chondrocytes (hPACs). Based on a panel of 20 relevant genes, we showed a 53% similarity between hiMSCs and hBMSCs, and a 65% similarity between hiCPC and hPACs neo-cartilage. In addition, hiCPCs neo-cartilage showed a higher expression of markers associated with articular cartilage matrix deposition, while hiMSCs neo-cartilage was more prone to hypertrophy. With hypertrophy as a hallmark of OA, this would make hiMSCs more suited to study cartilage and bone related diseases.

By following the hiMSC approach, we differentiated the hiPSC-OPG-XL line into neo-cartilage and neo-bone and characterized the effects of the mutation in **Chapter 4**. To prove causality, Clustered Regularly Interspaced Short Palindromic Repeats (CRISPR) and CRISPR-associated protein 9 (Cas9) technology was used to repair the OPG-XL mutation. This technology recognizes and cleavages specific strands of DNA complementary to the CRISPR sequence, generating an isogenic control to OPG-XL. This resulted in two CRISPR/Cas9 OPG-XL repaired hiPSC lines where neo-cartilage and neo-bone tissue were generated. Comparison between the OPG-XL repaired and OPG-XL tissues revealed that this mutation had a fibrotic effect in neo-cartilage, while neo-bone tissue had a stronger mineralization, likely via function of MGP and DIO2 respectively.

Immobilization of secreted OPG on the osteoblast membrane via binding to heparan sulphate is necessary for RANKL mediated osteoclast inhibition. Since immobilization results from the C-terminal binding of OPG to heparan sulphate and the OPG-XL mutant is changed at the C-terminus, we hypothesize that the effects on MGP and DIO2 might be triggered by interference with binding

between RANKL, heparan sulphate and OPG. Additionally, osteoclast formation was studied with monocytes from OPG-XL carriers and matched healthy controls. This revealed a higher osteoclast activity as measured by gene expression, despite similar bone resorption levels were observed in culture. To determine how these results were translated into the OPG-XL carriers phenotype, we performed MRI and DEXA scans. This revealed a pleiotropy of OPG-XL with cartilage calcification accompanied by low subchondral bone mineralization, both hallmarks of OA pathophysiology, and in consonance with the observed higher osteoclast activity.

Altogether, this thesis highlights the role of OPG in OA development by generating an OPG overexpression system in primary chondrocytes and by studying a rare mutation in *TNFRSF11B*. By further generating neo-cartilage, neo-bone and osteoclasts from the OPG-XL family members, we showed a bidirectional interplay of OPG-XL characterized by higher bone resorption and higher cartilage mineralization. Novel treatments for this family and extrapolation to common OA could be addressed on highly differentially expressed genes such as *MGP* and *DIO2*. Finally, the pleiotropy that OPG-XL showed indicates a beneficial or detrimental stage depending on the tissue, making OPG-XL, and likely OPG, a double-edged sword in OA development.

Nederlandse samenvatting

Artrose (OA) is een degeneratieve aandoening van de gewrichten die wordt gekenmerkt door afbraak van kraakbeen, subchondrale botremodellering, osteofytvorming en synoviale ontsteking. Klinisch wordt artrose gekenmerkt door chronische pijn, gewrichtsstijfheid en invaliditeit van patiënten. OA treft over het algemeen handen, heupen en knieën en kan worden beïnvloed door meerdere risicofactoren zoals body mass index (BMI), botmineraaldichtheid (BMD), letsel en erfelijkheid. Momenteel zijn er in Nederland ongeveer 1,2 miljoen mensen met artrose en dit aantal zal naar verwachting alleen maar toenemen. Als zodanig verwacht de Wereldgezondheidsorganisatie dat in 2050 15% van de wereldbevolking ouder dan 60 jaar aan artrose zal lijden. Tot nu toe is gewrichtsvervanging de enige effectieve therapie, maar dit is een zeer kostbare procedure die geen volledig herstel garandeert. Als gevolg hiervan wordt geschat dat 1-2,5% van het bruto nationaal product wordt besteed aan OA-gerelateerde behandelingen.

Om de ontwikkeling van effectieve OA-behandelingen te bevorderen, is een beter begrip van de pathofysiologische mechanismen nodig. Door het bestuderen van een familie met juvenile artrose en hoge kraakbeenmineralisatie, werd een vermoedelijk causale mutatie in het TNF-receptor-superfamilielid 11b (*TNFRSF11B*) dat codeert voor osteoprotegerine (OPG) geïdentificeerd. Deze mutatie veroorzaakt een verlenging van 19 aminozuren aan het C-terminale domein van OPG (OPG-XL). OPG is een receptor die concurreert met receptoractivator van de nucleaire KB-factor (RANK) voor de binding van nucleaire factor KB-ligand (RANKL). Deze triad staat bekend om het reguleren van de vorming van osteoclasten en speelt daarom een cruciale rol bij botremodellering. Gezien het feit dat *TNFRSF11B* ook een van de genen is met de hoogste upregulatie in kraakbeen met aangedaan een nicht aangedaan kraakbeen, is dit gen waarschijnlijk de oorzaak van de ontwikkeling en progressie van OA, maar de implicatie ervan in kraakbeenhomeostase is tot nu toe onbekend.

Om de rol van *TNFRSF11B* in de ontwikkeling van artrose te onderzoeken, werd *TNFRSF11B* in **Hoofdstuk 2** tot overexpressie gebracht in een *in vitro* cel model van neo-kraakbeen afgezet door chondrocyten van negen patiënten die een gewrichtsvervangende operatie ondergingen vanwege artrose. Vervolgens werden karakteristieke markers van OA-ontwikkeling en botvorming gemeten. Dit liet een opregulatie zien van genen die gewoonlijk worden geassocieerd met OA-ontwikkeling en matrixomzetting, zoals *MMP13*, *COL2A1* en *COL1A1*. Bovendien suggereerde de consistente hogere expressie van genen geassocieerd met osteoblastvorming en mineralisatie zoals *RUNX2*, *ASPN* en *OGN*, een overgang van chondrocyten naar osteoblasten. Opmerkelijk was dat neo-kraakbeen vertoonde geen veranderingen in expressie van de andere twee

leden van de triad: *TNFSF11* (RANKL) en *TNFRSF11A* (RANK). Dit wijst erop dat een verschil bestaat in het OPG-mechanisme in kraakbeen in vergelijking met bot.

Om meer informatie te verkrijgen over het intrinsieke mechanisme van OPG bij de ontwikkeling van artrose, gingen we verder met het bestuderen van de OPG-XL-familie. Hiervoor gebruikten we geïnduceerde pluripotente stamcellen (iPSC's). iPSC's zijn stamcelachtige cellen afkomstig van gespecialiseerde cellen die weer in staat zijn om te her-specialiseren in verschillende weefsels, terwijl de genetische achtergrond van de donor behouden blijft. Dit maakt ze tot een uitstekende benadering voor ziektemodellering voor ziektemodellering voor het ontwikkelen van (regeneratieve) therapieën. In dit proefschrift hebben we iPSC-technologie toegepast om een stamcellijn te genereren uit huidfibroblasten van een drager van de OPG-XL-mutatie. Aangezien toegang tot kraakbeen en botweefsel van leden van deze familie zeldzaam is, stelde de beschikbaarheid van de iPSC's ons in staat om een hernieuwbare bron van neo-kraakbeen en neo-bot weefsel te genereren dat deze mutatie draagt voor verder onderzoek.

Er waren verschillende protocollen beschikbaar om neo-kraakbeen uit menselijke iPSC's te genereren. Deze protocollen volgden verschillende ontwikkelingsroutes, hetzij door vorming van mesenchymale stromale cellen (hiMSC) of door chondroprogenitorcellen (hiCPC) te genereren. Toch was de kwaliteit van het gegenereerde neo-kraakbeen in vergelijking met articulair kraakbeen onbekend. Om de beste methode voor het genereren van neo-kraakbeen voor ons OPG-XL-model te bepalen, vergeleken we in **Hoofdstuk 3** het neo-kraakbeen gegenereerd uit beide protocollen met neo-kraakbeen afgezet door respectievelijk mesenchymale stromale beenmergcellen (hBMSCs) en humane primaire articulaire chondrocyten (hPAC's). Op basis van een panel van 20 relevante genen toonden we een overeenkomst van 53% tussen hiMSC's en hBMSC's, en een overeenkomst van 65% tussen hiCPC en hPAC's neo-kraakbeen. Bovendien vertoonde het neo-kraakbeen van hiCPC een hogere expressie van markers geassocieerd met kraakbeen, terwijl het neo-kraakbeen van hiMSC meer vatbaar was voor hypertrofie. Aangezien hypertrophy een belangrijk aspect is van het atrose process, meer geschikt van hiMSCs is om kraakbeen- en botgerelateerde ziekten te bestuderen.

Door de hiMSC-benadering te volgen, hebben we de hiPSC-OPG-XL-lijn gedifferentieerd in neo-kraakbeen en neo-bot en de effecten van de mutatie in **Hoofdstuk 4** gekarakteriseerd. Om causaliteit van de mutatie te bewijzen, hebben we Clustered Regularly Interspaced Short Palindromic Repeats (CRISPR) en CRISPR- geassocieerde eiwit 9 (Cas9) technologie gebruikt om de OPG-XL-mutatie te herstellen. Deze technologie herkent en splitst specifieke DNA-strengen die complementair zijn aan de CRISPR-sequentie, waardoor de perfecte

isogene controle voor OPG-XL wordt gegenereerd met identieke genetische achtergrond. Dit resulteerde in twee CRISPR/Cas9 OPG-XL gerepareerde hiPSC-lijnen waarvan neo-kraakbeen en neo-botweefsel werd gegenereerd. Vergelijking tussen de OPG-XL herstelde en OPG-XL weefsels toonde aan dat deze mutatie een fibrotisch effect had in neo-kraakbeen, terwijl neo-botweefsel een sterkere mineralisatie had, waarschijnlijk via functie van respectievelijk MGP en DIO2.

Immobilisatie van uitgescheiden OPG op het osteoblastmembraan via binding aan heparansulfaat is noodzakelijk voor RANKL-gemedieerde osteoclastremming. Aangezien immobilisatie het gevolg is van de C-terminale binding van OPG aan heparansulfaat en de OPG-XL-mutant aan de C-terminus is veranderd, veronderstellen we dat de effecten op MGP en DIO2 kunnen worden veroorzaakt door interferentie met binding tussen RANKL, heparansulfaat en OPG. Daarnaast werd osteoclastvorming bestudeerd met monocyten van OPG-XL dragers en gematchte gezonde controles. Dit onthulde een hogere osteoclastactiviteit zoals gemeten door genexpressie, ondanks dat vergelijkbare botresorptieniveaus werden waargenomen in kweek. Om te bepalen hoe deze resultaten werden vertaald in het OPG-XL-dragerfenotype, hebben we MRI- en DEXA-scans uitgevoerd. Dit onthulde een pleiotropie van OPG-XL met kraakbeenverkalking vergezeld van lage subchondrale botmineralisatie, beide kenmerken van OA-pathofysiologie, en in overeenstemming met de waargenomen hogere osteoclastactiviteit.

Al met al belicht dit proefschrift de rol van OPG in de ontwikkeling van artrose door het genereren van een OPG-overexpressiesysteem in primaire chondrocyten en door het bestuderen van een zeldzame mutatie in *TNFRSF11B*. Door verder neo-kraakbeen, neo-bot en osteoclasten van de OPG-XL-familieleden te genereren, toonden we een bidirectioneel effect van OPG-XL aan, gekenmerkt door hogere botresorptie en hogere kraakbeenmineralisatie. Nieuwe behandelingen voor deze familie en extrapolatie naar gewone artrose zouden kunnen worden aangepakt op sterk differentieel tot expressie gebrachte genen zoals *MGP* en *DIO2*. Ten slotte wijst de pleiotropie die OPG-XL liet zien op een gunstig of nadelig stadium, afhankelijk van het weefsel, waardoor OPG-XL, en waarschijnlijk OPG, een tweesnijdend zwaard is in de ontwikkeling van OA.

List of publications

Mutation in the CCAL1 locus accounts for bidirectional process of human subchondral bone turnover and cartilage mineralization.
Alejandro Rodríguez Ruiz[§], Marcella van Hoolwerff[§], Sara Sprangers, Eka Suchiman, Ton Schoenmaker, Petra Dibbets-Schneider, Johan L. Bloem, Rob GHH Nelissen, Christian Freund, Christine Mummery, Vincent Everts, Teun J. de Vries, Yolande F. M. Ramos[#], and Ingrid Meulenbelt[#]
Rheumatology (Oxford). 2022;00:1-13.

The role of *TNFRSF11B* in development of osteoarthritic cartilage.
Alejandro Rodríguez Ruiz, Margo Tuerlings, Ankita Das, Rodrigo Coutinho de Almeida, Eka Suchiman, Rob G. H. H. Nelissen, Yolande F. M. Ramos, Ingrid Meulenbelt.
Rheumatology (Oxford). 2022;61(2):856-864.

High-impact *FN1* mutation decreases chondrogenic potential and affects cartilage deposition via decreased binding to collagen type II.
Marcella van Hoolwerff[§] , **Alejandro Rodríguez Ruiz**[§], Marga Bouma, Eka Suchiman, Roman I. Koning, Carolina R. Jost, Aat A. Mulder, Christian Freund, Farshid Guilak, Yolande F. M. Ramos, and Ingrid Meulenbelt.
Sci Adv. 2021 Nov 5;7(45):eabg8583. [§]Shared first coauthors.

Cartilage from humaninduced pluripotent stem cells: comparison with neocartilage from chondrocytes and bone marrow mesenchymal stromal cells.
Alejandro Rodríguez Ruiz, Amanda Dicks, Margo Tuerlings, Koen Schepers, Melissa van Pel, Rob G. H. H. Nelissen, Christian Freund, Christine L. Mummery, Valeria Orlova, Farshid Guilak, Ingrid Meulenbelt & Yolande F. M. Ramos.
Cell Tissue Res. 2021;386(2):309-20.

RNA sequencing data integration reveals an miRNA interactome of osteoarthritis cartilage.
Rodrigo Coutinho de Almeida, Yolande F. M. Ramos, Ahmed Mahfouz, Wouter den Hollander, Nico Lakenberg, Evelyn Houtman, Marcella van Hoolwerff, Eka Suchiman, **Alejandro Rodríguez Ruiz**, P. Eline Slagboom, Hailiang Mei, Szymon M Kiełbasa, Rob G. H. H. Nelissen, Marcel Reinders, Ingrid Meulenbelt.
Ann Rheum Dis 2019;78:270–277.

WWP2 osteoarthritis risk allele rs1052429-A confers risk by affecting cartilage matrix deposition via hypoxia associated genes
Margo Tuerlings, G.M.C. Janssen, Ilja Boone, Marcella van Hoolwerff, **Alejandro Rodríguez Ruiz**, Evelyn Houtman, Eka Suchiman, Robert J. P. van der Wal, Rob

G.H.H. Nelissen, Rodrigo Coutinho de Almeida, Peter A. van Veelen, Yolande F. M. Ramos, and Ingrid Meulenbelt.
In revision in Osteoarthritis and cartilage.

The role of epigenetics as a stable marker to monitor cartilage quality in hiPSC chondrogenesis
Ghazaleh Hajmousa, Rodrigo Coutinho de Almeida, **Alejandro Rodríguez Ruiz**, Marga Bouma, Roderick Sliecker, Hailing Mei, Rob G.H.H. Nelissen, Christian Freund, Judith Bovee, Keito Ito, Yolande F M Ramos, Ingrid Meulenbelt
In preparation for submission.

Curriculum vitae

Alejandro Rodríguez Ruiz was born on the 19th of November of 1992 in Valencia, Spain. He attended high school education in San Pedro Pascual. In 2010, he started his bachelor in Biotechnology at the Polytechnic University of Valencia (UPV), where he specialized in biotechnology applied to biomedical research.

For his bachelor thesis, he worked at the Centre of Biomaterials and Tissue Engineering (CBIT), where he generated three different biomaterials to achieve a controlled release system of growth factors upon brain injury. In 2014, he started a two years masters in Biomedical Sciences at the KU Leuven in Belgium, which he finished *cum laude*. During his masters, he performed two minor internships at the Genetics Laboratory and the Stem Cell institute in Leuven. For his final internship he moved to London to investigate osteosarcoma disease in a 3D *in vitro* biomaterial system and enter into the fascinating skeletal system field at the University College London (UCL).

In 2017, he started his PhD in the Biomedical Data Sciences group at Leiden University Medical Centre (LUMC) under the guidance of Prof. Dr. Ingrid Meulenbelt and Dr. Yolande Ramos. During his PhD he established and worked with an induced pluripotent stem cell (hiPSC) model of cartilage and bone to unravel the role of osteoprotegerin in osteoarthritis (OA). In August 2021, he became a postdoctoral researcher at the department of Pulmonology at the LUMC in the group of Prof. Dr. Pieter Hiemstra and Dr. Anne van der Does to generate hiPSC-derived alveolar models for lung repair.

Acknowledgments

After five years of doctoral research, I can say that this exciting journey has come to an end. A rollercoaster full of ups and downs, unexpected turns, short and long cuts and some detours that finally conclude with a title: Doctor. This journey would not have been possible without the help of many people to whom I would like to dedicate some words.

Dear Prof. Ingrid Meulenbelt. Thank you for offering me the opportunity to form part of your team. Your guidance and mentorship taught me valuable lessons for the rest of my professional career.

Dear Dr. Yolande Ramos. Thank you for your supervision and guidance both in the laboratory and while writing our manuscripts. Your mentorship and kindness strongly supported me throughout these years.

Dear members of my doctorate committee: Prof. Mummery, Prof. van Osch, Dr. Geurts. Thank you for reading this manuscript and for your suggestions to improve this thesis. Dear Dr. de Vries, thank you for your valuable input and fruitful discussions about the OPG-XL mutation paper.

I would also like to thank my colleagues in the osteoarthritis (OA) group. First of all, I would like to thank my paranymphs Eka and Evelyn. Dear Eka, thank you for asking for help whenever I was doing RT-qPCRs, Fluidigms, or any particularly difficult experiment, which you seemed to smell from your office. Also, your ccultural and culinary curiosity introduced me to discover many new places to visit in the Netherlands. Dear Evelyn, Evelyne or Evelin, thank you for teaching me all your vast SPSS knowledge and showing me the ABC of the lab. I will always remember how you used to hit your samples with that hammer to isolate RNA. You also kindly introduced me to the Dutch culture (and their directness) which really helped me during my first years here. Dear Marcella, thank you for your constant supply of sweets and for eating all the cakes (and fries) I couldn't finish during birthdays and other celebrations. Together we were able to defeat the CRISPR and the hiSPC differentiation projects and successfully finish our PhDs. I would also like to thank the rest of my awesome colleagues including Margo, Ritchie, Rodrigo, Ghazaleh, Ilja, Matthew, Niek, Nico and Nicoline. Also, the excellent students who came to work under my supervision Luuk and Ankita. I would like to thank the rest of the MolEpi group, and especially Eline, who always gave an incredible positive energy to the team. Thank you Inge for your kind help regarding the logistics during my PhD.

Moreover, I would like to thank all our collaborators Prof. Guilak, Prof. Nelissen, Prof. Bloem, Prof. Everts, Christian, Sara, Koen, Melissa, Petra and Ton. I would

A

also like to thank the OA patients and especially the OPG-XL family members for their enthusiastic cooperation in this study.

Finally, I would like to thank my new lab, friends and family for their constant support. Thank you PulmoScience lab for your great atmosphere. Thank you Pieter and Anne for welcoming me to your team. Thank you Sijia, Ying, Abilash, Doris and Shewanti for all the fun activities, food, laughs, advice and also for your support during the final steps for writing this thesis.

Next, I would like to thank the Biotechs, and especially Alejandra, Miriam and Evy, for always being a family where the laws of time and space don't seem to change anything. Thank you for being there. I would also like thank Ari, Schef, and Katja for our lovely meetings, dinners and little trips. Por supuesto, no me puedo olvidar de mis amigas del colegio María y Julia. Valencia no sería lo mismo sin vosotras.

Likewise, I would like to thank the Gang of Leiden, with Jacopo and Francesca for showing us Imperia, and Akane for introducing us to Osaka and Tokyo. I would also like to thank Nerea, Laura, Ruplu and Joseph for the time spent together. For our laughs, movie nights, museum days, warm lunches, adventures (and misadventures) and exhausting but marvelous trips.

Por último quisiera dar las gracias a mi familia. Gracias Mamá, Papá, Guillermo, Ita, Lucky y Merlín. Gracias por ofrecerme vuestro constante apoyo, consejo, alegrías, paseos y viajes de vuelta a casa donde podía recargarme de energía para seguir afrontando este periplo. Gracias por ser mis duendes, ayudándome en todo lo posible a pesar de la distancia. Este doctorado está dedicado a vosotros.

A